

Model-based Design of Hybrid Electric Marine Propulsion System Using Modified Low-Order Ship Hull Resistance and Propeller Thrust Models

by

Siyang Liu

Bachelor of Engineering, University of Victoria, 2018

A Thesis Submitted in Partial Fulfillment of the Requirements for the Degree of
MASTER OF APPLIED SCIENCE
in the Department of Mechanical Engineering

©Siyang Liu, 2020

University of Victoria

All rights reserved. This dissertation may not be reproduced in whole or in part, by photocopying or other means, without the permission of the author.

Supervisory Committee

Model-based Design of Hybrid Electric Marine Propulsion System Using Modified Low-Order Ship Hull Resistance and Propeller Thrust Models

By

Siyang Liu

Bachelor of Engineering, University of Victoria, 2018

Supervisory Committee

Dr. Zuomin Dong, Department of Mechanical Engineering

Supervisor

Dr. Brad Buckham, Department of Mechanical Engineering

Departmental Member

Abstract

Supervisory Committee

Dr. Zuomin Dong, Department of Mechanical Engineering

Supervisor

Dr. Brad Buckham, Department of Mechanical Engineering

Departmental Member

Transportation is a primary pollution source contributing to 14 percent of global greenhouse gas emissions, and 12 percent of transportation emissions came from maritime activities. Emissions from the ferry industry, which carries roughly 2.1 billion passengers and 250 million vehicles annually, is a major concern for the general public due to their near-shore operations. Compared to the rapidly advancing clean automotive propulsion, fuel efficiency and emissions improvements for marine vessels are more urgent and beneficial due to the significantly higher petroleum fuel consumption and heavy pollutants and the relatively slow adoption of clean propulsion technology by the marine industry. Hybrid electric propulsion, proven to be effective for ground vehicles, presents a promising solution for more efficient clean marine transportation. Due to the diversified hull/propulsor design and operation cycle, the development of a hybrid electric marine propulsion system demands model-based design and control optimization for each unique and small batch production vessel. The integrated design and control optimization further require accurate and computation efficient hull resistance and propulsor thrust calculation methods that can be used to predict needed propulsion power and gauge vessel performance, energy efficiency, and emissions. This research focuses on improving the low-order empirical hull resistance and propulsor thrust models in the longitudinal direction by extracting model parameters from one-pass computational fluid dynamics (CFD) simulation and testing the acquired models in integrated design optimization of the marine propulsion system. The model is implemented in MATLAB/Simulink and ANSYS Aqwa and validated using operation data from BC Ferries' ship Tachek. The modified low-order model (M-LOM) is then used in the integrated optimizations of propulsion system component sizes and operation control strategies for another BC Ferries' ship, Skeena Queen. The performance, energy efficiency, and emissions of various propulsion options, including nature gas-mechanical and natural gas-electric benchmarks, and hybrid electric alternatives of series hybrid, parallel hybrid, and battery/pure electric are compared to demonstrate the benefits of the new method in completing these complex tasks and hybrid electric marine propulsion. The research forms the foundation for further studies to achieve more accurate propulsion demand prediction and a more comprehensive lifecycle cost assessment of clean marine propulsion solutions.

Table of Contents

Supervisory Committee	ii
Abstract.....	iii
Table of Contents	iv
List of Table	vii
List of Figure.....	viii
Acknowledgments.....	x
Dedication	xi
Glossary of Acronyms and Abbreviations	xii
Chapter 1. Introduction	1
1.1. General Background	1
1.2. Research Motivation	3
1.3. Research Objective	4
1.4. Thesis Organization	5
Chapter 2. Application of Hybrid Electric Propulsion on Marine Vessels – A General Review	6
2.1. Hybrid Electric Propulsion System.....	6
2.1.1 Architectures of Hybrid Electric Propulsion System	6
Series HEPS.....	6
Parallel HEPS	7
Series/Parallel HEPS	8
2.1.2 Degree of hybridization	8
Micro Hybrid.....	8
Mild Hybrid.....	9
Medium Hybrid	9
Full Hybrid	9
Plug-in Hybrid.....	9
2.1.3 Operation Modes	9
2.2. State-of-the-art Hybrid Maritime Application	10
2.2.1 Architecture	10
2.2.2 Components	11
Energy converter.....	12
Energy Storage System (ESS).....	13
Electric Machines	15
Electric Power Grid	15

2.2.3	Technology Trend	16
2.3.	Hybrid Electric System Control.....	17
2.3.1	Rule-Based Control	18
	Deterministic Rule-Based.....	18
	Fuzzy Rule-Based.....	18
2.3.2	Optimization-Based Control.....	18
	Global Optimization	18
	Online or Real-Time Optimal Control.....	19
2.4.	Lifecycle Assessment.....	19
Chapter 3. Ship Power Demand Prediction Using Modified Low-Order Hull Resistance and Propeller Thrust Models		21
3.1.	Vessel Hull Resistance Model.....	21
3.1.1	Total Ship Resistance.....	21
	Water-induced Hull Resistance.....	22
	Wind-induced Upper Decks Resistance	24
3.1.2	Hull Resistance Models and Calculation Methods.....	25
	Hull Resistance Based on Vessel Sea Trial Data	26
	Towing Tank Hull Resistance Prediction Method	26
	Full-Scale CFD	26
	Reduced-Order Hull Resistance Prediction Model	27
	Low-Order Hull Resistance Prediction Model	27
	Generic Parametric Mathematical Model Estimation Method.....	28
3.2.	Vessel Propeller Efficiency and Thrust Model	28
3.2.1	Propeller Efficiency Model.....	28
3.2.2	Propeller Thrust Calculation.....	29
3.3.	Modified Low-Order Model and Calculation Method (M-LOMCM).....	30
3.3.1	Model Related Work.....	30
3.3.2	Numerical Estimation of Stability Characteristics Using CFD.....	32
	Conventional NX CFD Package.....	35
	FloEFD Toolbox for NX.....	35
	Ansys Aqwa.....	36
	Ansys Fluent.....	37
3.4.	Modified Low Order Propeller Thrust/Torque/Speed Model	38
3.4.1	Modified Holtrop and Mennen’s Drag Based Surging Power Deduced Model....	38
3.4.2	Pre-calculated Propeller Efficiency	39

Direct Efficiency Calculation	39
Efficiency Diagram Lookup	39
Computational Fluids Dynamic Simulation	41
Model Comparison	42
3.4.3 Iterative Propeller Speed Estimation Model.....	44
3.5. Software Implementation and Model Validation	47
3.6. Key Improvements - Stability Data-Based Model.....	51
Chapter 4. Comparison of Different Marine Propulsion Systems	53
4.1. Selection of a Benchmark Marine Vessel – BCFS Skeena Queen.....	53
4.2. Natural Gas (NG) Engine Mechanical Drive.....	56
4.3. Natural Gas Engine Electric Drive	58
4.4. Pure Electric Drive.....	59
4.5. NG Engine Hybrid Electric Drive.....	60
4.5.1 Series Hybrid Electric Drive.....	60
4.5.2 Parallel Hybrid Electric Drive	60
4.6. Benchmark Performance Comparison	61
Chapter 5. Application to Integrated Hybrid Electric Ship Design	64
5.1. Propulsion Power Prediction.....	64
5.2. Hybrid Electric Propulsion System Design	68
5.3. Operation Control of the Hybrid Electric Vessel	69
5.3.1 Rule-based Stateflow Control.....	69
5.3.2 Dynamic Programming (DP).....	73
5.4. Integrated Propulsion System Design and Control Optimization.....	77
Chapter 6. Conclusion and Future Works	89
6.1. Summary.....	89
6.2. Conclusions.....	90
6.3. Research Contributions.....	91
6.4. Future work.....	92
Reference	94
Appendix A Coefficients for Holtrop’s method of resistance calculation	102
Appendix B Coefficients for wind resistance calculation.....	104
Appendix C Coefficients for propeller efficiency calculation	105

List of Table

Table 1: Comparison of the critical characteristics between series and parallel hybrid electric architectures	11
Table 2: Propeller efficiency lookup table for function implementation	40
Table 3: BCFS MV Skeena Queen design details [108].....	54
Table 4: Optimized benchmark model result comparison.	62
Table 5: Detailed results comparison of two different dynamic programming strategies	76
Table 6: Simulation results of two nested optimizations using fixed ICE power output strategy and variant ICE power generation	81

List of Figure

Figure 1: Series hybrid electric architecture on ship	7
Figure 2: Parallel hybrid electric architecture on ships or vehicles	7
Figure 3: Series-parallel hybrid electric architecture on ships.....	8
Figure 4: Complex integration of series-parallel hybrid electric architecture for ship application	11
Figure 5: Summary of available control strategies [32].....	17
Figure 6: Types of resistance experienced by ships during sailing.....	22
Figure 7: Typical hull resistance estimation methods.....	26
Figure 8: Efficiency diagram of Wageningen B-Series propeller with four blades $AE/AO = 0.45$ [104].	29
Figure 9: Comparison between the dedicated ship drag regression and numerical results [102]	31
Figure 10: Rough CAD model for Tachek upper decks.....	33
Figure 11: NX CAD model measurement report	33
Figure 12: Measure the corresponding volume for determining draft.....	34
Figure 13: Ansys Aqwa hydrodynamic diffraction set up	34
Figure 14: Ansys hydrostatic position results report.....	34
Figure 15: Conventional build-in NX CFD solver setup	35
Figure 16: FloEFD NX version simulation setup and results	36
Figure 17: Ansys Aqwa simulation setup.....	37
Figure 18: Ansys Fluent setup and results	37
Figure 19: Tachek propeller efficiency based on the efficiency diagram	40
Figure 20: Propeller CFX simulation set up and results	41
Figure 21: Results of three tested propeller efficiency calculation methods	42
Figure 22: Power results using fixed and real RPM.	43
Figure 23: Tachek propeller thrust and torque coefficient	45
Figure 24: Comparison between measured shaft speed to the predicted shaft speed using the backpropagation method.....	46
Figure 25: Processes flow for the subfunction contains resistance and efficiency calculation	48
Figure 26: Predefined functions for setting up propeller efficiency lookup table and stability data calculation	48
Figure 27: Main LOM function flow	49
Figure 28: Results comparison between predicted and actual measured shaft power profile.	50
Figure 29: Hull resistance models comparison visualization.	51
Figure 30: A simple representation of the low-order model	52
Figure 31: BCFS MV Skeena Queen [108]	53
Figure 32: Integrated propulsion system design processes using low-order model	55
Figure 33: Benchmark model for the NG-mechanical drive propulsion system	57
Figure 34: The low-order model block representation	57
Figure 35: Benchmark model for the NG-electric drive propulsion system.....	58
Figure 36: NG generator block representation.....	59

Figure 37: Benchmark model for the pure battery-electric drive propulsion system	59
Figure 38: Benchmark model for the series hybrid electric drive propulsion system	60
Figure 39: Benchmark model for the parallel electric drive propulsion system.....	61
Figure 40: SKQ propeller parameter computation setup using Ansys CFX.....	65
Figure 41: SKQ propeller efficiency results from Aqwa CFD simulation.	65
Figure 42: SKQ propeller parameter results from Aqwa CFD simulation.	66
Figure 43: SKQ acceleration results in comparison.	67
Figure 44: Fully integrated series-parallel hybrid-electric propulsion system design layout for SKQ.....	68
Figure 45: Rule-based control scheme for SKQ series-parallel system.	70
Figure 46: Engine operation curve.....	71
Figure 47: Simulation result for series-parallel configured SKQ using rule-based control. ...	72
Figure 48: Comparison between simulation results and recorded results.....	73
Figure 49: Dynamic programming processes demonstration	74
Figure 50: ICE power production comparison between two DP strategies	76
Figure 51: NG generator power generation comparison between two DP strategies	76
Figure 52: Battery SOC comparison between two DP strategies	77
Figure 53: Comparison between simulated power output and recorded power demand for both control strategies.	77
Figure 54: Flowchart demonstration of nested two-layer optimization.....	79
Figure 55: NG generator power production for two different control strategies.	82
Figure 56: NG generator power profile filtrated using a 60-second moving average filter.....	82
Figure 57: Battery SOC profile comparison between control strategies.	83
Figure 58: Comparison between simulated ship velocity and the VDR recorded velocity data.	84
Figure 59: Improved simulated ship speed comparing to the recorded ship speed.	85
Figure 60: Ship “helmsman” speed PID controller implementation	86
Figure 61: Speed controller module regulated ship speed in comparison to recorded ship speed.	87
Figure 62: Predicted shaft power, torque, and speed demand after PID controller implementation.	88

Acknowledgments

I would like to thank my supervisor, Dr. Zuomin Dong, whose continuous support, guidance, and feedbacks were essential in completing this research work. His expertise greatly inspired me for this research work, and will continuously do in my future work. I would also like to acknowledge the valuable inputs from my research mates: Li Lily Chen, Haijia Alex Zhu, Michael Grant, and Mostafa Rahimpour. Their works are the foundations of this extended research.

Dedication

I would like to dedicate this thesis to my family members who have supported me during the past many years. Especially for my parents, without their encouragement and good faith, I would not be able to complete this work in a place far from home.

Glossary of Acronyms and Abbreviations

AC	Alternate current
BCFS	BC Ferries
CAD	Computer-aided design
CD	Charge depleting
CFD	Computation fluids dynamic
CS	Charge sustaining
DC	Direct current
DE	Diesel-electric
DG	Diesel generator
DOE	Department of energy
DP	Dynamic programming
EFCM	Equivalent fuel consumption method
EMS	Energy management system
ESS	Electric storage system
EV	Electric vehicle
FC	Fuel cell
FCHS	Fuel cell hybrid system
GHG	Greenhouse gas
GPS	Global positioning system
HC	Hydrocarbon
HEPS	Hybrid electric propulsion system
HEV	Hybrid electric vehicle
HIL	Hardware in loop
ICE	Internal combustion engine
IMO	International maritime organization
ITTC	International towing tank conference
LCC	Lifecycle cost
LCCA	Lifecycle cost assessment
LNG	Liquified natural gas
LOM	Low-order model

MAPE	Mean absolute percentage error
MCFC	Molten carbonate fuel cell
M-LOM	Modified low-order model
MPC	Model predictive control
MSSR	Multi-start space reducing
NG	Natural gas
PEMFC	Proton exchange membrane fuel cell
PHE	Parallel hybrid electric
PHEPS	Parallel hybrid electric propulsion system
PM	Particle matters
RANS	Reynolds Averaged Navier Stokes
RNG	Renewable natural gas
ROM	Reduced-order model
RPM	Rotation per minute
SHE	Series hybrid electric
SHEPS	Series hybrid electric propulsion system
SOC	State of charge
SOFC	Solid oxide fuel cell
SPHEPS	Series-parallel hybrid electric propulsion system
VDR	Voyage data record

Chapter 1. Introduction

1.1. General Background

With the increasing world population and growing economic activities, transportation is a primary pollution source contributing to 14 percent of global greenhouse gas emissions [1]. With increasing environmental concerns, using clean transportation technologies to achieve decarbonization has become the priority. Among the transportation sector, ground vehicles contributed most of the emissions and attracted most of the research efforts and investments. Maritime activities, which contribute to about 12 percent [2] of the transportation emissions, have fallen behind in adopting clean propulsion technologies. At present, more than 90 percent of world trade is carried by ships [3]. On the other hand, the ferry industry alone has a similar size to the commercial airline industry. The world ferry industry carries roughly 2.1 billion passengers and 250 million vehicles annually [4], even without considering countries with a vast population like China. As the largest North American ferry operator, BC Ferries (BCFS) transport 21 million passengers and 8 million vehicles in 2019 [5]. As reported by multiple institutes, such as the International Maritime Organization (IMO), 4.5 percent of global CO_2 emissions are produced by ships [6]–[8]. This amount, if left untreated, will increase by 25 percent in 2050 [8]. Compared to the rapidly advancing clean automotive propulsion, fuel efficiency and emission improvements for marine vessels are more urgent and beneficial due to the significantly higher petroleum fuel consumption and heavy pollutants and the relatively slow adoption of clean propulsion technology by the marine industry. The maritime industry sector is smaller than other transportation segments, but investment in clean transportation for marine vessels is more effective than in the automotive industry [9].

The inherent reason for maritime pollutions is the usage of large-scale diesel engines. With operation cost as the primary consideration, the conventional diesel engine is the first choice for marine vessel propulsion and power generation [7]. Much research has been carried out on sustainable maritime transports. Since the inherent pollution source is fossil fuels, cleaner alternative energy is a generic area of interest. One of the most adopted alternatives is liquefied natural gas (LNG), followed by renewable electricity, biodiesel, methanol, hydrogen, and even nuclear. Those fuels have no or low carbon, sulphur, and nitrogen content, which can drastically reduce the exhausts' pollutive contents [10]–[17].

On the other hand, researchers also focus on advanced propulsion technologies for energy efficiency and emission improvements. Using gas turbines to replace diesel engines or switching to auxiliary power units during docking can improve fuel efficiency [18]–[21]. Hybrid electric propulsion systems (HEPS), with optimally controlled mechanical and electric power flow, allow the engines to operate more efficiently and supporting prolonged heavy-duty operations, which have become a promising solution. The new and cleaner propulsion technology may take over maritime propulsion soon. With cleaner fuels and improved engine technologies, hybrid electric marine propulsion would resolve a large portion of the outstanding marine emission issue.

Geertsma *et al.* [18] performed a detailed review of different hybrid propulsion systems with

corresponding control strategies. That study showed that the hybrid system benefits a ship that sails at 40 percent or below its top speed for most of the mission. Meanwhile, if the power demand is well spread across the mission cycle, a hybrid electric propulsion system tends to perform better. The review also suggested that a DC power bus can considerably reduce energy conversion losses and boost performance. Optimization of the power control strategy and energy management system can significantly improve the performance of a HEPS. Molloy *et al.* [22] detailed the potential of applying hybrid electric or pure electric technology onto small marine vessels and thoroughly investigated HEPS's benefits and drawbacks from the overall concept to specific components and potential market. Researchers also suggested that hybrid electric marine propulsion technology can only be successfully developed through collaboration between ship designers, builders, and researchers. Only then, can technology become mature and accepted by customers. Menanan *et al.* [23] reviewed the HEPS applications on small ships. Researchers argue that the hybrid system is suitable for applications that have stochastic conditions. Different propulsion systems, depending on the applications, require different configurations. This review concludes that hybrid-electric propulsion is capable of minimizing fuel consumption, especially for ships that need a high degree of freedom during maneuvering. Other researches [24]–[26] also assess the applications of different hybrid alternatives on ships' applications.

The propulsion systems of ground vehicles and marine vessels are comparable due to many similar elements, such as electric drive, battery energy storage system (ESS), fuel cell powerplant, power control, and energy management strategies, and layout of the hybrid electric powertrain. Maturing hybrid electric technologies can be applied with some modifications. However, several challenges prevent the quick adoption of clean transportation technology. The demand for propulsion can be accurately predicted for vehicular applications based upon widely accepted driving cycles and established vehicle dynamics models. The performance, energy efficiency, and emissions of different propulsion systems can be obtained using model-based simulation tools. On the other hand, the needed propulsion power for marine vessels cannot be quickly and accurately calculated due to the following two reasons:

- Most large marine vessels are different with distinct and diversified hull geometry, propulsor design, and operating environments. The hydrodynamics based, accurate hull drag and propulsor thrust prediction methods require computation-intensive full-scale computational fluids dynamic (CFD) simulations, either in direct numerical/simulation studies [27] or for obtaining the parameters for the reduced-order hull drag and propulsor thrust prediction models [28]. The traditional low order empirical equations for hull drag and propulsor thrust calculations are inaccurate and not reliable [29].
- Depends on their missions, the operation profile of marine vessels varies significantly [28], including travelling velocity, sailing route, cargo load, and marine weather conditions.

These factors determine that no standard propulsion system design and operation controls can be representative enough. In addition, the propulsion systems for large marine vessels require massive investment, have long operation life, and small batch production without prototype testing and design revision opportunity. Using model based design (MBD) technology to

identify the optimized propulsion system design and associated control strategies for a specific marine application becomes essential, especially for the complex hybrid electric propulsion system with various possible design and control solutions. Integrated propulsion system design and optimization using multiphysics simulations and hardware in the loop (HIL) testings, introduced in hybrid electric vehicle research, are not yet available for the optimal design of hybrid electric marine vessels. These advanced techniques need to be developed urgently to pave the road for clean marine propulsion.

1.2. Research Motivation

This research's primary motivation is to address the previously stated issues in generating optimal design and control solutions through MBD for hybrid electric marine vessels. A new method for obtaining the low-order vessel hull resistance, propulsor thrust, and propulsion power with balanced modelling accuracy and computation intensity are to be introduced and validated using a ferry ship's acquired operation data. The method will be integrated with the hybrid electric powertrain design and control optimization tools and implemented using the same MATLAB/Simulink platform. The newly introduced methods and integrated modelling tool will be applied to compare various marine propulsion options of another benchmark vessel. The tests are used to verify the new approach's capability for identifying the best clean, hybrid electric propulsion solution with optimal energy efficiency and emission improvements.

Traditionally, ship design is dominated by diesel-mechanical drives. Several reasons make such a selection an "obvious" choice. Low-cost diesel fuel has a large energy density. The diesel engine has a high torque capability, and the mechanical propulsion system is the most inexpensive drivetrain installed on ships. Modern, clean propulsion technologies require high investment costs for additional generators, electric propulsion motors, high power AC or DC power bus, battery ESS, hydrogen fuel cells, etc. The high initial costs of adopting these new technologies and the inability to accurately predict the fuel and operation cost savings hold back the progress of clean marine propulsion technology. Moreover, after decades of development, diesel engine technologies are mature. When running in the peak efficiency zone, the engine and propulsion system efficiency is comparable to other technologies. However, the fuel efficiency and emissions of a diesel engine are heavily influenced by the vessels' propulsion power demand. This power demand changes dramatically for fully loaded, partially loaded, or empty ships and under unpredictable marine weather conditions with varying wind, wave, current, and tide. Since the engine's most efficient operation zone is only associated with a limited range of speed and torque, the diesel-mechanical propulsion system of a near-shore vessel only operates at its peak efficiency for a fraction of time.

A hybrid electric marine propulsion system with a combination of mechanical power flow from the diesel engine and electric power flow from the electric ESS, generator, and propulsion motor can overcome the stated drawbacks of traditional diesel-mechanical and diesel-electric drives. The series hybrid electric marine propulsion system simply adds the electric ESS and hybrid electric powertrain control to the diesel-electric propulsion system. This new design allows the diesel generator to operate continuously at its peak energy efficiency operation zone, leading to improved fuel efficiency and reduced emissions and fuel cost. The variant propulsion

power demand from the vessel operation is met by charging or drawing electric power from the onboard battery ESS through optimal power control and energy management from the added hybrid propulsion system control. The parallel and series/parallel hybrid electric marine propulsion system further improves the system's energy efficiency and reduces power loss by avoiding unnecessary energy conversions in the hybrid electric powertrain under advanced controls. The hybrid electric marine propulsion system better utilizes the existing diesel and natural gas (NG) fueling infrastructure. Meanwhile, high fuel energy density, low engine cost, and long operation life are benefits of the HEPS but are often obstacles of pure electric and hydrogen fuel cell electric vessels.

In this research, the new modified low-order Holtrop and Mennen's (H&M) hull resistance regression model and H&M drag and vessel surging power deduced model (two models in combined is known as M-LOM) are first validated using the real-world vessel operation data acquired from the BC Ferries ship Tachek [30]. Integrated marine propulsion system modelling, design, and control optimization are then conducted based on the BC Ferries ship Skeena Queen (SKQ). The ship's present diesel-mechanical propulsion system is used as the performance, energy efficiency, and emission benchmark. Using the newly introduced modelling and simulation tools, advanced clean marine propulsion system design and control solutions are studied.

1.3. Research Objective

As previously mentioned, the hybrid system is influenced by the ship power profile, and such power profiles are hard to predict under certain situations. Meanwhile, based on the power profile and sailing conditions, the hybrid system performance is not guaranteed better than other conventional systems. To solve the difficulties and concerns, the research objective of this study include:

- Develop a capable and accurate ship propulsion power profile prediction method based on the low-order hull resistance and propulsor thrust models, using available vessel operation data and one-pass CFD simulations on a PC workstation;
- Validate the new M-LOM using real vessel operation data;
- Test the new M-LOM model through the modelling, simulations, and performance studies on a benchmark ferry for further improvement;
- Apply the newly introduced modelling method and tools in the integrated modelling and design and control optimizations of an advanced hybrid electric propulsion system for the testbench ferry ship to carry out the further development of the new technique.

The ultimate goal of this research is to make the integrated modelling, design, and control optimization of the hybrid electric marine propulsion system a more practical clean vessel design tool without the burden of sea trial and computation-intensive full-scale CFD simulations requiring the use of a supercomputer.

1.4. Thesis Organization

The thesis is organized as:

Chapter 2 reviews hybrid electric propulsion technology in general and its application on ships. The review studies the hybrid configurations, operation modes, state-of-art components and system design, controls, and lifecycle assessment. The review aims at studying the feasibility of hybrid-electric propulsion technology on ships.

Chapter 3 presents the development of the M-LOM, a low-order hull resistance and propeller thrust model for ships' power profile prediction using speed, hull geometry data, and vessel stability data, in detail. The goal of this study is to establish a modularized Simulink model for power prediction that can be integrated into the overall designed system.

Chapter 4 focuses on modelling the benchmark and advanced marine propulsion systems, including natural gas-mechanical drive, natural gas-electric drive, series hybrid, parallel hybrid, and pure electric drive. To compare the energy efficiency of these systems, this work optimizes the system and converts all system consumptions to equivalent fuel consumptions for total costs measurement.

Chapter 5 introduces a fully integrated model-based hybrid electric ship design using the M-LOM and a representative benchmark ferry ship. To simultaneously optimize the component sizes and control strategies of the hybrid electric propulsion system, a nested two-layer optimization problem is formulated and solved using dynamic programming (DP) and the multi-start space reducing (MSSR) global optimization algorithm. In addition, the research considers electric energy equivalent fuel consumption and battery degradation penalty. System optimization is based on balanced fuel consumption and battery life loss.

Chapter 6 summarizes the work, draws conclusions, and outlines the steps for future developments.

Chapter 2. Application of Hybrid Electric Propulsion on Marine Vessels – A General Review

A hybrid electric propulsion system (HEPS) is a maturing technology for improving fuel efficiency and reduce emissions of ground vehicles. This technology also presents great potential for various marine applications. On the other hand, the enabling model based design (MBD) tools for developing the HEPS of various marine vessels are still not available due to the more complex and much diversified marine applications. To better understand the key requirements of developing the MBD tools for marine applications, this chapter presents a review of the system architecture, key components, and control methods of HEPS and uses the understanding to select the appropriate HEPS design for the targeted marine vessel, including the series-parallel hybrid electric drive with natural gas (NG) engines, electric motors, DC power bus, li-ion batteries, and system design and control optimizations.

2.1. Hybrid Electric Propulsion System

As suggested by its name, HEPS combines at least two energy sources to provide propulsion power jointly. Conventional HEPSs utilize internal combustion engines (ICE) and battery energy storage systems (ESS) to boost efficiency by distributing the energy based on the external working condition and internal system device properties. Depending on the energy distribution methods, the HEPS can be categorized into three major groups: series, parallel, and series-parallel. Meanwhile, based on the degree of hybridization, HEPSs are grouped into micro, mild, medium, full, and plug-in hybrid.

In this section, the ICE and battery are considered as the default energy converter and energy storage system to illustrate the system configuration. These two devices are the most commonly used energy sources for the HEPS; other devices such as fuel cells or flywheels are reviewed in the later section but not demonstrate here.

2.1.1 Architectures of Hybrid Electric Propulsion System

Series HEPS

The principal characteristic of series-configured HEPSs (SHEPS) is, there is no direct mechanical link between ICE and the final drive. The ICE is coupled with a generator for electricity generation. Together with the ESS, two energy sources power the electric motor(s) to propel the final drive (wheels for vehicle and propellers for vessel). ICEs suffer from low efficiency in the low-speed region. For vehicles in urban driving conditions or vessels under variant loading conditions, the overall system efficiency will be low since the engine frequently enters the low-efficiency zone. SHEPS resolves the problem by allowing ICE to work in a high-efficiency zone for electricity generation. The battery will charge or discharge depending on the working conditions and the level of charge (also known as the state of charge). Figure 1 shows the typical series hybrid electric propulsion system architecture.

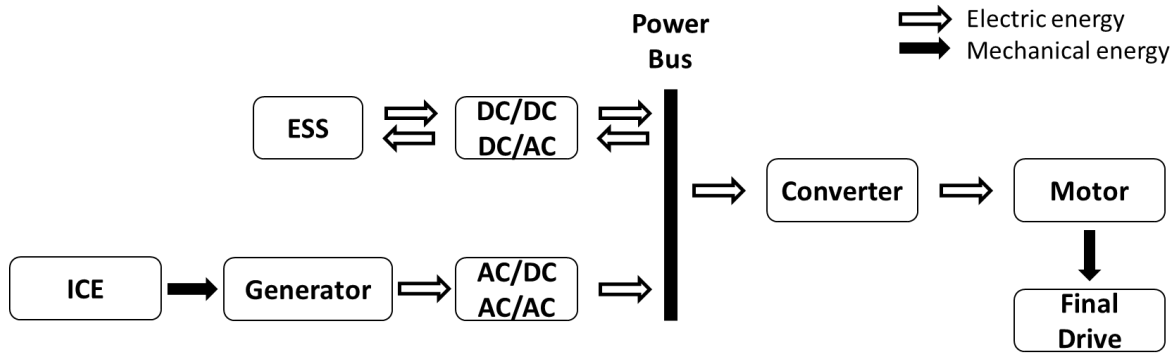


Figure 1: Series hybrid electric architecture on ship

The engine can potentially be downsized in SHEPS since it is mainly responsible for maintaining the battery's level of charge. During a mission, ICE idles or shuts down when the battery state of charge (SOC) is high. When battery SOC is low, ICE will operate at a high-efficiency zone for electricity generation to charge the battery or provide propulsion power. On vehicle applications, SHEPS is suitable for urban driving conditions where the vehicle stops frequently. For maritime applications, SHEPS offers an excellent range extension ability for long-distance sailing.

Parallel HEPS

Parallel HEPSs (PHEPS) keep the mechanical link between the ICE and final drives and allow mechanical power flows through the gearbox. Meanwhile, the additional ESS and electric motor provide assistive power to the final drive to enhance the propulsion performance. Figure 2 shows the parallel drivetrain architecture [31].

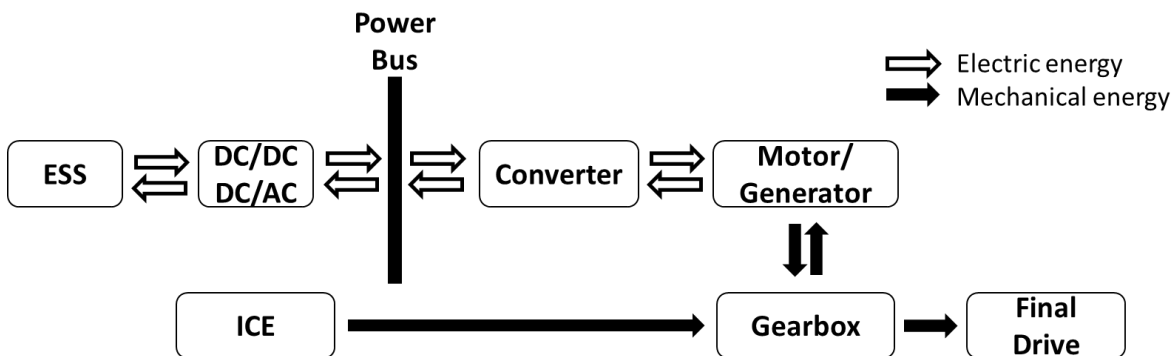


Figure 2: Parallel hybrid electric architecture on ships or vehicles

For PHEPS, ICE and electric motor are on for the entire operation duration. In this case, the control strategy can be more complex to determine power distributions and match the speed and torque requirements. The ICE and motor need to be synchronized in output speed since two devices jointly power the final drive. However, the parallel configuration is more compact than SHEPS, which requires fewer energy converters and hence will have fewer conversion losses. PHEPS is a better suit for rural driving conditions for the vehicle since speed can be well maintained at a constant level. At a consistent power level, an ICE will have high efficiency, and direct mechanical links enhance efficiency since no energy formation

conversion is required. Ferries that have pronounced cruising phases are a good fit for PHEPS with a similar reason to ground vehicles.

Series/Parallel HEPS

The series/parallel or power-split HEPS is a unique hybrid propulsion architecture that supports both series and parallel hybrid electric propulsion. This advanced design allows the propulsion system to operate as a conventional ICE drive, pure electric drive, PHEPS, SHEPS, or series-parallel HEPS (SPHEPS). A few designs achieve alternative modes by splitting the drivetrain into sub-systems (front and rear axis) and simultaneously applying different configurations. In contrast, others use internal connectors such as clutch, planetary gear, and electric convertor to achieve multiple drive modes. Figure 3 shows the general configuration of the series-parallel structure.

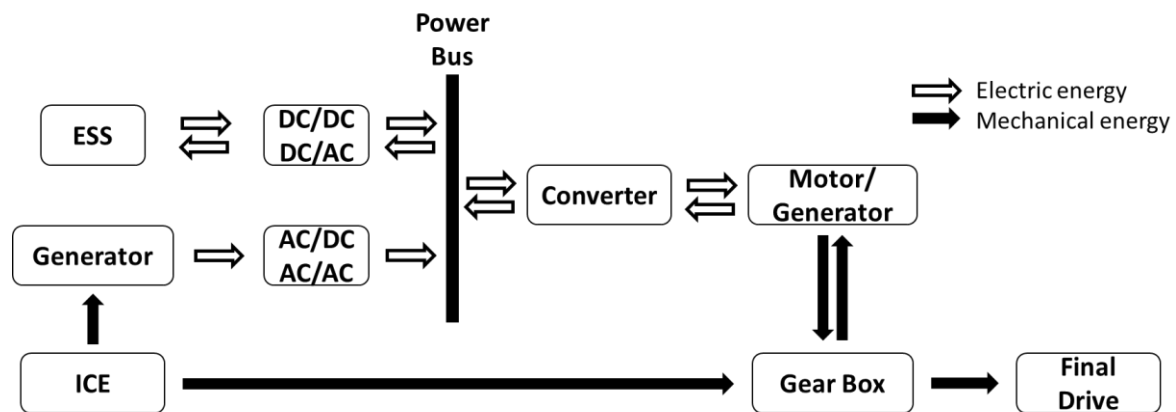


Figure 3: Series-parallel hybrid electric architecture on ships

Power-split HEPS is one of the most advanced HEPS designs with the most considerable potential for fuel consumption reduction. However, since many modes are to be switched under different conditions, the control scheme can be complex to optimize and implement. Meanwhile, a vast amount of simulations need to be done to achieve smooth transitions between various modes.

2.1.2 Degree of hybridization

The degree of hybridization measures the percentage of involvement of the additional energy sources. For ground vehicles, the degree can be tiered up as micro, mild, medium, full, and plugin hybrid [31]–[35]. However, due to the large power demand for vessels and ships, a full hybrid with an optional plugin functionality is commonly used. The smaller degree of hybridization is not generally considered in marine applications.

Micro Hybrid

Micro hybrid is the minimum amount of hybridization that can be achieved in a vehicle, which only ranges from 3 to 5 kW [32][35]. Micro hybrid aims at harvesting energy from regenerative braking for battery charging. Combined with an engine stop-start system, this hybrid system can typically reduce up to 4 percent of the CO_2 emissions [32].

Mild Hybrid

Mild hybrid is the next tier, which typically rates at 7 to 12 kW of hybridization. A motor/generator can harvest energy from regenerative braking, and the system benefits from engine stop-start. Meanwhile, the motor provides assistive power during some driving conditions. However, the battery and motor are not big enough for electric drive mode [31]–[34].

Medium Hybrid

Medium hybrid is also known as a motor assistive hybrid. For medium hybrid, the primary energy is the ICE, and ESS provides assistive power. Two energy sources are parallel connected, allowing ESS/electric motor to assist with propulsion or take over when ICE is idling. With a motor/generator installed between ICE and transmission, the medium hybrid can achieve EV mode for a short period. Meanwhile, regenerative braking is still available for energy recovery.

Full Hybrid

Combined with a powerful ESS with large capacity, a full hybrid system can achieve ICE mechanical, battery-electric, and hybrid drive. The full hybrid requires complex control strategies to control the power flow and manage energy allocation. As ESS SOC is high, the vehicle/vessel operates in EV mode, known as charge depleting mode. When the SOC of ESS is low, the system will maintain the charge level using the fossil fuel operated ICE to produce more power through the charge sustaining mode of operation. Depending on the mission cycle, a full hybrid system can utilize all possible configurations aforementioned.

Plug-in Hybrid

The plug-in hybrid is an enhanced version of the full hybrid. Plug-in hybrid suggests the battery can be plugged into the power grid for charging (known as cold ironing for ships and vessels application) [36][24][37][7]. The plug-in hybrid system can further reduce fuel consumption and overall emissions, especially when the grid power is generated from clean sources. Plug-in hybrid often requires a larger ESS comparing to other hybrid configurations to achieve a longer EV drive. Since the battery for a hybrid electric marine propulsion system is generally more massive than the battery on a vehicle, the batteries are swapped for some ships after each mission. Other ships are connected to the grid through cold ironing over the night for hotel loads and battery charge.

2.1.3 Operation Modes

The operation modes describe the possible working configuration a hybrid system can achieve. The switch between each different mode depends on the mission and the corresponding control strategy. For series configurations, the following modes can be achieved:

- 1) Diesel-electric propulsion
- 2) Battery-electric propulsion
- 3) Diesel-electric propulsion with battery power assistance
- 4) Diesel-electric generation for propulsion and battery recharge

For parallel systems, the available modes are:

- 1) Mechanical drive through ICE
- 2) Battery electric drive
- 3) Mechanical drive with power generation for battery recharge
- 4) Mechanical drive with battery power assistance

For series-parallel architecture, the different operation modes are the combinations of the previous two configurations:

- 1) Pure ICE mechanical drive
- 2) Pure Battery electric drive
- 3) Diesel-electric drive
- 4) Diesel-electric propulsion with battery power assistance
- 5) Diesel-electric generation for propulsion and battery recharge
- 6) Mechanical drive with power generation for battery recharge
- 7) Mechanical drive with battery power assistance
- 8) Full hybrid mode: mechanical output with diesel-electric propulsion and/or generation and battery charge and/or discharge

Regenerative braking is an essential and unique operating mode in automotive applications for energy recovery; however, since ships have no braking system, the regenerative recovery method is not feasible. In fact, a better control strategy or operation method is required to minimize the energy consumption during ship ‘braking’ since thrust from the opposite direction is the most common method for vessel deceleration [38].

2.2. State-of-the-art Hybrid Maritime Application

Hybrid electric propulsion for marine applications is less advanced than the automotive industry; however, with raising attention to climate change due to maritime activities, more researchers have stepped into the field and published innovative works. This section reviews the state-of-the-art hybrid-electric technology implemented into the marine application.

2.2.1 Architecture

The automotive industry already recognizes the aforementioned typical hybrid propulsion system architectures; however, for the marine industry, diesel generators are commonly used in parallel with the ESS to provide electric power. The primary reason is that diesel-electric technology is currently dominating the ship propulsion system. The additional battery pack can be installed onboard to convert the design into a hybrid drive. Moreover, a properly sized battery module may be too large and expensive to implement onboard. If the diesel-electric system is implemented, the series architecture remains the same with no modification; however, the parallel system can be automatically modified into a series-parallel architecture if the diesel-electric generation system is implemented.

Currently, the most complex hybrid propulsion architecture builds up from the series-parallel system as shown in Figure 4. With additional motor generators, the system allows bidirectional power flow and can achieve enhanced parallel drive. Such an approach enables the battery to power two motors: one for direct output for the final drive and the other one for assisting the

engine shaft output [39].

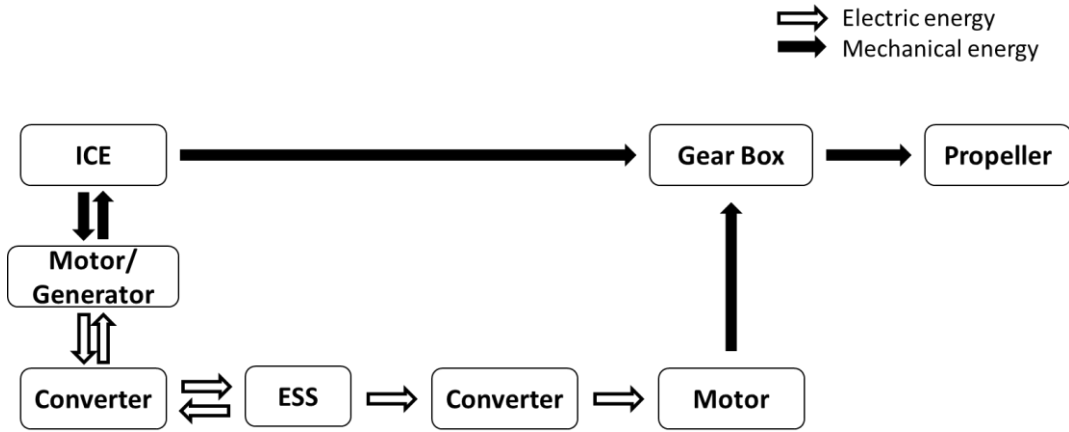


Figure 4: Complex integration of series-parallel hybrid electric architecture for ship application

Since ships are built to order, there is less room for prototyping and system iteration. Therefore, the basic hybrid electric powertrain configurations, namely, the series, parallel, and series-parallel, are commonly used on ships.

Table 1 compares the series and parallel architecture applied to the ships and vessels.

Table 1: Comparison of the critical characteristics between series and parallel hybrid electric architectures

	Series	Parallel
Engine operation	Constant operation point at efficient zone The engine can be sized down to reduced initial cost	Fluctuating operation points Engine power directly output, fewer conversion losses
ESS operation	Battery responsible for peak power	Less battery power variation
Electric motor	Motors need to be sized up for full power output	Motors can be sized down since the engine provides power
Overall system	No mechanical linkage between engine and propeller. Engines can be placed as desired for stability purpose	Better efficiency due to reduced conversion losses
Control strategy	Simpler control strategy	More complex control to balance the energy output

2.2.2 Components

The core idea of hybrid propulsion is to combine several energy sources to power the final drive jointly for peak performance. For optimal design, components need to be selected and sized according to the mission and control. This section reviews the state-of-the-art components used in the maritime hybrid propulsion application.

Energy converter

When hybrid technology is introduced, one default power source is ICE. However, conventional ICEs are responsible for primary greenhouse gases (GHG) emissions; therefore, the fuel converters and the conversion processes have become the main focus area for emission reduction, fuel efficiency improvement, and decarbonization.

Internal Combustion Engine (ICE)

ICE has been the most commonly used fuel converter. Converting chemical energy from fuel to mechanical energy, ICE is responsible for all the operation emissions, including GHG emissions, SO_x , NO_x , and particle matters. For the past decades, research has focused on ICE to increase efficiency and reduce emissions, and the technology is close to mature.

The majority of the ships on the current market are powered by diesel, either through the direct diesel engines mechanical drive or diesel-electric drive, where diesel-electric can be diesel generator or combined gas turbine electric. In recent decades, the diesel-electric system dominated the market since it can provide both propulsion power and hotel load. Meanwhile, no transmission is required between the ICE and the final drive in a diesel-electric drive. The diesel engines have large power/energy density, low operation cost, and high efficiency at rated power [7][41][42].

To meet the hotel loads, peak power requirements, and redundancy required from regulations, diesel engines for marine propulsion applications are often oversized, causing more maritime air pollution [42]. When the engine is oversized or operating at a fixed rotational speed to meet the electric load frequency, the engine efficiency is not optimized [7][40]. Meanwhile, under partial loads (<75 percent of the maximum load capacity for diesel generators and <80 percent for gas turbine combined systems), the efficiency of diesel generator and turbine-based systems is low [40]. The low-efficiency operation results in insufficient combustion processes, which is the consequence of a large amount of harmful pollution.

Different fuels, such as natural gas (NG), bio-diesel, methanol, ethanol, hydrogen, propane, and other alternatives have been proposed and tested to reduce carbon emissions. Among all alternative fuels, compressed NG and liquefied NG have drawn significant attention in the marine propulsion application. With minor modifications, many existing ships can be fueled by liquified natural gas (LNG) to achieve cleaner emissions profiles. Being stored in compressed and liquid form, NG has a better energy density than other alternatives such as hydrogen [43]. NG mainly contains CH_4 and C_2H_6 , which has a low percentage of carbon content contrasting from crude oil products [7]. Meanwhile, short on sulfur and nitrogen content, harmful air pollutants can be reduced using NG. The current marketing products are mostly fossil NG; however, renewable natural gas (RNG) can be produced through biomass [7][14][44]. NG technology, from the engine to fuel, is relatively cheap compared to high-end technology such as hydrogen fuel cells, which is critical for its expansion over the ship/vessel industry. However, it has to be noted that the NG engine has issues with hydrocarbon (HC) release, which needs to be addressed by unique control strategies.

Hydrogen Fuel Cell System

The hydrogen fuel cell (FC) is an advanced fuel converter with “zero tailpipe emissions.” FC converts chemical energy into electric energy through electrochemical reactions. The most

recognized FC types are proton exchange membrane FC (PEMFC), solid oxide FC (SOFC), and melt carbonate FC. PEMFC is used in maritime and automobile industries for its low operating temperature, whereas SOFC is commonly used in marine propulsion applications on large ships (for example, cross-continental cargo ships). FC can reduce carbon emissions during operation with hydrogen as primary fuel and other high hydrogen content fuel as secondary fuels or hydrogen carriers. At present, most PEMFC modules remain at the kW level. Multiple modules are required to fulfill the high power demands of ships at a high cost. SOFC and MCFC, on average, have larger power output, but the system start time is an issue due to the high operating temperature. Meanwhile, FCs produce electricity through electrochemical reactions, which require time to reach steady-state and output consistent electricity. Such characteristic makes FC unsuitable for handling the transient load.

Hydrogen has the highest energy content and no carbon content, which is an ideal fuel for any purpose [45]. However, H_2 is naturally rare in the atmosphere and cannot be directly harvested. At the current stage, most of the H_2 supplies on the market are from the industry by-products. To mass produce the hydrogen fuel, the most adopted methods are natural gas reforming [7] and electrolysis [46]–[48]. However, both ways introduce a large amount of pollution, which violates the purpose of using H_2 as a clean fuel. Moreover, H_2 has low fuel volumetric density and the storage is a major issue. H_2 is often stored under high pressure at 350 or 700 bar or liquified form [45][49]. It can also be stored in other chemical and physical means such as metal compound hydrides. However, the volumetric density of hydrogen is still incompatible to fossil fuel even under compressed or compound form [14][48][49].

Due to the illustrated issue of transient load, peak power constraints, and hydrogen volumetric density, the standalone FC system is more feasible for smaller-scale vessels. FC provides both propulsion and onboard electricity loads [7]. For large ship propulsion systems, additional battery packs are installed to form a hybrid propulsion system [7][18][51].

Energy Storage System (ESS)

Typically, the battery is the most commonly used energy storage system in the hybrid electric propulsion system. Other common storage or sources include super/ultracapacitor and hybrid ESS. The less commonly used method includes pneumatic, hydraulic, and flywheels.

Battery

The battery is the most commonly used ESS for the transportation industry and is arguably the most critical component in state-of-the-art hybrid or pure electric applications. From the traditional lead-acid batteries to the more advanced nickel-based batteries (Ni-Fe, Ni-Zn, Ni-Cd, and Ni-MH) and lithium (ion and polymer) batteries, the battery technology has been largely researched and still has great space for advancement.

Battery technology is a broad topic of discussion which involves the electrochemical area. However, when mentioning the hybrid system's application, the major points of interest are cost, capacity, and lifespan. The battery's cost is responsible for up to 40 percent of the total cost of a HEPS [37][59], and the number can increase for maritime propulsion applications, especially when the rated power is much higher. The main benefit of the battery is the large energy density for energy storage. However, with a massive amount of energy stored, the battery suffers from a low charge/discharge rate. Ideally, the hybrid architecture should have a

plug-in ability to recharge the ESS from the grid since the cost of grid electricity is lower and cleaner than onboard generation using fuel. However, for ships with large battery capacity (long recharge time) or vessels under frequent operation (lack of time between each mission for recharge), the battery cannot be charged regularly for the best operational performance. Some applications feature battery swap when docked. This method allows battery charge through the grid without a ship in place.

Quick charge, on the other hand, can help with the situation; however, charging efficiency, battery temperature control, and grid power supply are well-recognized issues but not detailedly reviewed here. The most critical and relevant topic is battery degradation. It is worth noting that battery degradation occurs naturally as the battery is used. Quick charge is a factor that accelerates battery degradation but not the sole reason for it. Degradation is critical to assess since it directly reflects the hybrid system's cost if the battery needs to be replaced frequently due to degradation. Therefore, various researches have been done on battery degradation, including modelling, life prediction, and degradation mitigations [51]–[61].

Super/ultra-capacitor

While batteries store electric energy in a chemical form, a capacitor stores energy in a “physical” form that can be released and recharged quickly. Such property makes the capacitor a strong ESS candidate for buses where the capacitors can be instantaneously charged during a stop. For marine applications, technology can be transferred to small ships such as water taxi where the mission cycle is short. Although the capacitors can be charged or release their charge in a short period, the capacity is much lower than batteries’ capacity since the electrical charge is simply held in between conductive plates [62]. With no energy form conversion, the supercapacitors do not significantly suffer from degradation. The capacitors’ quick charge and discharge character is commonly used in some heavy-duty applications or the starting phase of a mission where a peak load is experienced.

Others

A few alternative energy storage methods are available, including pneumatic, hydraulic, and flywheel; however, the real applications of these three techniques on ships are limited. The flywheel converts energy into a mechanical form to store in the form of a rotating wheel. But the energy in/output is in the form of electricity through a motor or generator. Pneumatic and hydraulic storage methods are very similar, where the pneumatic system stores energy using compressed air, and the hydraulic system uses liquid.

Hybrid Energy Storage System (HESS)

Hybrid ESS combines multiple ESSs to enhance the performance of energy storage. The most commonly used hybrid ESS is the battery/capacitor hybrid system. As illustrated, the battery suffers from low power density but features in high energy density, whereas the capacitor has the opposite properties. The combination of two devices allows larger energy density and sufficient power density for different applications. However, the control strategy for hybrid ESS is more complicated; an advanced control strategy or specially designed circuits are needed to prevent internal charge transfer between multiple storage devices [63]–[65]. Meanwhile, the balance of system equipment such as DC/DC converter is required to regulate the voltage and current.

Electric Machines

Brushed/Brushless DC Motor

The DC motor is one of the most commonly used motors for propulsion applications. Featuring a high torque at low speed, the DC motor is excellent for start-up and power assistance at lower speed range. DC motors are generally cheap to build, with permanent magnets or wire winding as the core, DC motors are mature and robust [32][66]. Depending on the applications, the brushed DC motor can be used to reduce the maintenance requirements. However, with low power density, it is typically used for light-duty applications. Meanwhile, a low level of efficiency is also limiting the use of DC motors. DC motors perform well for hybrid or pure electric applications since devices such as battery and FC output DC. With DC generators and DC bus, the energy conversion losses can be vastly reduced.

Induction Motor

As the most developed AC motor, the induction motor is inexpensive but still robust and reliable. Induction motor is widely used worldwide and has been well regulated by different standards. Featuring excellent speed control through vector control or other methods, the induction motor is a great candidate for HEPS applications. Meanwhile, the induction motor is easy to construct and is almost maintenance-free. However, at high speed, the motor efficiency drops as losses increases. Meanwhile, in the constant power region, there is a break-down torque [32][66]. Comparing to the permanent magnet motor, the loss of the induction motor is higher due to the rotor winding.

Synchronous Motor

For synchronous motor, the rotor spins at synchronous speed without influences from the load [32][66]. Synchronous motor is also known as AC brushless motor since its stator is excited by a 3-phase AC supply. Depending on the rotor's excitation method, there are the permanent magnet synchronous motor and the DC excited synchronous motor. For a non-self-excited synchronous motor, to excite the rotor winding, DC needs to be run through the winding to create a magnetic field. However, the excitation current is responsible for half of the motor loss in the form of heat loss [32][66]. Therefore, the permanent magnet synchronous motor has higher efficiency. However, a significant amount of heat can be generated during motor operation, and the permanent magnet can be demagnetized.

Electric Power Grid

The AC bus is the most commonly used grid for ship applications. Since modern ship design consists of diesel generators as primary or backup hotel load suppliers, AC alternators and AC buses have been widely adopted in the marine vessel industry. Using high voltage, the AC bus minimizes the transfer losses through wires. Meanwhile, AC technology is nearly mature, and the AC system's cost is low with high capability. The major drawback of the AC system is that when generating electricity, the alternator needs to operate at a fixed speed to match the phase of the electrical loads connected to the bus. This may put the ICE in a less efficient operation zone resulting in higher fuel consumption and emissions. The other drawback is the potential conversion losses due to the balance-of-system equipment such as AC/DC converter.

Besides the AC bus, DC buses are experiencing a rising trend, especially for cruise ships and some special-task ships [67][68]. The DC bus is not a new technology; however, applications

of the DC bus has challenges. An outstanding one is that most of the equipment is built for the AC system, customized equipment that adopts DC can introduce high initial costs during shipbuilding. Meanwhile, alternatives such as using additional converters induce energy losses, which reduce efficiency and increase fuel consumption. In terms of advantages, the major benefit of the DC bus is that, without electricity phase constraint, the DC architecture allows variable ICE speed based on the load situation, leading to reduced fuel consumption since the operating points can be controlled. This is favourable for ships that require a large amount of hotel load so that engines do not experience a fixed operating point for frequency requirements. Meanwhile, since ESS often outputs DC, a DC bus has a natural advantage for hybrid or pure electric systems, which can further reduce losses and boost efficiency. Moreover, a DC bus gathers more attention for naval applications since DC power can generate pulse output for weapons and a remarkable resilience ability [18][68].

2.2.3 Technology Trend

It is generally recognized that HEPS is an intermedia solution for clean transportation propulsion and decarbonization since it reduces carbon emissions but does not eliminate them. However, with the advancement of balance-of-system components, the hybrid system can grow significantly parallel with the pure electric drive.

With the aforementioned FC technology in the marine application, FC hybrid could be the next step of a hybrid solution. With industrial collaborations, many projects and proof-of-concept designs and simulations have demonstrated the potential of such clean transportation technology. On the one hand, considering the hydrogen fuel or hydrogen carrier's energy density, the fuel cell hybrid system (FCHS) has better rangeability compared to the battery-electric system. Accordingly, with battery enhancing the design, FCHS can handle transient loads better than other standalone systems. However, the major concerns are related to FC manufacture, hydrogen production, and other balance-of-system components. Meanwhile, establishing the FC degradation mechanism, life prediction model, and life-prolong methods are essential for FC to be used in the propulsion system, especially for marine applications where the mission cycle varies greatly. Only when all corresponding technologies are well adopted and become cheap, FC application in the marine industry will show its full potential.

The next vital technology to be advanced is the battery. Since the beginning of battery electric propulsion, the advancement of battery technology has never stopped, yet the results have not fulfilled the rising demand completely. Several issues, including capacity, charging, footprint, and cost, are still in the way to implement battery-electric systems on ship propulsion. This is the primary reason for using hybrid technology. The central focus of battery technology involves increasing capacity and reducing cost and size. Meanwhile, similar to FC, degradation is also a major topic of discussion for the battery. Battery degradation models and mitigation methods are required for advanced marine propulsion applications considering the long travel distance and variant load conditions. The hybrid ESS system can be improved as well to boost efficiency and reduce battery degradation.

On top of the mentioned improvement, any afore-reviewed systems or components can be improved to achieve better HEPS performance. Different areas such as

- Onboard clean energy generation
- Efficient energy conversion and storage
- Quick charging
- Clean fuel production
- Power control and energy management

are worth investigating as future technology trends.

2.3. Hybrid Electric System Control

Control is arguably the most critical area in HEPS. Depending on the application, the main control objective varies; however, the most common goals are to reduce fuel usage/emissions level and increase overall system efficiency, as these are the main reasons for developing the HEPS [69]–[72]. The HEPS control is commonly regarded as a two-level system: upper-level supervisory control and lower-level components control. Due to the existence of multiple energy sources, the power control of each element and the energy management between sources can directly influence the performance of HEPSs, which is decided by the upper supervisory control scheme. The lower-level is responsible for components functionality, such as when the motor controller drives the motor based on the upper level's command. The lower level control is essential for HEPS to function correctly; however, such control strategies, such as PID commonly used for motor control, have no significant effects on overall energy management; hence it is not in the scope of this review.

The upper-level energy management system (EMS) is responsible for managing each component's energy flows and power generation/consumption. The EMS is divided into two major categories shown in Figure 5: rules-based control and optimization-based control. This section below reviews the control strategy commonly used for propulsion system control [31][32].

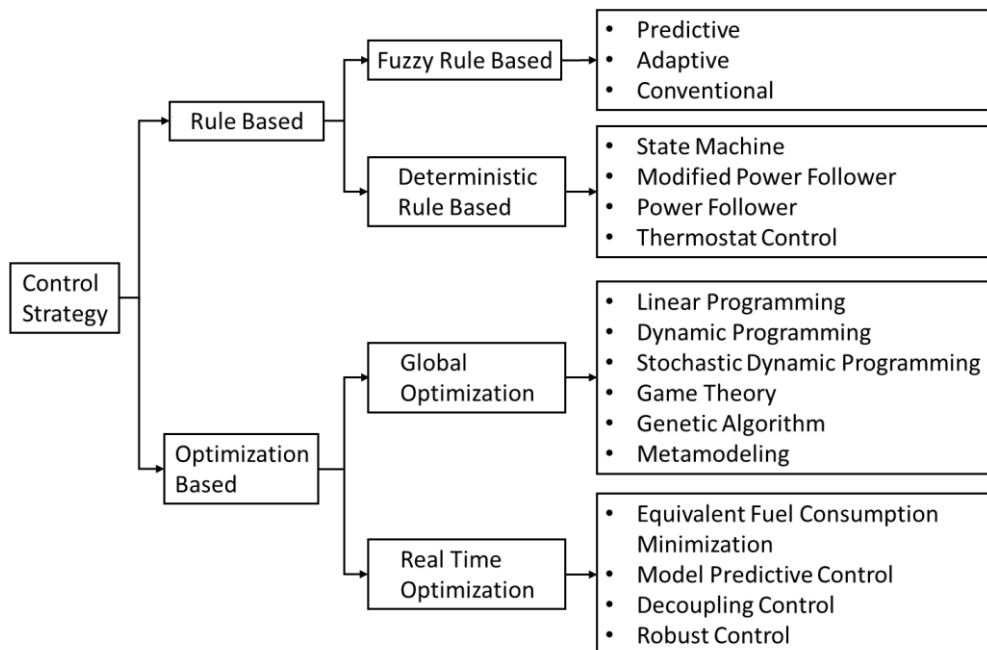


Figure 5: Summary of available control strategies [31]

2.3.1 Rule-Based Control

Rule-based control is one of the most basic control strategies. Typically, a set of rules are constructed for different stages or modes of the operation processes. The rules are developed based on heuristic, common sense, human experience, or even optimization results. It is noted that the optimization-based rule is developed through optimization algorithms; however, the main control scheme is laid out as rule-based; hence, such a method is still regarded as rule-based control. Rule-based control action can be simply understood as a set of “if-then”; that is, if a group of conditions are met, a specific action will be executed [31]. The rule-based control can be categorized into two major parts: deterministic rule and fuzzy rule-based.

Deterministic Rule-Based

By its name, deterministic rule-based control has a set of fixed rules. The rules can be developed from the aforementioned methods (stochastic, etc.). The state machine is one of the most commonly-recognized examples of such a strategy. The power follower strategy is also a commonly used method that allows the engine generator to follow the power demand and the battery's available power. Similarly, the thermostat strategy is another well-recognized method in this family. Deterministic rule-based control is easy to implement and can achieve quality results on the fly. Thus, complex control schemes obtained through optimization are often rewritten into rules for simple implementation and real-time operation [31].

Fuzzy Rule-Based

Fuzzy rule-based control is considered as an extension to the conventional deterministic rule. Instead of using hard go/nogo conditions, the fuzzy logic is embedded to increase the condition's tolerance, hence increasing the robustness of the control system. Fuzzy logic can be easily tuned, which enables the wide adoption of the fuzzy rule-based strategy. On the other hand, looking at the nature of the HEPS powertrain, the plant is multidomain, nonlinear, and time-varying. The decision-making strategy of fuzzy logic is a better suit for HEPS control applications than the deterministic rule [31].

2.3.2 Optimization-Based Control

Optimization-based control uses optimization algorithms to maximize system efficiency and minimize energy losses [73]. Optimization-based control performs well since different algorithms can be applied to extract the best performance point based on other optimization objectives and constraints. Especially for a predefined or fix driving cycle, with final drive rotational speed or torque information available, various global optimization methods can be used to find the corresponding optimal control that suits the driving conditions. However, optimization processes generally take a long time to compute; thus, online implementation is not feasible. Therefore, optimization can be used for generating optimal rules for the aforementioned rule-based control. For on fly application of the optimization-based control method, different equivalent methods are used instead.

Global Optimization

Global optimization is a well-recognized tool in different fields. For HEPS control purposes, global optimization is often used when the driving cycle is defined. With the entire domain's information, algorithms such as sequential quadratic programming, genetic algorithm, and

metamodelling methods can accurately identify the optimal solution for the best possible control performance. However, with bounds and constraints, the obtained results can be limited. On the other hand, dynamic programming searches for all possible solutions and has been proven to be one of the best methods for optimization-based control. As mentioned, global optimization methods have a drawback on computational time. Control actions are generally applied on a fraction of a second basis. Therefore, global optimization-based control is often computed offline and implemented onto a fixed mission cycle.

Online or Real-Time Optimal Control

In comparison, real-time control optimization requires decision making on the fly. The conventional global optimization method is not feasible for this application due to the intensive and time-consuming numerical computation. Therefore, different model predictive control (MPC) and equivalent consumption minimization strategy (ECMS) are commonly used.

2.4. Lifecycle Assessment

HEPS has great potential for reducing fuel consumption and improving system efficiency; however, whether the hybrid system can achieve its goal has been significantly debated. This concern arises because although the HEPS's regular operating cost is less than the conventional system, the HEPS's upper and lower stream costs are potentially higher instead. Meanwhile, as the system's key component, ESS induces a tremendous amount of pollution during the manufacturing stage. Different strategies need to be compared to a lifecycle point of view to identify potential issues.

For a HEPS, one primary driver of the lifecycle cost is the battery. It is well recognized that the battery suffers from degradation, which needs to be replaced periodically if not adequately controlled and used. Although most manufacturers claim that the battery pack in HEPS can last for a lifetime, most manufacturers limit their battery warranty to seven or eight years [74]. Life cycle assessment converts the inflow and outflow of a product into a quantitative, measurable value for comparison, which unveils its actual advantages and disadvantages.

Lifecycle analysis (LCA) and/or lifecycle cost assessment (LCCA) have been widely applied to different fields. Especially the automotive, where hybrid technology plays an important role, numerous studies (Ref. [33][34][75]–[87]) have presented LCAs and LCCAs to evaluate the performance of various hybrid systems in comparison to battery electric, FC electric, and the conventional systems. Those studies prove the necessity of the LCA on drivetrain designs and analyses. Although more studies have been done on the ground vehicle, the fundamental reason and the general approaches for doing LCA remain the same for watercraft. LCA is essential for ship application since ships' building costs are usually high; a systematic analysis of ships' lifecycle is critical for decision-making. For the maritime industry, a significant amount of LCA studies have been conducted, as summarised below.

Manouchehrinia *et al.* [88] systematically assessed the lifecycle cost and GHG of implementing a hybrid electric and pure electric system to a lobster fishing boat. By simulating the system based on the real data collected from a fishing boat, the results suggested that both systems have great potential for reducing GHG; however, battery-electric has a high lifecycle cost comparing to HEPS.

Jeong, Wang, Oguz, and *et al.* did several studies involving LCA on hybrid ships. Wang *et al.* [89] analyzed the LCA of a short route hybrid ferry in ship maintenance. Oguz *et al.* [90] performed a hybrid architecture selection and component size optimization for a tugboat using the LCCA approach. Combining the results from two case studies, Jeong *et al.* [91] established a framework for performing LCA on the hybrid vessels. In combination, three works jointly emphasized LCA's importance during the comparison between the hybrid system and conventional or alternative systems. Results showed a 30-year lifespan is ideal for ship/vessel lifecycle analysis, and the studied hybrid electric ships have better cost-benefits over the proposed lifespan compared to conventional systems. Meanwhile, the LCA has massive impacts on the initial sizing of HEPS.

Ling-Chin and Roskilly detailedly compared the different propulsion systems to a conventional system using the LCA approach [92]. A detailed LCA study was then carried on a roll-on/roll-off cargo ship case study to investigate the system's cost efficiency and environmental impact [93]. The conclusion from the research suggested that LCA is essential for decision making when comparing different propulsion systems.

Blanco-Davis and Zhou [94] performed a study on the economic effects of selecting alternative retrofitting on hull using LCA as a primary tool. The study intended to show the advantages of using LCA in maritime applications.

There is no doubt that LCA or LCCA are complex processes to analyze. When considering cradle to grave, a significant number of parameters and factors need to be considered. However, most of the elements are either hard to measure or impossible to obtain due to confidentiality. Some models are susceptible to various parameters; different cost factors can affect the decision making significantly. Some commercial software is available on the market for LCA; however, the lifecycle analyses are still not universally done due to the complexity of the assessment. The aforementioned researches have proved the importance of LCA or LCCA.

Chapter 3. Ship Power Demand Prediction Using Modified Low-Order Hull Resistance and Propeller Thrust Models

Hybrid electric technology can potentially increase the marine propulsion system's fuel efficiency only if the system components are adequately sized and the system is optimally operated. Correct component sizes ensure sufficient power output and reduce waste from redundant overpowering (not referring to the reserved power for emergencies and only related to waste due to oversizing). For the propulsion system's custom or optimal design, the power demand profile of a ship needs to be provided.

The ship propulsion power profile contains three major parts: ship speed profile, ship hull resistance profile (also known as load profile), and ship propulsor thrust model. The ship speed profile depends on the mission cycle, which needs to be measured onboard or cross-referenced from similar ships. Ship resistance includes various modes. The exposed upper decks suffer from wind drag, which is widely studied by the automotive and aviation industry. The lower submerged hull experiences drag induced by water, involving viscous drag, current drag, and wave-induced force. Those combined water-induced drags contribute the majority of the ship resistance, for which a detailed prediction model is necessary for power profile prediction. The propeller thrust model measures the forces required to carry the shiploads under the desired speed profile. The ship's propulsion power demand can be estimated by combining all three models, and correct component sizes can be selected to design the propulsion system.

At the current stage, the hull resistance and propeller thrust are estimated through physical tests such as sea trial and towing tank methods or full-scale numerical methods such as full-scale CFD simulations. These methods have limitations on ship models and computational time, which cannot be well adapted for some design purposes. This chapter introduces a modified low-order model and calculation method for hull resistance estimation based on Holtrop and Mennen's hull resistance regression model and ship stability characteristics. Meanwhile, a Holtrop and Mennen's drag and vessel surging power deduced model using iterative propeller speed estimation model is proposed as a propeller thrust/performance model. The combined hull resistance and propeller thrust model is referred to as the modified low-order model (M-LOM) from this section.

3.1. Vessel Hull Resistance Model

3.1.1 Total Ship Resistance

Like the automobile and aviation industry, studying the vessel's resistance is critical for estimating the propulsion power demand. Different from the other two, ship resistance is more complicated due to the additional wave-making resistance. The *hull resistances* are mainly the wave/current-making pressure resistance and viscous surface drag. A small section of the hull that remains above the waterline will experience wind resistance as well. The primary source of the *wind resistance* comes from a marine vessel's upper decks, including air viscous drag and wind pressure-making resistance. Figure 6 summarizes the typical type of resistance

experienced by ships.

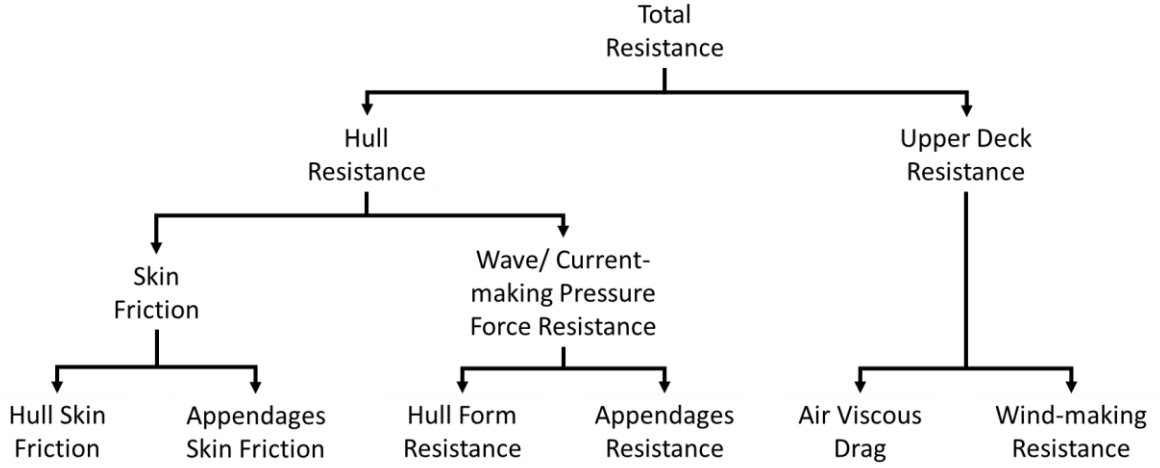


Figure 6: Types of resistance experienced by ships during sailing

Water-induced Hull Resistance

Hull resistance is the primary drag during vessel sailing. As shown in Figure 6, the water-induced hull resistances are mainly viscous friction and pressure resistance. A significant number of works have been done on the subject, and various resistance models are introduced. Since the M-LOM is built up based on the Holtrop and Mennen's regression method [95], this section outlines the basic theory of water-induced resistance using Holtrop and Mennen's regression method.

The hull skin friction can be calculated as:

$$R_f = 0.5\rho V^2 S C_f \quad (3.1)$$

where ρ is the fluid density, V is ship speed, S is the surface area, and C_f is the coefficient of frictional resistance established by ITTC 57 (International Towing Tank Conference) based on Reynolds number R_n :

$$C_f = \frac{0.075}{[(\log_{10} R_n) - 2]^2} \quad (3.2)$$

The equation is well established for the viscous friction of an object in fluids. However, considering the irregular shape a ship hull has, an additional hull form factor must be introduced to capture the extra surface area from the hull geometry. The factor k_1 can be calculated as

$$k_1 = c_{13} * [0.93 + c_{12} \left(\frac{B}{L_R}\right)^{0.92497} * (0.95 - C_p)^{-0.521448} * (1 - C_p + 0.0225 * lcb)^{0.6906}] \quad (3.3)$$

In the formula, lcb is the location of the longitudinal center of buoyancy measured from the ship center point, C_p is the prismatic coefficient, which is the ratio of block coefficient C_b , and the midship section coefficient C_m .

$$C_P = \frac{C_b}{C_m} = \frac{V_d/(L * B * T)}{A_{mid}/(B * T)} \quad (3.4)$$

L_R is the parameter that reflects the length of run

$$\frac{L_R}{L} = 1 - C_P + \frac{0.06C_P lcb}{4C_P - 1} \quad (3.5)$$

The required coefficients are typical ship geometric data where V_d is the vessel moulded displacement volume, L is the length of the ship at the waterline, B is moulded breadth, and T is the average moulded draft. It is noted that the numbered coefficients introduced here and in the following section are detailed in the Appendix.

The appendages friction is similar to equation (3.1) with S representing appendages surface area and corresponding k_2 coefficient. Appendages typically involve rudder, shaft brackets, skeg, bossings, shafts, dome, bilge keel, and stabilizer fins.

For ships with bow thrusters, the bow thruster tunnel also contributes to additional resistance as an appendage. The resistance can be calculated as:

$$R_{bow} = \rho V^2 \pi d^2 C_{BTO} \quad (3.6)$$

where d is the tunnel diameter and C_{BTO} is a coefficient ranging from 0.003 to 0.012.

The pressure making resistance is the more complex subcomponent of the overall ship resistance. The hull pressure resistance includes wave-making/breaking resistance R_W , the pressure resistance of bulbous bow R_B , and pressure resistance of immersed transom stern R_{TR} . The sum of these resistances is described in Froude's hypothesis and known as residuary resistance. Proposed by Froude, the previously mentioned frictional resistance is a function of Reynolds number, whereas the residuary resistance only depends on corresponding speed, which is known as Froude number F_r [96]. Researchers continuously develop Froude's method over the past decades, and a leading method is from ITTC. Referred to as residuary resistance (ITTC 57/87) or wave resistance (ITTC 2017), the resistance is obtained by wave resistance coefficient:

$$C_w = C_{TM} - (1 + k)C_{FM} \quad (3.7)$$

where the k and C_{FM} is the aforementioned hull form factor and frictional force coefficient and C_{TM} is the total resistance coefficient. Such a method relies on the towing tank method, which is well regulated by ITTC; however, when the scaled test cannot be performed, the illustrated Holtrop and Mennen method can provide a direct empirical regression method:

$$R_W = c_1 c_2 c_5 \nabla \rho g \exp[m_1 F_n^d + m_4 \cos(\lambda F_n^{-2})] \quad (3.8)$$

$$R_B = \frac{0.11 \exp(-3P_B^{-2}) F_{ni}^3 A_{BT}^{1.5} \rho_w g}{1 + F_{ni}^2} \quad (3.9)$$

$$R_{TR} = 0.5 \rho_w V^2 A_{IT} c_6 \quad (3.10)$$

where

$$\lambda = \begin{cases} 1.446C_p - 0.03L/B & \text{if } L/B < 12 \\ 1.446C_p - 0.36 & \text{if } L/B > 12 \end{cases} \quad (3.11)$$

$$P_B = \frac{0.56\sqrt{A_{BT}}}{T_F - 1.5h_B} \quad (3.12)$$

$$F_{ni} = \frac{V}{\sqrt{g(T_F - h_B - 0.25\sqrt{A_{BT}}) + 0.15V^2}} \quad (3.13)$$

In the equations, F_n is the Froude number, A_{BT} is the area of transverse bulbous, ∇ is ship displacement, and A_{IT} is the area of immersed transverse area of transom.

To describe the effect of ship hull roughness and resistance in still air, the model-ship resistance can be calculated as

$$R_A = 0.5\rho V^2 S C_A \quad (3.14)$$

where the correction coefficient is

$$C_A = 0.006(L + 100)^{-0.16} - 0.00205 + 0.003 \sqrt{\frac{L}{7.5}} C_B^4 c_2 (0.04 - c_4) \quad (3.15)$$

Wind-induced Upper Decks Resistance

The wind resistance is calculated based on the model established by Journée and Massie [97]. The wind has two effects on the ship during sailing. The direct impact is the wind resistance induced by the pressure acting on the projected area. The alternative effect is the wind-induced wave causing hull resistance. The wind-induced wave resistance follows the analogy made in the previous section. This section only calculates the direct wind resistance experienced by the ship.

The wind resistance is relevant to wind speed. However, when detailed wind data is unavailable or not yet determined, a simplification using the Beaufort wind scale can be used to estimate the wind speed. The Beaufort wind force scale calculates the wind speeds based on the Beaufort scale, and an empirical equation written as:

$$v_{wind} = 0.836B^{1.5} \text{ (m/s)} \quad (3.16)$$

where B is the Beaufort scale number. However, the equation calculates the wind speed at 10 meters above the sea level, which needs to be converted to the ship level. The equation that can be used is

$$\frac{v_z}{v_{10m}} = \left(\frac{z}{10}\right)^{0.11} \quad (3.17)$$

where the z value is typically the height of the vertical ship center of gravity above the waterline.

Then, the transverse and longitudinal wind resistance is calculated as

$$X_{wind} = 0.5\rho_{air} V_{rw}^2 C_{Xwind} A_T \quad (3.18)$$

$$Y_{wind} = 0.5\rho_{air}V_{rw}^2C_{Ywind}A_L \quad (3.19)$$

where V_{rw} is the relative wind speed, $C_{X,Ywind}$ is the wind load coefficient, which is a function of wind angle α , $A_{T,L}$ is the transverse and longitudinal projected wind area.

The relative wind speed is calculated as

$$V_{rw} = \sqrt{V_s^2 + V_{tw}^2 + 2V_sV_{tw}} \quad (3.20)$$

where V_{tw} is the true wind speed and V_s is the ship's sailing speed. The relative wind angle is shown as

$$\alpha_{rw} = \arctan\left(\frac{V_{tw} \sin \alpha_{tw}}{V_s + V_{tw} \cos \alpha_{tw}}\right) \quad (3.21)$$

with α_{tw} representing the true wind angle.

The formally mentioned C_{XYwind} is the function of the wind angle, which is calculated as

$$C_{Xwind} = A_0 + A_1 \frac{2A_L}{L_{oa}^2} + A_2 \frac{2A_T}{B^2} + A_3 \frac{L_{oa}}{B} + A_4 \frac{S}{L_{oa}} + A_5 \frac{C}{L_{oa}} + A_6 M \quad (3.22)$$

$$C_{Ywind} = B_0 + B_1 \frac{2A_L}{L_{oa}^2} + B_2 \frac{2A_T}{B^2} + B_3 \frac{L_{oa}}{B} + B_4 \frac{S}{L_{oa}} + B_5 \frac{C}{L_{oa}} + B_6 \frac{A_{SS}}{A_L} \quad (3.23)$$

where A_L is the lateral projected area, B is the beam at the waterline, and L_{oa} is the overall ship length, and A_S is the lateral projected area of the superstructure. Coefficients A and B are tabulated in Appendix B.

3.1.2 Hull Resistance Models and Calculation Methods

The hull resistance is widely studied as it is a critical parameter to be measured during ship design. Various hull resistance models are established and can be largely categorized into three tiers. Based on the level of fidelity, the three tiers are full-scale models, reduced-order models, and low-order models. The full-scale model involves full-scale CFDs and sea trials. The reduced-order model scales and simplifies the full-scale model to reduce the computation time with a consequence of a lower level of fidelity. The low-order models are largely based on theories and equations illustrated previously. The Holtrop and Mennen's regression model is a well-known low-order model, which serves as the foundation of the proposed M-LOM. Figure 7 compares the typical hull resistance estimation model in terms of the level of fidelity and computation intensity. Based on the applications, each method has benefits and disadvantages. For example, for industry use, sea trial, towing tank methods, or full-scale CFD are costly or not feasible to perform and are normally avoided or done at the end of the design phase. Some of the methods are briefly discussed below. Some disadvantages of the illustrated models are the motivation of proposing the M-LOM.

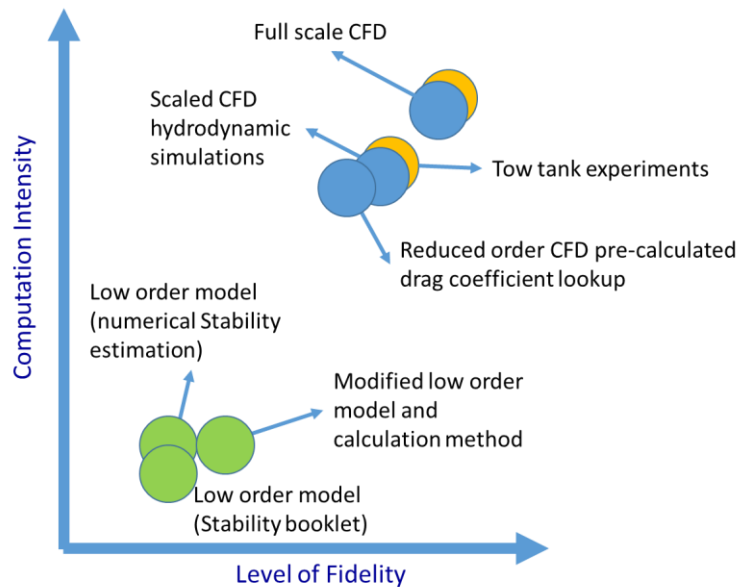


Figure 7: Typical hull resistance estimation methods

Hull Resistance Based on Vessel Sea Trial Data

For existing vessels, the directly measured operation data are arguably the most accurate reflection of the vessel's behaviour. Not only can the power demand be measured, but also a complete operation profile can be obtained. Such driving cycle data is valuable for the propulsion system and control strategy design. As an example, to understand the ship operation profile data of BC Ferries's M.V. Tachek, including ship speed, heading, wind speed, wind direction, shaft speed, shaft power, engine speed, rudder angle, GPS coordination, and electricity usage, are collected during ship operations with the assistances from BC Ferries as part of the M.A.Sc. research by Haijia Zhu [30] and the UVic research work supported by Transport Canada [29]. The project collected all information and data that affected ship propulsion, including main engine power and speed, and wind speed. Electric loads were also measured to investigate electrical energy consumption and power flow in the electric system. Ship operation data, such as rudder angle, propeller speed, and ship heading, were also collected.

The method, however, can only be applied to existing and operating marine vessels. For a new vessel under design, these data could not be obtained. For commercial ships, the acquisition of these data may involve a considerable amount of effort and disruptions to the normal operation of the vessel.

Towing Tank Hull Resistance Prediction Method

The towing tank method is a direct measuring method for hull resistance; however, done on a scaled model. Well regulated by the International ITTC, the towing tank method is an accurate way of measuring hull resistance [98][99]. Although the technique is regarded as accurate, the approach requires costly special facilities and operations.

Full-Scale CFD

A full-scale CFD simulation models and simulates the behaviours of the entire ship, or a portion of the hull, to numerically estimate the hull resistance [27]. Comparing to the real towing tank

method, CFD is more accessible for most of the research facilities, which can be performed at will at different stages of the design phase. However, the major drawback is the aforementioned intensive computational time using a dedicated CFD package. Considering a large scale ship model with detailed hull geometry in a large open water environment with additional current, wave, and wind, the full six degrees of freedom RANS can take weeks to solve. If several iterations are required, a Supercomputer, which is not always accessible to all, is often used.

Reduced-Order Hull Resistance Prediction Model

The reduced-order model (ROM) is an accurate non-physical model for hull resistance and power demand estimation at slightly reduced and acceptable fidelity. Kevin Andersen introduced the reduced-order hull resistance and propeller thrust prediction models in his M.A.Sc. thesis [29]. He used full-scale CFD simulations to obtain the drag coefficient and propeller thrust/torque lookup tables first. These CFD-formed metamodels are then used to support the compact ROMs within the integrated marine propulsion system model. The models can replace the conventional computation-intensive, full-scale CFD-based hydrodynamic hull resistance and propeller thrust simulations by carrying out the intensive CFD simulations ahead of time. In this approach, the hull and propeller coefficient matrices are obtained using the full-scale CFD simulations first. The compact and easy to calculate parameter based reduced-order models with the obtained hull and propeller coefficient matrices are then embedded into the integrated system model in MATLAB/Simulink codes. These parameter-based models can be executed quickly in Simulink with accurate results. The calculated results' verification showed resistance and propulsion force prediction errors at about 5 percent [29][30]. Comparing to the most conventional hull drag models, where only the forward direction is considered, the implemented reduced-order model considers 3 degrees of freedom. This method is favourable for analyzing the vessels' dynamic maneuvering, including turning and docking, where at least three degrees of freedom need to be used.

However, this approach still needs the full-scale CFD simulations to obtain the parameters of the reduced-order models for calculating the hull resistance and propeller thrust before these models can be used in the integrated marine propulsion system modelling in MATLAB/Simulink.

Low-Order Hull Resistance Prediction Model

The low-order model is primarily based on the theoretical equations, corresponding hull parameters and ship stability characteristics. An outstanding example of the low order model is Holtrop's and Mennen's hull resistance regression model, as illustrated. The model is adopted by Tiffany Jaster in her M.A.Sc. thesis [100], and the technique is integrated into a MATLAB based code by Rahimpour [101]. The low-order model is a simplified version of the computational model. Considering only one degree of freedom, the low-order model requires less time for computation and maintain acceptable accuracy for ship propulsion system design and control development. The required ship stability characteristic is listed in the Trim and Stability Booklet for any existing ships, which makes the model simple to using by parameters substitution and calculation. For ships under design where stability booklet is absent. Numerical methods can be used to obtain the ship stability data. The proposed modified low order model and calculation method in this work belong to the low order model.

Generic Parametric Mathematical Model Estimation Method

To avoid CFD modelling and full-scale or one-pass simulation, a method for generating representative load cycles for arbitrary monohull surface vessels from a generic, parametric mathematical model was introduced by Anthony Truelove in his M.A.Sc. thesis [102]. In this approach, assumptions are made that the hull shapes and the propeller of a vessel can be approximated using a surrogate model of the Wigley N43 hull geometry and a surrogate model of the Wageningen B-Series propeller geometry. The method takes a hull geometry and propeller placement, vessel loading condition, vessel mission, and weather data (wind, waves, currents) and, from that, generates the propeller states (torque, speed, power) and steering gear states (torque, speed, power) necessary to accomplish the given mission. Together with the steering gear states, the propeller states determine the load cycle corresponding to the given inputs (vessel, mission, weather). The method includes the use of a surge-sway-yaw model for vessel dynamics and the use of surrogate geometries for both the hull and propeller. The technique is modest on input requirements, fast in calculations, easy to generalize, reasonably accurate, and provides valuable insights on required propulsion power. However, due to the generic assumptions on hull and propeller geometry, this load cycle estimation method may have relatively large errors without fine tuning.

3.2. Vessel Propeller Efficiency and Thrust Model

3.2.1 Propeller Efficiency Model

After obtaining the hull resistance using the various resistance mode, the propeller thrust model needs to be carried out to estimate the ship's shaft power demand. Considering the fundamental physics, the product of the ship's speed and thrust force is the propulsion power. Additional forces for achieving specific mass acceleration needs to be considered as well. However, when propulsion power is delivered to the final drive, the power is partially lost due to the propeller efficiency. Hence, to capture the real shaft power, the propeller efficiency is a determining factor.

Propeller efficiency has been widely studied throughout decades, and a series of empirical equations have been established systematically. On the other hand, alternative solutions such as CFD simulations are widely accepted for their accuracy and visualization. This section introduces the basic theory used for the empirical calculation of propeller efficiency.

For the empirical equation [103]–[106], the propeller efficiency can be calculated based on the propeller thrust coefficient K_t , torque coefficient K_q , and advance ratio J as

$$\eta_o = \frac{J K_t}{2\pi K_q} \quad (3.24)$$

where K_t and K_q can be calculated based on the propeller geometry and rotation speed. Both coefficients are a function of advance ratio J , pitch diameter ratio $\frac{P}{D}$, the blade area ratio $\frac{A_E}{A_o}$, Reynolds number Re , the number of propeller blades Z , and the ratio of the maximum propeller blade thickness to the length of the cord at the characteristic radius $0.7R$. The advance ratio can be calculated as

$$J = \frac{V_A}{nD} \quad (3.25)$$

where V_A is the speed of advance, n is the shaft speed in rev/sec, and D is the propeller diameter.

Throughout the decades, the equations are widely used and tuned. Instead of calculating the efficiency each time, a series of diagrams are generated for easy access. Figure 8 shows the efficiency diagram of a typical propeller [103]. Based on the advance ratio and pitch to diameter ratio, the propeller's efficiency, torque coefficient, and thrust coefficient can be looked up.

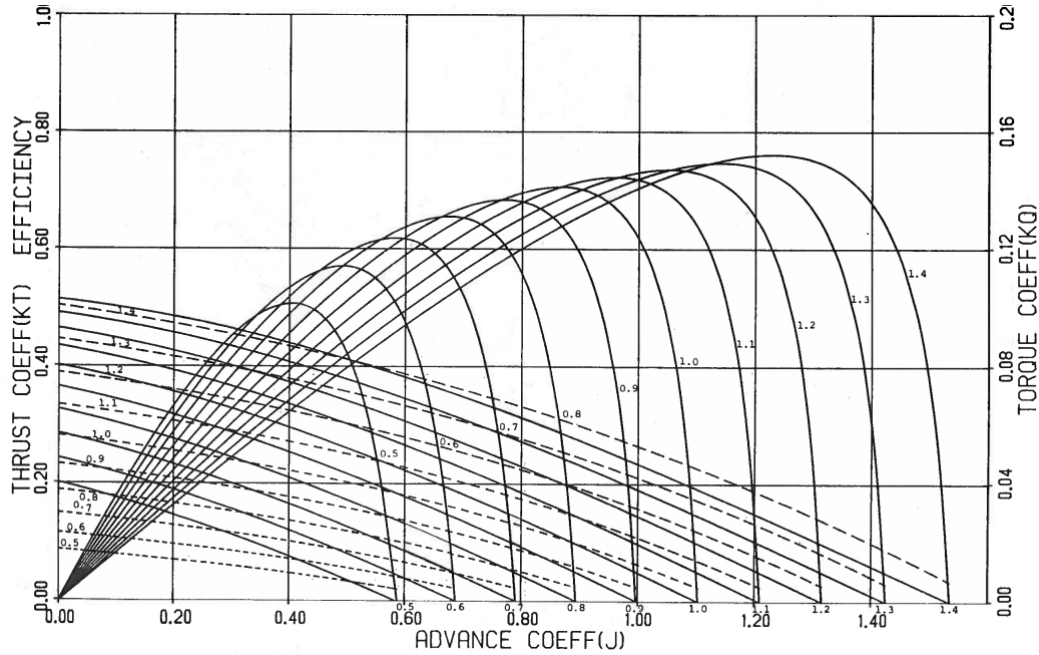


Figure 8: Efficiency diagram of Wageningen B-Series propeller with four blades $AE/AO = 0.45$ [103]. The reference numbers beside the curves are pitch to diameter ratio.

3.2.2 Propeller Thrust Calculation

Like the propeller efficiency, propeller thrust is also a critical value to be measured in the power prediction model since the thrust is the direct counter of the ship resistance representing the shaft output. The aforementioned propeller efficiency shown by the equation (3.25) is calculated based on the thrust coefficient K_T and torque coefficient K_q , which are also determining factors for the propeller thrust calculation. Equation (3.26) and (3.27) [103] demonstrate the relation between the propeller's thrust generation and the K_T value as well as the torque and the K_q .

$$K_T = \frac{T}{\rho n^2 D^4} \quad (3.26)$$

$$K_q = \frac{Q}{\rho n^2 D^5} \quad (3.27)$$

The K_T value can also be obtained from the efficiency diagram shown in Figure 8. It can be observed from the equation that the thrust is proportional to n^2 , which suggests that the thrust is sensitive to the rotational speed, and high rotational speed corresponding to larger thrust

generation. However, the situation only holds when the thrust is aligned with the sailing direction. To be discussed in detail in later sections, the current M-LOM considers only the sailing direction. Such a propeller thrust calculation method may induce large errors during the vessel's departing and approaching phase where the propeller may be angled for ship turning. Except for the empirical equation shown previously, propeller thrust can be obtained through CFD simulation as well. Section 3.4.2 shows the CFD simulation for extracting the propeller thrust and torque for efficiency calculation.

3.3. Modified Low-Order Model and Calculation Method (M-LOMCM)

3.3.1 Model Related Work

The *low-order ship resistance model and calculation method* is based on the regression approach that originated from the method published in 1982 by Holtrop and Mennen. The technique is developed through regression analysis based on the full-scale data from the Netherlands Ship Model Basin [95].

In Holtrop and Mennen's original work [95], the total hull resistance is subdivided into the following parts:

$$R_T = R_F(1 + K_1) + R_{APP} + R_W + R_B + R_{TR} + R_A \quad (3.28)$$

where, R_T is the total resistance, R_F is the friction resistance, $1 + K_1$ is the hull form factor, R_{APP} is the resistance of appendages force, R_W is the wave-making and wave-breaking resistance, R_B is the additional pressure resistance of a bulbous bow near the water surface, R_{TR} is the additional pressure resistance of immersed transom stern, and R_A is the model-ship correlation resistance.

Aiming at predicting the propulsion power of high-block ships with low length to beam ratio or slender naval ships, the method provides a series of empirical equations that can be implemented without significant modification.

The method was adopted as a part of the M.A.Sc. research by Jaster [100]. The method was detailedly reviewed in Jaster's thesis, and a Simulink model was built for the study on a coast guard ship (formerly known as the RV Tsekoa II) and performance evaluation. Then, the method was implemented in the MATLAB environment by Mostafa Rahimpour during the research of the Transport Canada Clean Transportation project [29]. The model was not fully established since the alternative reduced-order model was proposed; however, a series of CFD was performed for evaluation on the BCFS ship Skeena Queen and Klitsa.

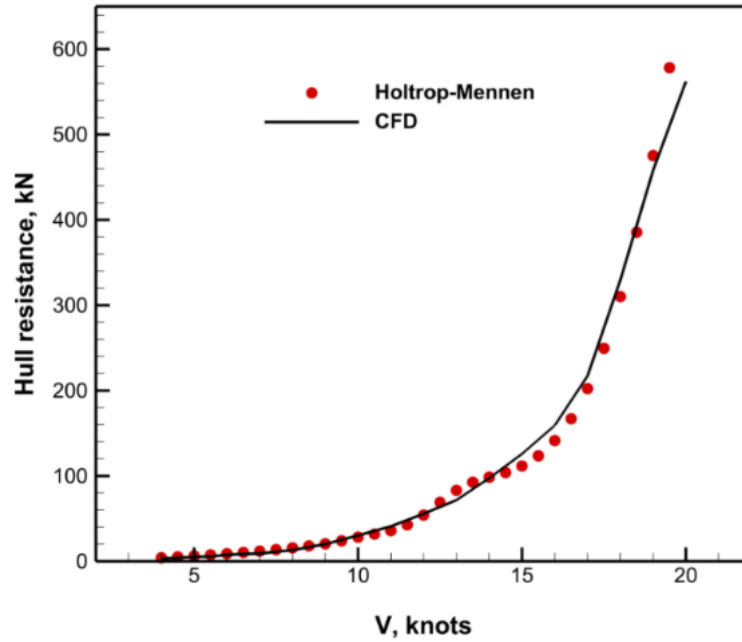


Figure 9: Comparison between the dedicated ship drag regression and numerical results [101]

In this study, a *modified low order hull resistance and calculation method* is proposed. The model is based on Holtrop and Mennen's (H&M) regression equation illustrated in section 3.1.1. There are three reasons for using H&M's method as the backbone of the modified model:

- a) Time-consuming and costly full-scale CFD, sea trial, and towing tank methods can be avoided when using H&M's method. The regression relationship is obtained through full-scale sea trial data, which by itself is a hydrodynamic model. When configured with the designated ship's parameters, the hull resistance can be predicted in a short period (in order of hours for the whole process). Although the level of fidelity is low compared to other methods, the results are critical and sufficient for industries to use at the early ship design phase.
- b) The method takes the ship's velocity, hull geometry data, and stability data as input, which are accessible at the early ship design phase. The required parameters can be captured through CAD models, one-pass pre-calculated CFD, and designed ship sailing conditions, which enhance the benefit of the method during its application at ships' design phase.
- c) As a calculation method, the model can be integrated as MATLAB functions or Simulink model. Such a characteristic is critical for integrated model-based system design and optimization. Since the control strategy is optimized during MBD, the power prediction model needs to be embedded in the system to determine the global optimized components' working conditions, power ratings (component size), and control schemes.

To extend the original H&M's method and increase the level of fidelity, the upper deck wind drag calculation is added to the model. Using the Beaufort wind scale method illustrated previously, the wind resistance can be estimated without sea trial data.

After the method is proposed, it needs to be constructed and tested using real ferry operation

data. The detailed model implementation is introduced in section 3.5, the remaining work in this section is to illustrate the procedures used for the ship's stability characteristic prediction using one-pass CFD.

3.3.2 Numerical Estimation of Stability Characteristics Using CFD

The benchmark ferry used for model developments and results validations is BC Ferry's Tachek, a roughly 50 meters long passenger/vehicle and cargo ship connecting Quadra Island and Cortes Island. The ship was built in 1969 with all documents, such as the stability booklet, available. The implementation includes CFD based stability data calculation, wind resistance model implementation, propeller efficiency model implementation, and results cross-validation. The Tachek voyage data used is collected by Zhu during his M.A.Sc. research work, as mentioned in [30]. The raw data is processed in Excel and imported into MATLAB as a discrete time table data type. The used data contains time, ship speed in knots, port shaft speed in RPM, port shaft torque in kN, starboard shaft speed in RPM, and starboard shaft torque in kN.

As aforementioned, the required stability data includes the center of buoyancy and draft, which are often listed in the vessel trim and stability booklet. When the booklet is missing or undetermined since no physical ship not yet available, such data needs to be calculated from the mathematical equation, measured from the CAD model, and computed from CFD simulation. To obtain this information, CAD models and loading conditions need to be available.

The processes for calculation the stability data include the following steps:

- a) Measure the location of the center of the gravity of the whole ship (require simple CAD modelling to create ship's upper deck geometry)
- b) Based on the weight distribution and loading condition, estimate the still water volume of displacement based on the conventional buoyancy force equation.
- c) Measure the hull volume corresponding to the water displacement to obtain the still water draft
- d) Based on the weight, CG location, and draft level, set up CFD for solving hydrostatic position and hydrodynamic response for stability data.

The first step is to estimate the ship's center of gravity since it is critical for hydrostatic position calculation. Among all three dimensions, the transverse and lateral CG position is more critical for the situation since it influences the center of buoyancy, which is a determining factor for the hydrostatic calculation. In order to estimate the CG position, the CAD model is constructed first. The hull model is created by Micheal Grant based on the geometric hull data provided by BC Ferries during the study for Transport Canada [29]. The upper decks are modelled based on the side views, section views, and floor plans provided by BCFS. The creation of the upper deck can also help with the surface area estimation during wind resistance calculation. The loading condition is assumed to be full load departure, which suggests the vehicle and passengers are fully loaded, and the fuel oil tanks and freshwater tanks are 98 percent full. Such a loading condition is for simulating the extreme situation where the maximum power demand may occur. The model is constructed using the NX platform, as shown in Figure 10.

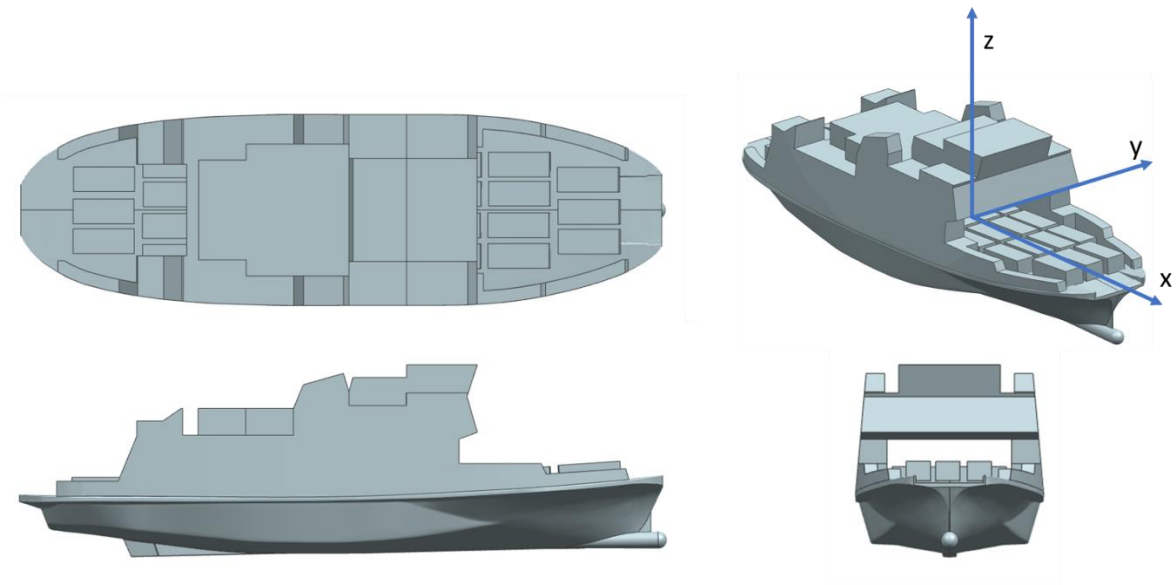


Figure 10: Rough CAD model for Tachek upper decks

The CG measurement shows the CG location to be (-361.4mm, -9.2mm, 5835.5mm) in x,y, and z from the center of the ship, whereas the stability booklet indicates the CG is at (-557.8mm, -2.1e-2mm, 5175.5mm). Comparing the results, a 35 percent error can be noticed for the longitudinal location of the CG. However, the absolute error is insignificant considering the length of the ship, the error can be ignored.

Measurement Mass Properties

Displayed Mass Property Values

Volume	=	3895470701615.094726563	mm ³
Area	=	4608729361.308423042	mm ²
Mass	=	27411261.388016358	kg
Weight	=	268812646.490790606	N
Radius of Gyration	=	11279.650624853	mm
Center of Mass	=	-361.426406553, -9.234571145, 5835.494526818	mm

Detailed Mass Properties

Analysis calculated using accuracy of 0.990000000

Density	=	0.000007037	kg/mm ³
Volume	=	3895470701615.094726563	mm ³
Area	=	4608729361.308423042	mm ²
Mass	=	27411261.388016358	kg
First Moments			
Mx, My, Mz	=	-9907153702.564004898	kg·mm, -253131243.462310016
			kg·mm, 159958265802.941528320
			kg
Center of Mass			
Xcbar, Ycbar, Zcbar	=	-361.426406553	mm, -9.234571145
			mm, 5835.494526818
			mm

Figure 11: NX CAD model measurement report

Under the loading condition, the total weight of the ship is 715388.5 kg. Therefore, the still water draft level can be roughly estimated using the conventional buoyancy equation:

$$F_f = \rho_{water} V_{displacement} g \quad (3.29)$$

Considering ocean water density to be 1024 kg/m^3 , the volumetric displacement of the ship

is 698.6 m^3 . After measuring the corresponding volume and height from the CAD model, the draft is obtained to be 2.495 m (8.185 ft), which is close to the given 2.515 m (8.25 ft) levelled water draft.

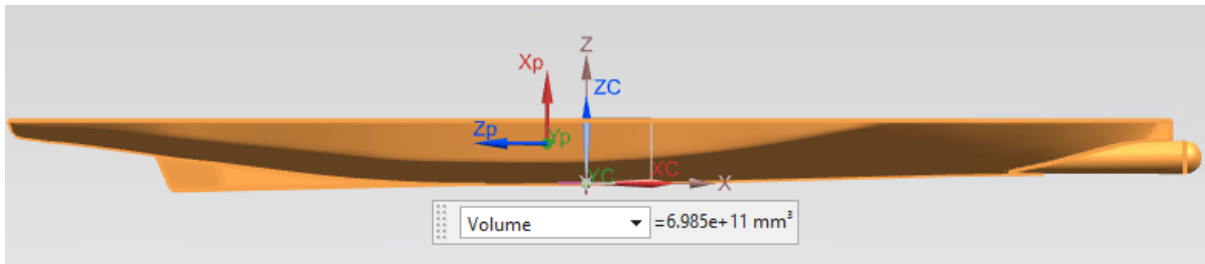


Figure 12: Measure the corresponding volume for determining draft

The calculated draft is then plugged into the Ansys Aqwa toolbox to evaluate the hydrostatic position and hydrodynamic response. The whole setup and results report is shown in Figure 13 and Figure 14. The result longitudinal center of buoyancy is -1.674 m, and the vertical CB is 1.589, whereas the given data is -1.703 m (5.59 ft) for longitudinal CB and 1.6 m (5.25 ft) for the vertical CB.

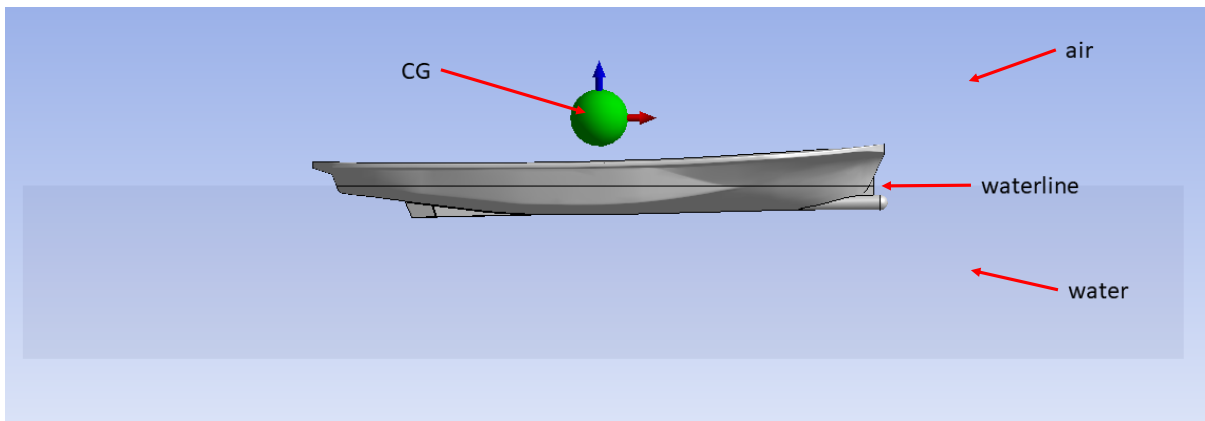


Figure 13: Ansys Aqwa hydrodynamic diffraction set up

Hydrostatic Results						
Structure	Hull					
Hydrostatic Stiffness						
Centre of Gravity (CoG) Position:	X:	-0.361 m	Y:	-9.2e-3 m	Z:	5.836 m
		Z	RX		RY	
Heave (Z):		4458189. N/m		715.08655 N/°		156826.72 N/°
Roll (RX):		40971.441 N.m/m		-681.36139 N.m/°		1425.9329 N.m/°
Pitch (RY):		8985509. N.m/m		1425.9329 N.m/°		8842121. N.m/°
Hydrostatic Displacement Properties						
Actual Volumetric Displacement:		694.35852 m³				
Equivalent Volumetric Displacement:		697.94 m³				
Centre of Buoyancy (CoB) Position:	X:	-1.6742766 m	Y:	7.6033e-5 m	Z:	-0.90591 m
Out of Balance Forces/Weight:	FX:	-8.986e-9	FY:	9.2984e-8	FZ:	-5.1308e-3
Out of Balance Moments/Weight:	MX:	9.2279e-3 m	MY:	1.3065403 m	MZ:	7.3028e-8 m

Figure 14: Ansys hydrostatic position results report

Except for the Ansys Aqwa toolbox, the conventional NX CFD solver, Ansys Fluent, and NX FloEFD are also tested for the CFD simulation. The following section briefly summarizes the tested packages.

Conventional NX CFD Package

NX built-in CFD is able to calculate the drag force of the hull; however, the calculations are for still water. Meanwhile, the conventional CFD cannot solve for the hydrostatic position of the ship hull. Therefore, the draft, center of buoyancy, and other stability data cannot be calculated. When performing the analysis, the draft has to be manually modelled. To evaluate the draft, a similar approach to the aforementioned method using in Ansys Aqwa is necessary. However, the center of buoyancy can not be assessed since no build-in feature is available.

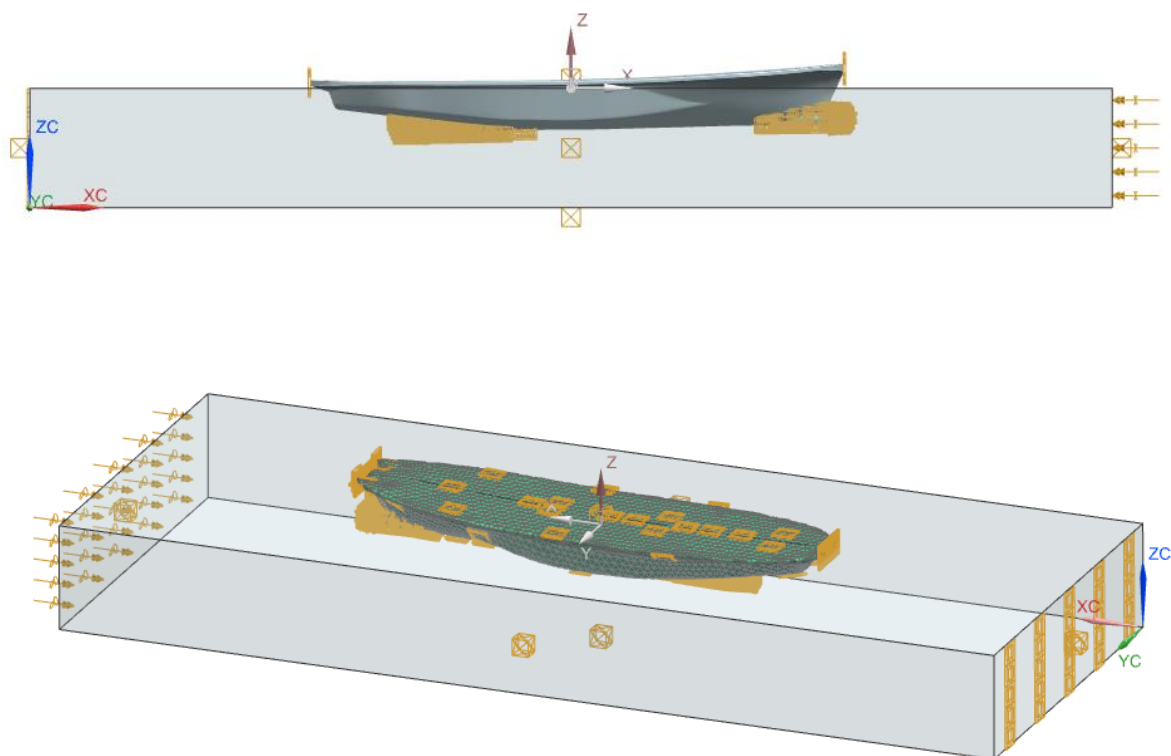


Figure 15: Conventional build-in NX CFD solver setup

FloEFD Toolbox for NX

FloEFD toolbox has more robust functionality than the conventional package. With the ability to define water and air condition, the program can generate a series of results, including surface drag, volumetric drag, and structural results. However, the program still cannot produce a hydrostatic position. Since UVIC does not have a toolbox license, a trial version was tested on a virtual desktop provided by the vendor. Since no file exchange can be made, a simple drafted model is tested instead of a hull model. With the free flow surface function (similar to SolidWorks wizard), the program is able to simulate ships in water conditions. However, due to the limited tutorial provided, a lot of the functions can not be performed. After testing,

FloEFD is stronger than the conventional CFD package; however, most of the functions do not aim for hydrostatic or hydrodynamic analysis of a floating body.

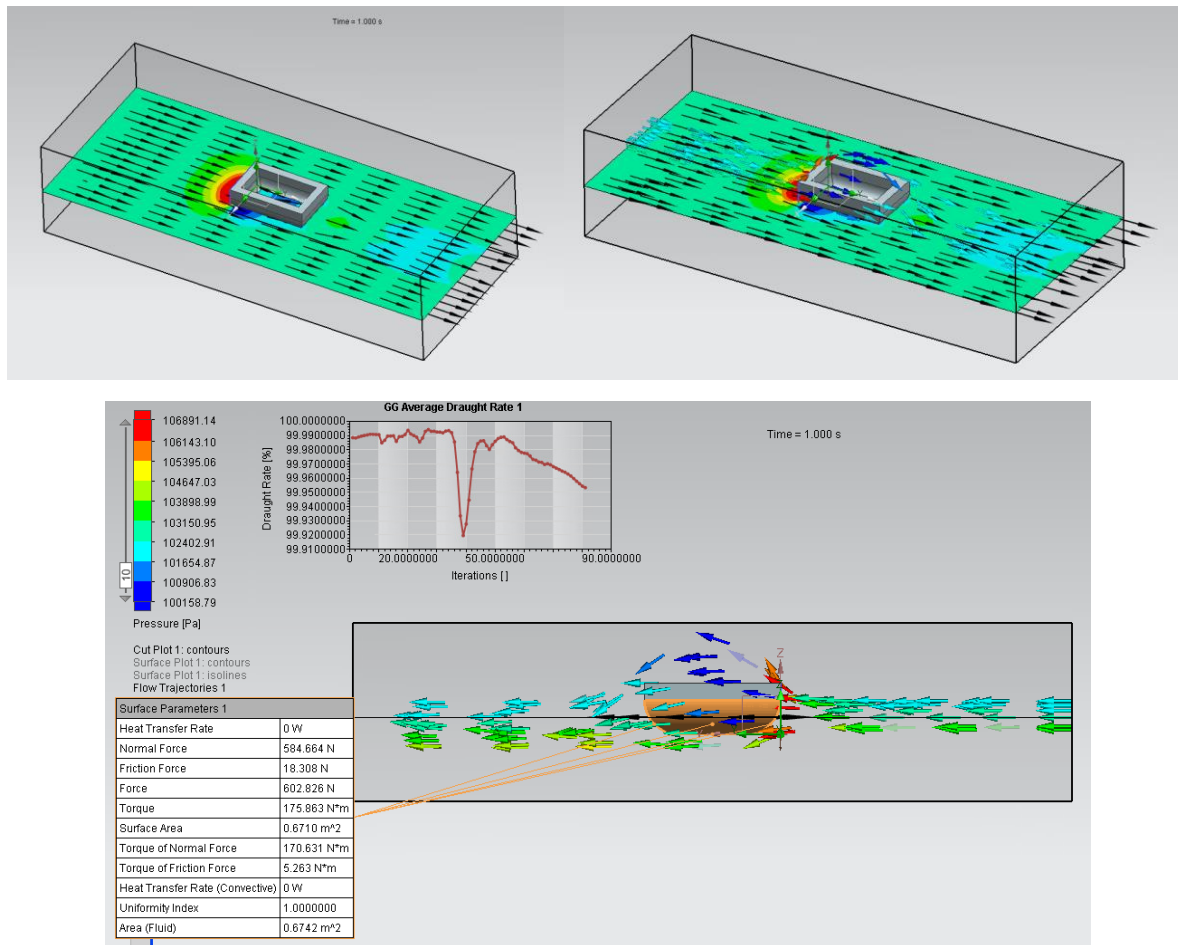


Figure 16: FloEFD NX version simulation setup and results

Ansys Aqwa

Ansys Aqwa is capable of solving the hydrostatic and hydrodynamic response of the hull. For a given draft, the program can calculate the center of buoyancy; however, the disadvantage is that the program requires a center of gravity value input. The program can evaluate the CG based on the geometric and material; however, with the absence of the upper-level components, the evaluated CG is for the hull. If used, the center of buoyancy cannot be accurately estimated. Explicitly designed for float object hydrodynamic analysis, Aqwa can evaluate the floating behaviours under the impacts of waves, currents, and winds. In addition, other stability data, such as the righting arm, can be calculated. However, when testing, it is found that Aqwa mainly calculates the passive response of an object under conditions such as waves. Ship speed cannot be defined, and the propeller cannot be set to rotate to see the propulsion force.

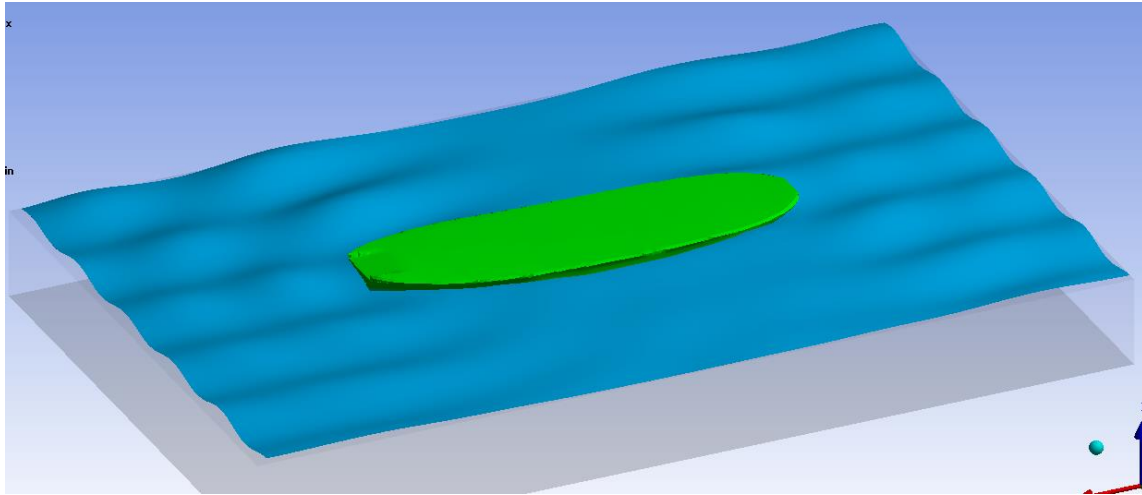


Figure 17: Ansys Aqwa simulation setup. The Ansys is able to implement the wave representation for solving the hydrodynamic model.

The major problem is that the system cannot calculate the draft. A test is performed by leaving the hull above the water surface and define the material properties and gravity. The purpose is to check if the program will reach the hydrostatic equilibrium, and thus draft can be evaluated; however, the program failed to assess the system and resulted in a 0 draft result. Therefore, the draft needs to be manually modelled prior to the hydrostatic simulation.

Ansys Fluent

Ansys Fluent is a well-developed and commonly used CFD package. Similarly, Fluent is able to calculate for the hull surface drag and other related fluids conditions; however, hydrostatic is still not obtainable using Fluent.

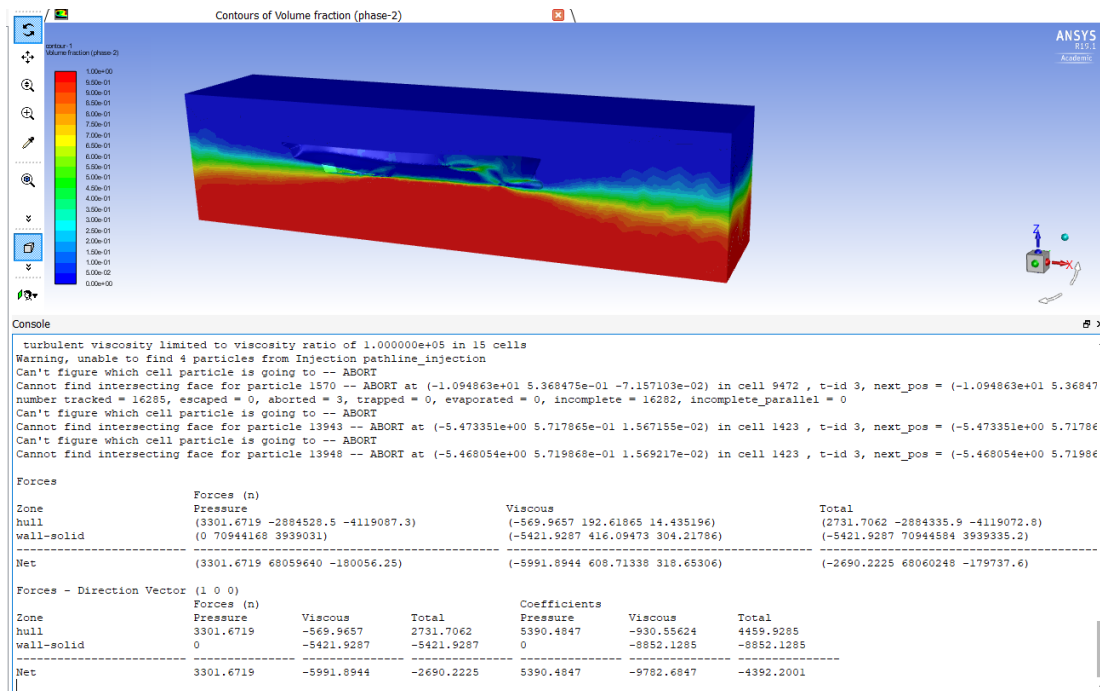


Figure 18: Ansys Fluent setup and results

3.4. Modified Low Order Propeller Thrust/Torque/Speed Model

After obtaining the vessel hull resistance, the ship's primary propulsion power can be estimated through the products of resistance force and velocity. However, the effective propulsion power (propulsion shaft power) is the more critical parameter to be measured for propulsion system design since its quantity directly affects the propulsion component's sizes. In order to get effective power, propulsor related data such as propeller's efficiency, operational coefficients, and torque/speed/thrust combination are necessary. This section illustrates a modified Holtrop and Mennen's drag based vessel surging power deduced model for predicting vessels' effective propulsion power utilizing the resistance characteristic and propeller related information.

3.4.1 Modified Holtrop and Mennen's Drag Based Surging Power Deduced Model

By its name, the proposed surging power deduced model is constructed based on the previously obtained vessel's resistance results using the modified H&M low order model and calculation method. Differ from the conventional propeller thrust models where the propeller thrust is calculated, the deduced model assumes that if the propeller produced thrust is known, the effective propulsion power can be calculated using the equation

$$\eta = \frac{\text{primary propulsion power}}{\text{effective propulsion power}} = \frac{\text{thrust} * \text{velocity}}{\text{torque} * \text{rotational speed}} \quad (3.30)$$

In order to use the equation to find the effective propulsion power, the propeller thrust and efficiency need to be calculated.

Instead of calculating the thrust from the propulsor, the method considers the Newton second law. The model assumes that considering only surge direction, the total amount of thrust needed for propulsion is equal to the sum of total resistance and mass acceleration. For the Tachek ferry, the acceleration can be obtained through the derivative of the velocity data. Combined with the assumed full-load departure loading condition, the mass acceleration can be predicted. The total ship resistance can be estimated using the previously introduced low order model and calculation method. Hence, the total thrust can be calculated. Once the propeller efficiency is obtained, the effective propulsion power can be deduced.

Several assumptions are made for such a deduced method:

- The thrust is assumed to have the same direction as the velocity, which is all in the surge direction. Under this assumption, the method only contains 1 DOF, which is the same as the modified low order model and calculation method. In consequence, the level of fidelity is low and the method belongs to the low order category.
- Since no maneuvering is not captured in the model, the thrust amount from each propeller is considered to share the total thrust equally.
- To achieve deceleration, thrust from the opposite direction is considered.

With the total amount of thrust estimated, the most critical process falls on propeller efficiency calculation.

3.4.2 Pre-calculated Propeller Efficiency

As reviewed in the previous section, propeller efficiency is governed by equation (3.24). For this study, three methods are tested and compared to find the best way to obtain the propeller efficiency.

Direct Efficiency Calculation

To directly calculate the propeller efficiency, equation (3.24) is added to the original LOM. The equation requires the torque and thrust coefficient, which are illustrated in the Appendix. An additional line of code is used to calculate the advance ratio. The pseudo-code reads as:

```
1  for each discrete vessel speed data
2      Set propeller diameter to 1.83 m
3      Calculate discrete ship wake fraction
4      Calculate discrete ship advance speed
5      Calculate the discrete advance ratio based on shaft rotational speed
6      Calculate torque and thrust coefficient
7      Calculate propeller efficiency based on thrust and torque coefficient and advance
      ratio
8      If efficiency > 1 || efficiency < 0
9          Correct the efficiency to 0
10     end
11 end
```

The calculation is done in matrix form since both port and starboard efficiencies are considered. The method requires actual ship speed and shaft speed as input. The remaining two methods also require the speed data and partial shaft speed as input. Later studies show that the ship's speed is a mandatory input, whereas the propeller's rotational speed can be replaced by the propeller designed rotational speed. The details are discussed in the Model Validation section.

Efficiency Diagram Lookup

Based on the Tachek propeller geometry, the propeller efficiency is read from Figure 8. Figure 19 shows the resulting propeller efficiency for the Tachek propeller.

It is worth noting that Figure 8 shows the efficiency of the Wageningen B series propeller, a typical water propeller geometry, with four blades and $A_E/A_o = 0.45$. The Tachek propeller also belongs to the B series propeller; however, the ratio of the propeller's extended area and disk area for the Tachek propeller is 0.43, which is not an exact match to the diagram used. Thus, further interpretations are used to capture the area ratio and the 0.87 pitch diameter ratio.

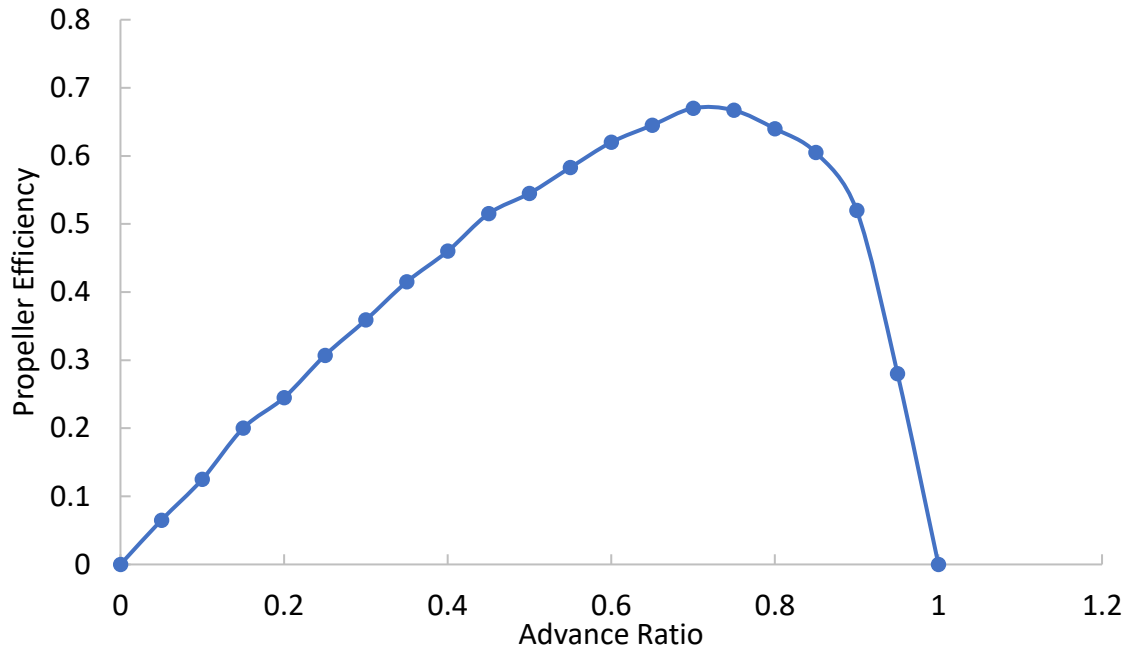


Figure 19: Tachek propeller efficiency based on the efficiency diagram

Base on the obtained data points, a 1-dimensional lookup table with linear interpretation is constructed in the original LOM file with the discrete advance ratio as input and propeller efficiency as output. The advance ratio is previously calculated during the direct calculation method, which can be adopted here. Table 2 shows the tabulated value used for the 1-dimensional interpretation. In between each data point, linear interpretation is used for approximation. If the calculated advance ratio is beyond the boundary, the efficiency is taken to be 0.

Table 2: Propeller efficiency lookup table for function implementation

Advance Ratio	Propeller Efficiency	Advance Ratio	Propeller Efficiency
0	0	0.55	0.583
0.05	0.065	0.6	0.62
0.1	0.125	0.65	0.645
0.15	0.2	0.7	0.67
0.2	0.245	0.75	0.667
0.25	0.307	0.8	0.64
0.3	0.359	0.85	0.605
0.35	0.415	0.9	0.52
0.4	0.46	0.95	0.28
0.45	0.515	1	0
0.5	0.545		

Computational Fluids Dynamic Simulation

As aforementioned, CFD is an excellent way of solving ship-related hydrostatic and hydrodynamic performance. However, a full-scale CFD requires a supercomputer and long computation time. Since this study aims to estimate power demand in a reasonable time, the CFD used for propeller efficiency calculation needs to be simplified and use a conventional academic CFD package.

The Ansys CFX platform is used for this case because of its reliability. As shown in Figure 20, the propeller CAD model provided by BCFS is imported to the simulation environment for model processing and meshing. It is worth noting that although the CFD is done to the propeller, the main interests of the study are not on the propeller geometry but the conditions of the fluid, including pressure and velocity. Thus, the primary method for setting up the CFD is to create a fluids domain and subtract the volume of the propeller geometry. This approach allows only fluids present in the design domain, and the boundary conditions are set up correspondingly to prevent fluid from entering the imaginary propeller's space. This is a typical method for CFD since the problem is reduced to a single phase. If a real propeller model is meshed in a fluid domain, two phases (materials) are present in the domain, and the computation can be slow.

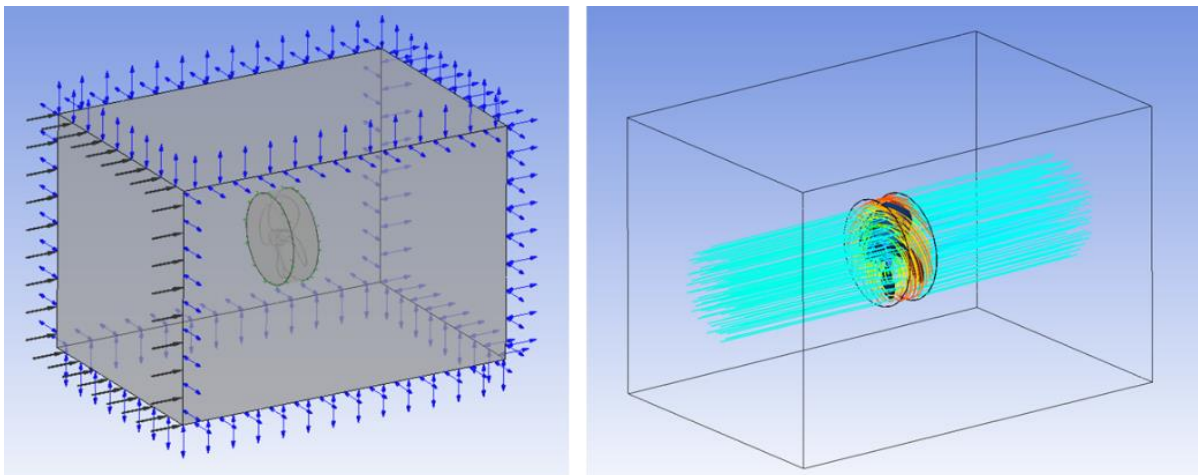


Figure 20: Propeller CFX simulation set up and results

However, this set up's major disadvantage is that the 'propeller' is fixed in the simulation environment. In order to capture the propeller's dynamic, the surrounding water is set to have an inlet velocity equal to the desired ship speed to simulate the forward motion. With a similar analogy, the subregion is created closely around the propeller, and the subregion is set to have a rotational speed equal to the propeller shaft speed. A similar problem occurs here since the ship velocity and shaft speed are required as inputs. The CFD does not directly yield propeller efficiency; however, the thrust generated and torque experienced can be obtained. It is generally understood that multiplying propeller rotational speed (input) by torque (output) reflects the real shaft power, and multiplying inlet speed (considered as the same as ship speed, input) by thrust (output) yields the propulsion power. The efficiency can be calculated as the ratio of propulsion power and shaft power. In this case, to ensure the input consistency, the 'propeller' rotation speed is set to be constant for the simulation, for which the propeller designed rotational speed is used. This assumption can introduce potential errors since the speed may

not correspond to the specific velocity input. The possible effects are discussed in the following section.

Model Comparison

The yielded efficiency curves are plotted in Figure 21 to compare the outcomes from three methods. Results from the three methods showed no significant variance, and the largest difference is 3 percent.

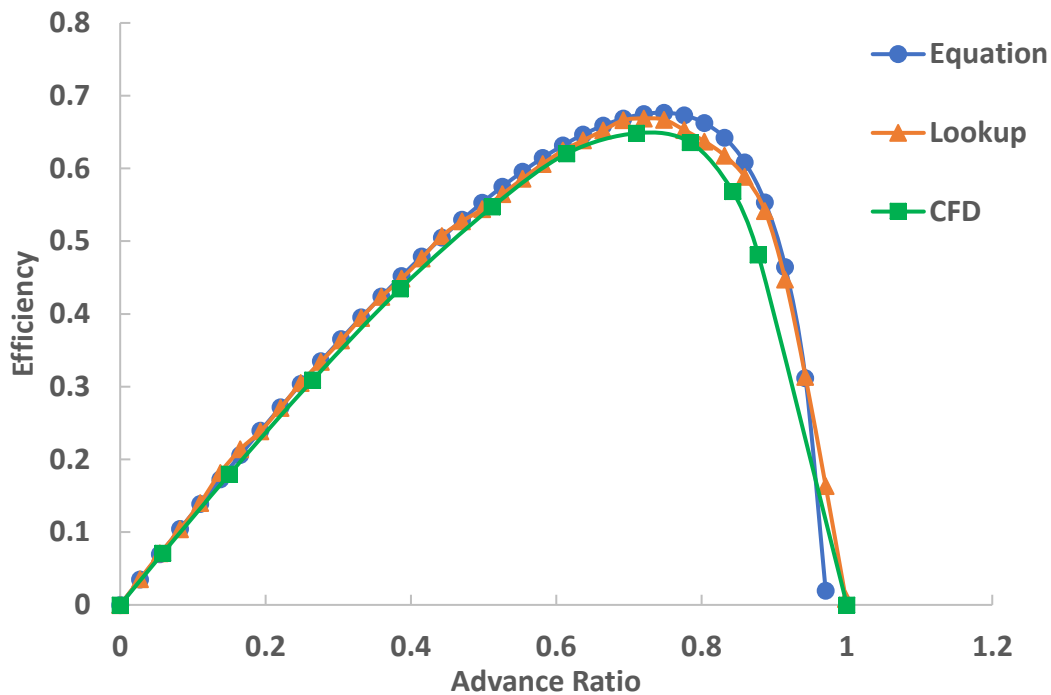


Figure 21: Results of three tested propeller efficiency calculation methods

There are several issues associate with each method. For the empirical equation method, the equation can lose its meaning when certain conditions occur. For example, when the ship is docking, propellers remain operating to generate thrust to push the vessel against the dock. However, the ship velocity is 0 during the stage, and the propeller efficiency is 0 based on the equation. To estimate the shaft power, the equation must divide the propulsion power by efficiency. In this case, division by zero will occur, resulting in an infinity shaft power demand while docking. This division is not feasible nor correct; however, the actual efficiency is not measurable. The situation is similar to the remaining methods. When the advance ratio is zero, the lookup table yields 0 for the efficiency, whereas CFD calculates the shaft power, but the propulsion power is zero; hence the efficiency is 0. Currently, the results are tuned by using a conditional division to eliminate dividing by zero situation. However, a method for solving the problem is required and needs further investigation.

On the other hand, the opposite situation occurs when the ship's speed is high and the propeller speed is low. Usually, when a vessel sails in a straight line, the ship speed increases when the propeller speed increases. However, during maneuvering, one side of the propeller may reduce velocity for turning. Such velocity difference will result in low shaft speed accompanied with high ship speed, and after calculation, the obtained propeller efficiency can be greater than one.

The problem associated with the CFD simulation is the shaft speed input. The designed propeller speed is used as a fixed input to shaft speed, yielding consistent results comparable to the empirical equation and lookup table method. The obtained operation data of the Tacheck have paired shaft speed and vessel velocity. However, the CFD simulation results could not produce the matched vessel velocity with the given propeller shaft speed as input. The method of using one fixed shaft speed for propeller efficiency calculation to cover all vessel velocity needs to be further investigated.

The propeller efficiencies are calculated using both real shaft speed and fixed design speed to test the problem. The measured shaft power is then multiplied by the two different sets of efficiencies to calculate propulsion power. In Figure 22, the blue line illustrates the propulsion power estimated using the real shaft speed, and the red line shows the power obtained using the fixed shaft power. A small disagreement with a maximum of 17 percent difference can be observed. Since the ferry with a well-defined mission cycle continuously sails at its design speed, the estimation presents a small error. A large error is expected for vessels with dynamically changing velocity and associated shaft speed. At the early design stage, the constant shaft speed can be used to roughly estimate propeller efficiency.

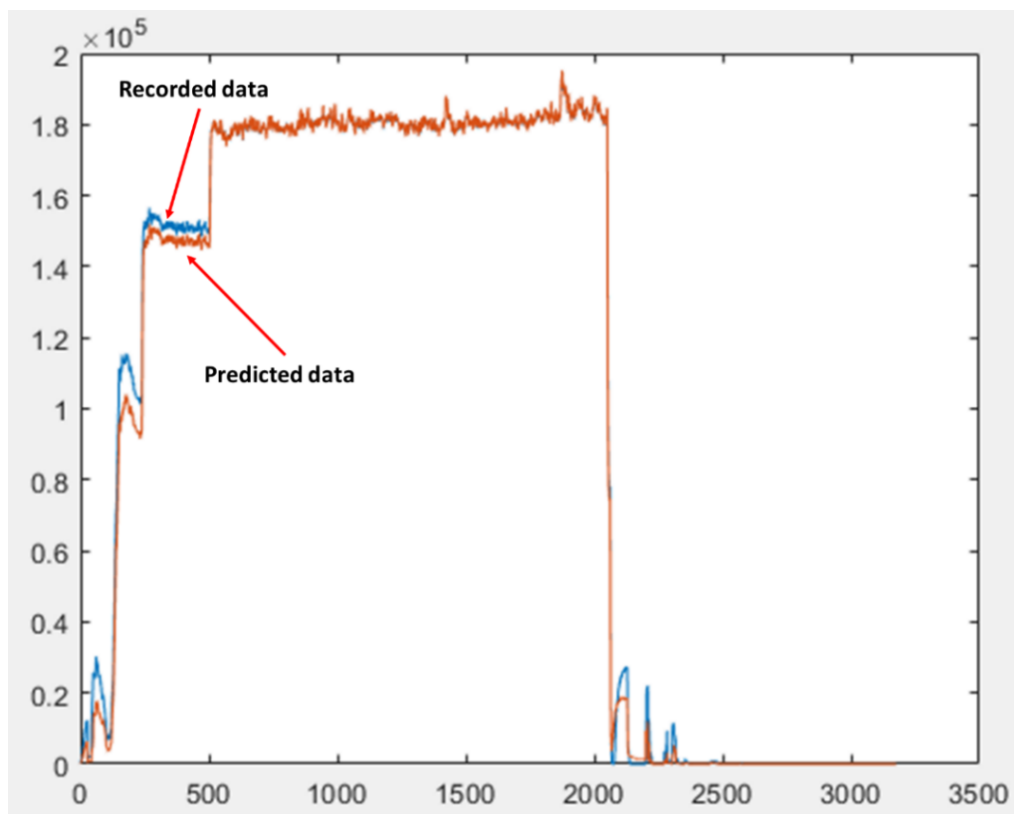


Figure 22: Power results using fixed and real RPM. Blue is the recorded data, whereas red shows the predicted results. The horizontal axis is time in [second], and the vertical axis is power in [W]

From the comparison, it can be concluded that using typical propeller speed as fixed input for propeller efficiency is a feasible estimation. However, to have acceptable estimation results, the ship's mission cycle should not have frequent fluctuation. For ferries with a “departing-accelerating- cruising- decelerating- docking” type mission cycle, the estimation is feasible.

Considering three methods, the lookup table derived from the efficiency diagram is the best method that should be implemented into the LOM. The equation calculation yields an unexpected negative or greater than one efficiency value; the process can not provide consistent results until the maneuvering is modelled in the LOM. The CFD method generates consistent results; however, at least ten simulations need to be performed to obtain a full list of efficiency. The time consumed by one-pass CFD is significantly less than full-scale CFD; however, each run still required an hour to compute. Any modification can be time-consuming to achieve. The efficiency diagram can be read to generate the lookup table, on the other hand. Throughout decades of propeller design modifications and interpretation, the propeller designs have become similar and can be generalized by several typical propeller geometries. An efficiency diagram with the same number of blades and a similar A_e/A_o ratio can be used for estimation. Meanwhile, with the empirical equation and CFD method, the lookup table method's accuracy can be proved. However, with the conclusion made, if the corresponding lookup table is not available, the CFD method needs to be performed since it can both calculate the efficiency as well as help obtain the efficiency lookup table.

For a marine vessel, the propeller(s) can be the conventional fixed-end type or the azimuth type. The former's pointing direction is fixed with fixed or variable pitch, while the latter can switch its pointing direction to improve the vessel's turning radius. With an azimuth propeller, the ship can be maneuvered by changing the direction of the thrust. When rotating 360 degrees, the advance ratio for the propeller is different for four quadrants. When the situation occurs, only the direct calculation method can be used for obtaining the propeller efficiency since the sign varies in different quadrants.

3.4.3 Iterative Propeller Speed Estimation Model

As aforementioned, the propeller designed rotational speed is used for the efficiency simulation. The results are compared to the real measured data, and the accuracy is adequate. However, for propulsion system design, the propeller required torque and rotational speed needed to be more accurately calculated since the engine and motor output torque, speed, and power are needed for component sizing and control strategy optimization. Therefore, estimating the propeller speed is an essential next step of the work.

From Figure 8, the thrust coefficient can also be obtained based on the advance ratio. Equation (3.26) illustrated the relation between the propeller generated thrust to the thrust coefficient. According to the equation, assuming the thrust is equal to the predicted drag force, with K_T available from the efficiency diagram, the propeller speed can be calculated accordingly. Figure 23 shows the interpreted thrust and torque coefficients for the Tachek propeller.

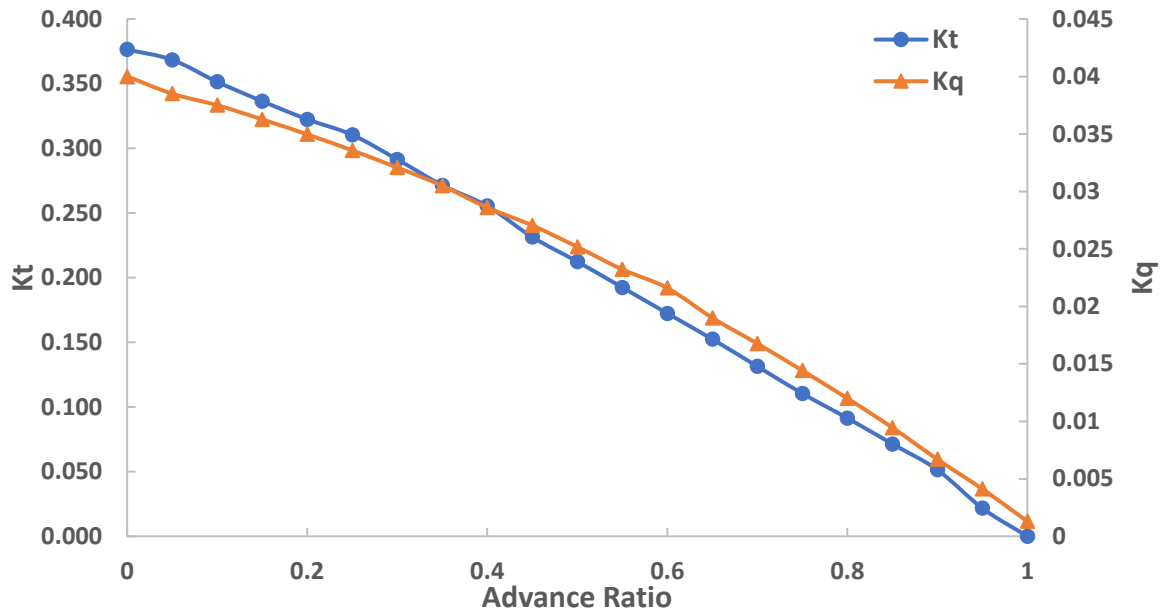


Figure 23: Tachek propeller thrust and torque coefficient

An iterative process is then undertaken to calculate the shaft speed to generate an equal amount of thrust. The pseudo-code reads as following

```

1   for the amount of the data point
2       set propeller speed  $n$  to be 280 RPM and error to 10
3       while  $|error| > tolerance$ 
4           calculate advance ratio
5           interpret thrust coefficient  $K_t$  and calculate thrust
6           error = calculated thrust – estimated drag
7           calculate the difference of  $n$  using yielded error
8           set  $n = n - dn$ 
9       end
10      record calculated  $n$  for each data point
11  end

```

Figure 24 compares the measured shaft speed to the predicted shaft speed using the backpropagation method. During the cruise sailing phase, the predicted shaft speed matches the measured speed accordingly; however, a significant difference can be observed during the departing and approaching phases. The reason for such difference is that the listed assumptions suggest that all propeller power is transferred into propulsion power under particular efficiencies and translated into ship speed. However, during the docking, leaving, and approaching phases, a part of the power delivered by propellers is used for maneuvering as well as stopping the ship. The predicted shaft speed is low since the ship's speed is low during

the stages. The maneuvering needs to be considered with additional DOFs to get a better-matching result.

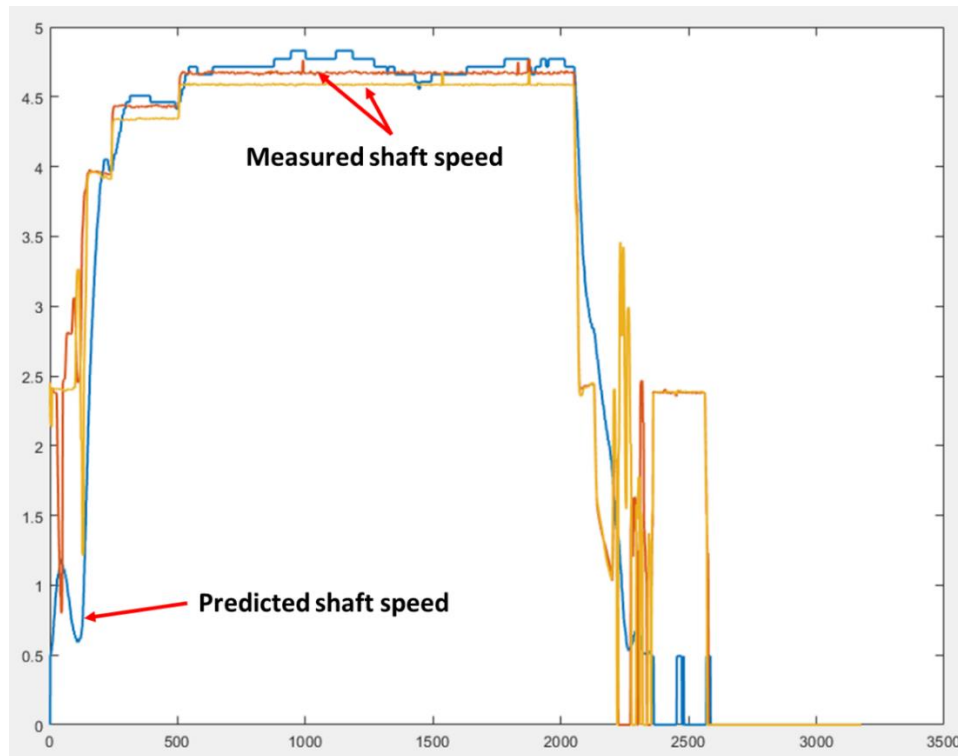


Figure 24: Comparison between measured shaft speed to the predicted shaft speed using the backpropagation method. The horizontal axis indicates the time in [second], and the vertical axis shows the shaft speed in [rads/s].

This study modified the existing low-order model and investigated the performance by comparing the model predicted ship shafts power profile to the real measured shaft data on the Tachek ferry. The model required inputs are obtained by solving well adopted empirical equations, simulating using CFD, and directly measuring from the existing ship. The model's overall accuracy is sufficient for powertrain design purposes since the peak, and continuous power outputs match the recorded data. Several shortages impact the overall accuracy, which will be discussed below in this section.

The active model captures almost all significant environment-induced resistance, including hull resistance caused by viscosity friction, wave, current, and upper deck resistance introduced by the wind. However, at the current model development stage, resistance direction is not captured; all modelled resistance is assumed in the sailing direction. Vessel turning and maneuvering is not considered in the model. This simplification vastly reduces the system degree of freedom and the overall complexity, which dramatically improves the reduced-order model without significantly damaging the accuracy. However, there is no doubt that inaccuracy will be introduced since the various directions of current, wind, and wave can influence performance, especially during the low-speed condition. Meanwhile, the direction of the forces encountered and generated will impact the propellers' efficiency, further introducing inaccuracy. As mentioned, a 3 DOF system generates better results since maneuvering is a critical area to be studied.

Similar to the water conditions, a few assumptions are made to simplify wind resistance calculation. First of all, the wind is assumed to be a headwind during the entire sailing. The wind direction affects the projected area, which is critical for wind resistance calculation. In addition to the direction, the magnitude is considered to be constant during the entire sailing. Jointly, the model yields a matching power profile; however, improvement can be expected when DOF increases. And a more accurate power profile helps with the powertrain component sizing and control design for energy management.

3.5. Software Implementation and Model Validation

The model related calculations, introduced in the previous two sections, have been implemented as MATLAB functions, and this section details the formed Simulink models. An existing MATLAB file was created by Mostafa Rahimpour that contains the original Holtrop's regression method [29]. The MATLAB codes are used as a baseline for implementing the modification. From the comparison in Section 3.4.2, the lookup table method interpreted from the efficiency diagram is used.

The inputs for the modified LOM includes:

- Length on the waterline (LWL)
- The length between perpendiculars (L_{pp}) (length of a ship along the waterline from the forward surface of the stem)
- Breadth moulded (B)
- Average moulded draft (T)
- Displacement volume moulded (V_d)
- Longitudinal center of buoyancy (LCB) (forward +, aft -)
- Draft moulded on F.P. (T_f)
- Draft moulded on A.P. (T_A)
- Transverse bulb area (A_{bt})
- Centre of bulb area above keel (h_b)
- Midship section area (A_{mid})
- Waterplane area (A_w)
- Transom area (A_t)
- The wetted area of the hull (S)
- Wetted area appendages (S_{app})
- Bow thruster tunnel diameter (d_{bto})
- Bow thruster tunnel openings coefficient (C_{bto})
- Beaufort wind scale (BN)
- Design shaft speed (n)
- Ship sailing speed (V)

The following flowchart depicts the process flows of the entire modified LOM. Figure 25 and Figure 26 show the predefined functions to be called or run before the primary MATLAB function, and Figure 27 shows the main function flow. The implemented code will be attached to the Appendix.

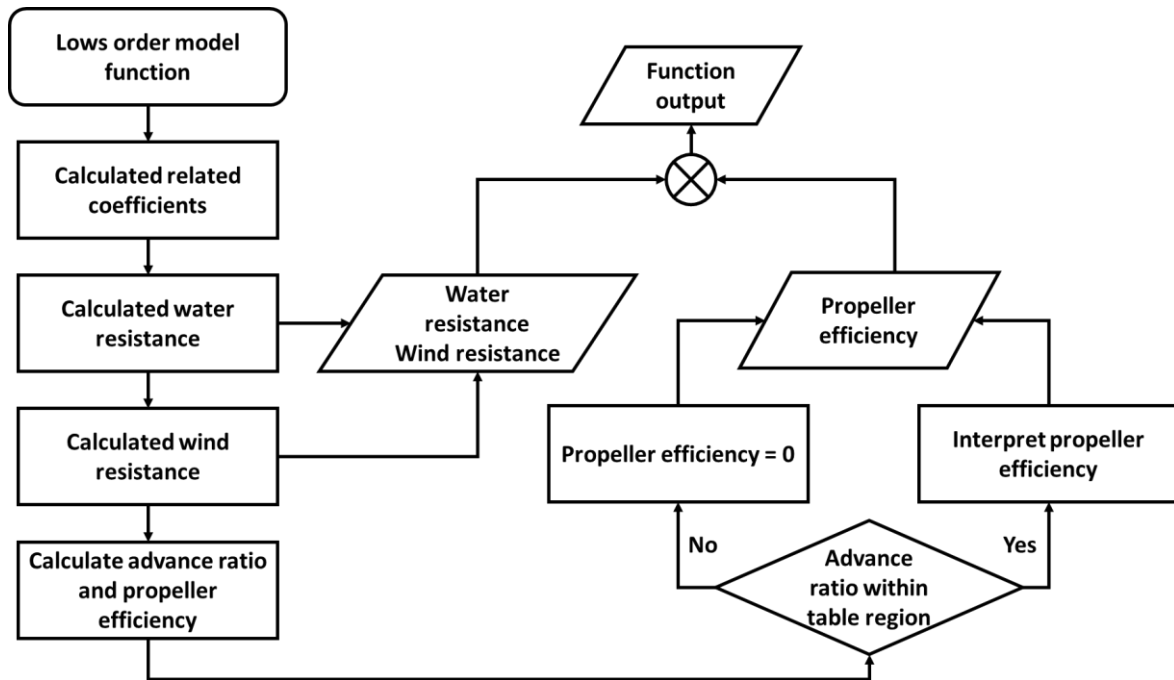


Figure 25: Processes flow for the subfunction contains resistance and efficiency calculation

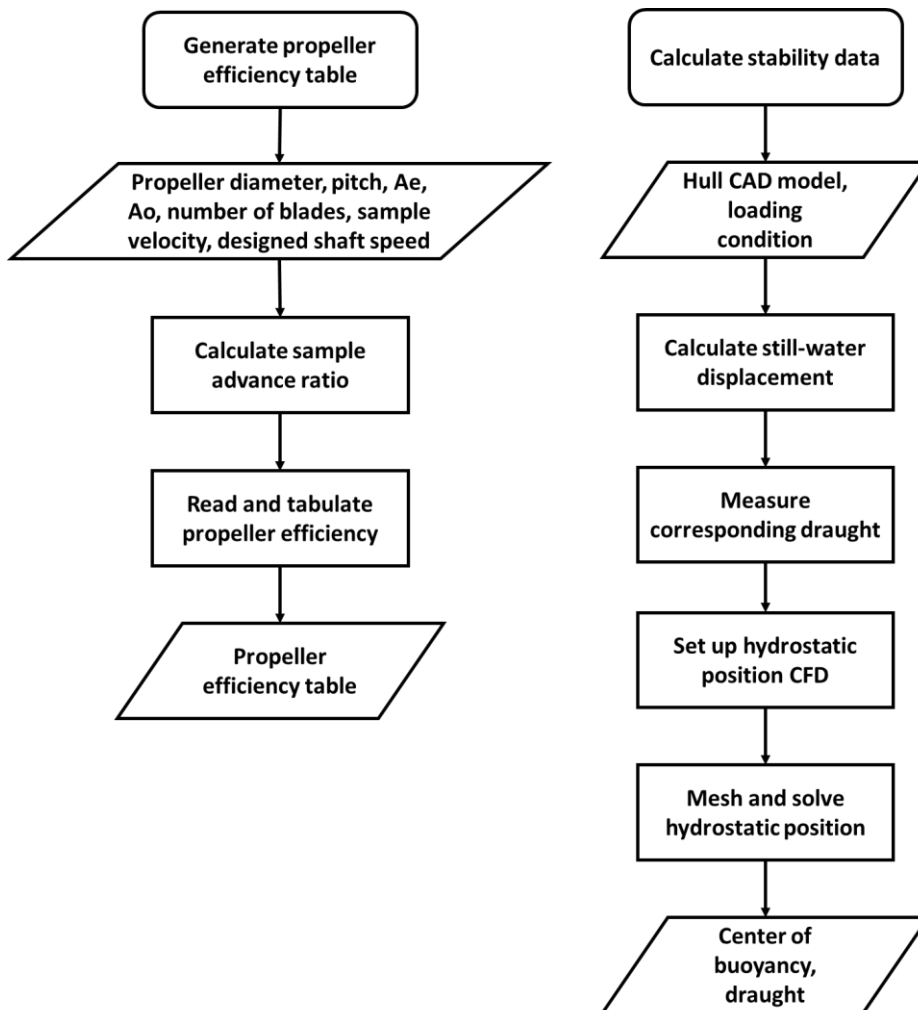


Figure 26: Predefined functions for setting up propeller efficiency lookup table and stability data calculation

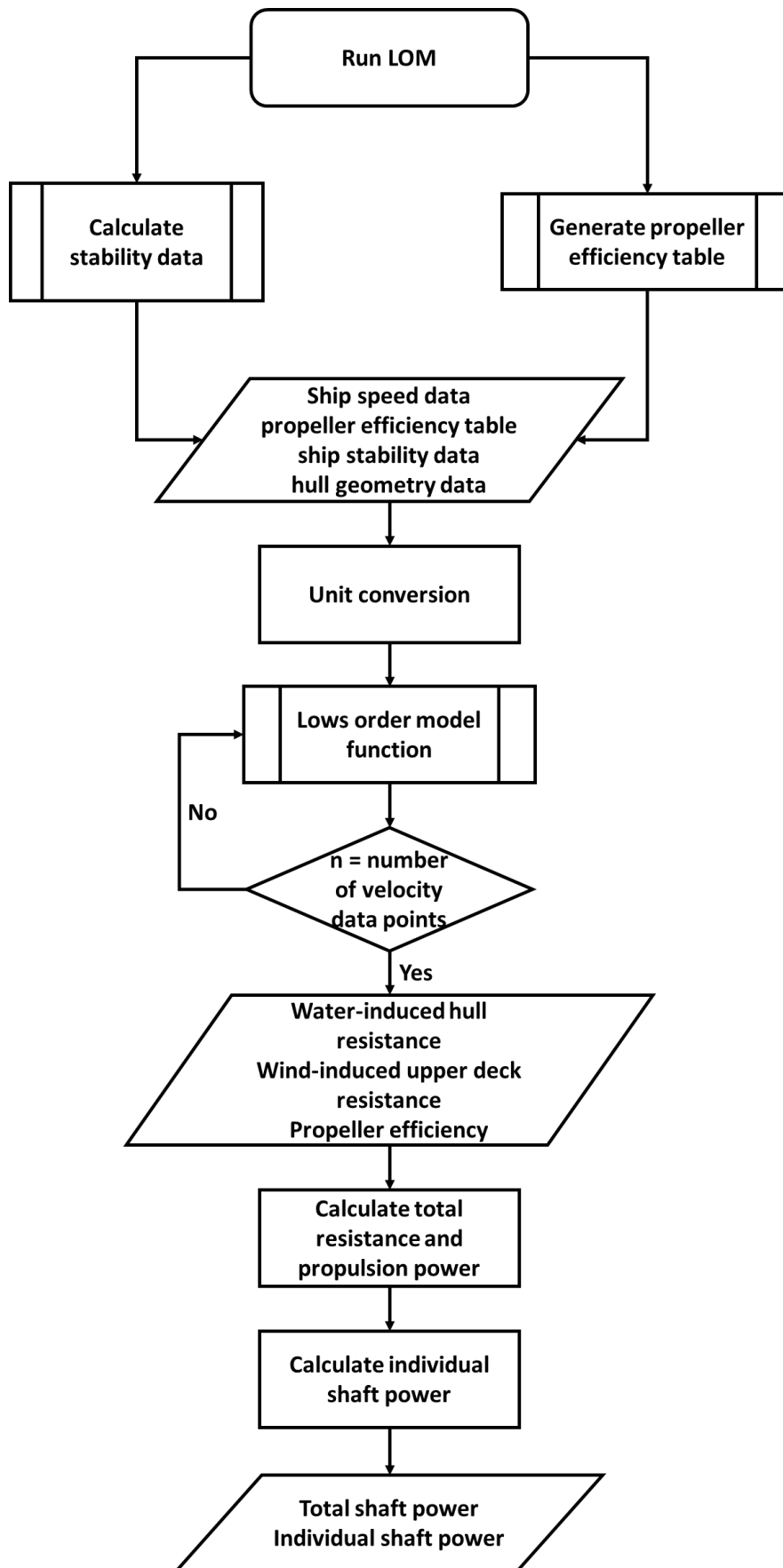


Figure 27: Main LOM function flow

After obtaining the predicted power profile, the results are compared to the real measure power profile for accuracy evaluation. It is worth noting that measured data by M.A.Sc. Zhu [30] reflects the real shaft power, which needs to be compared to the ratio of predicted propulsion power and estimated propeller efficiency. However, as aforementioned, predicted efficiencies contain zero when the ship is docking, a division by zero is not feasible. The measured shaft power is multiplied by the propeller efficiency to yield an estimated propulsion power profile for making the comparison. Then, the estimated propulsion power profile is compared to the modified LOM's predicted propulsion power profile.

Figure 28 shows a comparison between the predicted and measured propulsion power profile. The blue line shows the modified LOM generated results, whereas the red line is the results obtained from the measured shaft power multiplied by the propeller efficiency.

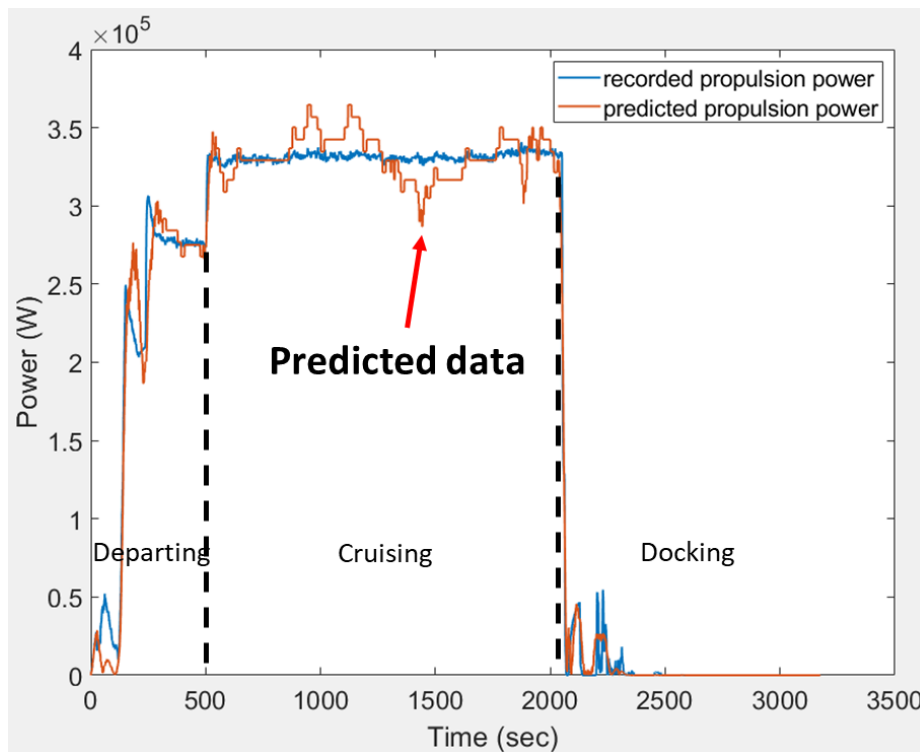


Figure 28: Results comparison between predicted and actual measured shaft power profile. The horizontal axis is time in [second], and the vertical axis is power in [W]

To quantify the difference between the predicted results and measured data, the mean absolute percentage error (MAPE) between the two data sets is calculated. The MAPE is the average percentage error between all data pairs, which is calculated as:

$$MAPE = \frac{1}{n} \sum_{i=1}^n \left| \frac{A_i - P_i}{A_i} \right| \quad (3.31)$$

Using equation (3.31), the directly calculated MAPE is 35.88 percent. The difference is partially caused by power output misprediction at the low-speed regions and a consistent minor time delay of the prediction. For this quasi-static power loss based propulsion system performance and energy efficiency models, the average power percentage errors are relevant. When considering the average power output at departing, cruising, and docking phases, the

differences between the measured and predicted values are only 2.13, 0.06, and 4.58 percent, respectively. During the cruising phase, which is the primary sailing period, the largest mismatch is 9.09 percent, occurred at the bottom peak pointed out by the red arrow in Figure 28 during constant velocity sailing. The general trend of the two data sets is consistent.

On the other hand, it is crucial to measure the total power consumption difference between the two data sets. The total power consumption affects overall fuel consumption and emissions, which are two critical parameters for hybrid power train design since they are treated as optimization objectives. The percentage difference in total power consumption between measured and predicted data is at 2.12 percent. When considering the entire mission cycle, the result suggests that the expected total consumed power matches the real data closely, even some largely distinguished data points exist.

3.6. Key Improvements - Stability Data-Based Model

When comparing the calculation method to the other model mentioned, the pronounced advantage is the computation time reduction without sacrificing accuracy. Figure 29 compares the modified hull resistance model to the aforementioned resistance estimation models. The sea trial and towing tank method require the physical ship or scaled prototype, whereas ROM and full-scale CFD rely on high-intensity calculation. The advantage of the M-LOMCM is finding the midpoint that balances the needs of software computation and the “physical” model.

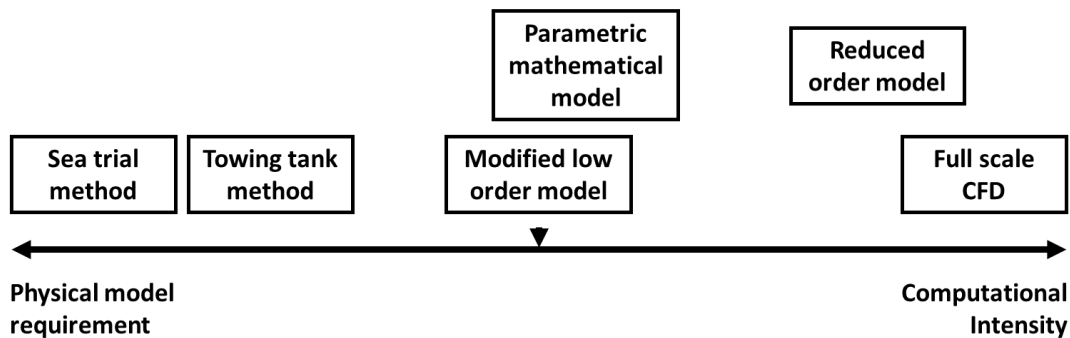


Figure 29: Hull resistance models comparison visualization. The scale is used to compare the needed model and computational power for each model. The further to the right, the more computational resource is required. The more to the left, the more physical model is necessary

The modified model has several noticeable improvements. First of all, M-LOMCM extends the original Holtrop’s method to formulate a complete vessel shaft power demand model based on the hull resistance model and propeller thrust model. Since the original Holtrop’s regression method only considers the still air resistance, the power profile estimation can be inaccurate and can potentially lead to incorrect component size selections. Instead, the M-LOMCM combines the full upper deck resistance with hull resistance to estimate the total ship resistance. When the wind data is missing, the Beaufort wind scale is used to generalize the wind conditions. The additional propeller efficiency model further upgrades the resistance model into a power profile prediction model. The original models only measure the hull resistance, which is less useful than the power profile when selecting components for the integrated system design. The additional propeller thrust/efficiency model converts the load profile into

propulsion power and shaft power profile, which can be directly used for integrated ship propulsion system design.

Secondly, with hull form geometry data from the computer-aided design (CAD) model and parameters obtained from the CFD simulations, the M-LOMCM only requires speed data as input. Unlike the methods mentioned previously, where information such as sea trial and stability data is needed for computation, the M-LOMCM unlocks the potential of “soft prototyping” during the ship’s early design phase. The speed data is generally measured from the physical ships; however, the ship’s top sailing speed is often determined at the design phase. A synthetic speed profile can be used as a reference for early-stage simulation. Meanwhile, the velocity profile from the ships that belong to the same class can be used as a reference.

Third, contrasting from the other complex models or full-scale CFD, the 6 DOF RANS is represented by low-order regression empirical equations, which vastly reduced the time needed for computation. The regression method relies on empirical equations and parameters obtained through the sea trial or experience. Such parameters are either not obtainable at an early stage of ship design or inaccurate. The CFD method is proven to be accurate by numerous researches and is able to deliver precise hydrostatic and hydrodynamic parameters. On the other hand, only one-pass CFDs through conventional CFD packages are required with the enchantment of the regression relation. Such simplification reduces the time and computational resources needed for the full-scale CFD. Without a physical model, the required stability data can be accurately obtained utilizing the CAD model and CFD simulation. A similar analogy can be applied to the propeller, where a single-pass CFD is used along with empirical equations for obtaining propeller efficiency without a prototype.

Lastly, M-LOMCM can be modified to customize for each ship. Unlike the mathematical model, the M-LOMCM is not a generic representation. Instead, for each vessel with unique hull and propeller designs and distinct mission cycles, the model can be applied to capture the unique hull resistance and power demand associated with the mission. Meanwhile, the M-LOMCM is well implemented as a module in the MATLAB/Simulink environment, which can be used along with the model-based design process. Since the resistance and power profile depends on the speed data, the power prediction may vary as the speed changes when the system control varies. The modularized M-LOMCM can be implanted into the design model, which is beneficial during the integrated system optimization.

To show the general relation, the proposed M-LOM can be visualized in Figure 30.

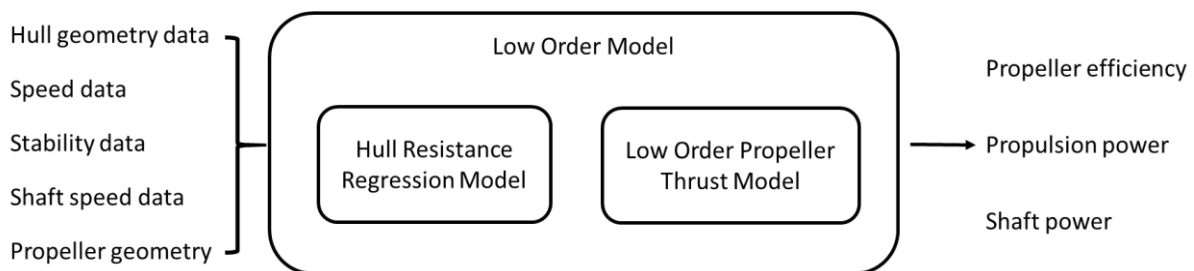


Figure 30: A simple representation of the low-order model

Chapter 4. Comparison of Different Marine Propulsion Systems

The benchmark comparison is the most commonly adopted method to study the different hybrid-electric propulsion system's feasibility and performance. The benchmark method selects a typical plant and applies various internal components, controls, or optimizations. Based on the different outputs, the comparison set's final results can be directly compared and visualized. This chapter details the benchmark vessel selection and modelling of various propulsion system comparison set, including direct mechanical drive, NG-electric drive, pure electric drive, parallel electric hybrid, and series electric hybrid.

4.1. Selection of a Benchmark Marine Vessel – BCFS Skeena Queen

In order to generalize the study, a representative benchmark vessel is needed. The first consideration to be made is the vessel's type and the weight level when selecting the benchmark vessel. Generally, the ships/vessels can be categorized into three major top-level groups: cargo ships, passenger vessels, and special-purpose vessels.

As detailedly reviewed in the first chapter, passenger ships such as ferries induce a large amount of pollution that needs immediate attention. With a strong correlation with the BC Ferries, the research group has been working on passenger ferries and has critical ship hull and internal components data. Due to the advantages listed, the BCFS ferry Skeena Queen (SKQ, shown in Figure 31) is selected as the benchmark vessel. The SKQ sails between Victoria and Salt Spring Island, BC. The overall vessel specs are listed in Table 3.



Figure 31: BCFS MV Skeena Queen [107]

Table 3: BCFS MV Skeena Queen design details [107]

Built:	1997, Vancouver
Overall Length:	110 meters
Maximum Displacement:	2942 metric tonnes
Car Capacity:	92
Passenger & Crew Capacity:	450
Maximum Speed:	17.3 knots
Horsepower:	6000

Unlike ferries such as Tachek that use typical fixed-direction propellers at the vessel's stern, the SKQ utilizes four azimuth propellers for both propulsion delivery and maneuvering. Such a layout is beneficial since the propellers can be orientated into the heading direction, under which condition the propeller efficiency can be maximized. Meanwhile, with four propellers in place, the ferry has enough redundant propulsors to meet the regulations, where at least two propellers must be under operation during the crossing [107].

The main focus of this thesis study is to use M-LOM in a complete vessel modelling process. The M-LOM is constructed initially based on the Tachek ferry. And in fact, the M-LOM performs better on the fix-direction propeller ship since the algorithms used for M-LOM propeller efficiency calculation only serves in surge direction. Because the SKQ varies the propellers' facing direction during the operation, the additional DOF makes M-LOM not ideal for the SKQ. However, the primary reason for selecting SKQ as the benchmark vessel is that some previous studies have been done on the ship. As mentioned in Chapter 3 of the thesis, the reduced-order ship hull resistance and propeller thrust model has been developed for the SKQ. The ROM serves as an excellent reference set for the M-LOM used in this study. Meanwhile, a dynamic model is available for the SKQ. When using the dynamic model, the research can predict the propulsion power only based on the speed profile. Without using additional measured data, the study can mimic the processes during the ship design phase, which is more generalized and representative.

To systematically analyze the hybrid-electric propulsion system's performance, comparisons to other conventional systems are essential. At the current stage, the ship design is volumetric driven, under which condition, the most volumetric dense fuel such as marine diesel or compressed NG is commonly used. Thus, the direct NG-mechanical drive through the internal combustion engines is to be modelled as a comparison set. Meanwhile, diesel-electric is more widely adopted on many ships to replace the conventional pure mechanical drive. In this case, an NG-electric drive is considered as another benchmark comparison set to match the NG ICE. With additional ESS in either parallel or series, the hybrid electric propulsion systems can be achieved. Both series and parallel architectures will be modelled for performance comparison. Lastly, a battery-driven pure electric propulsion system will also be compared.

The mainframe of the multiphysics model is shown in Figure 32. The only external input used

in the model is the vessel's speed profile. Using the modified low-order ship hull resistance model and calculation method, the corresponding thrust demand can be estimated. Based on the ship's speed, acceleration, and thrust demand, the modified low-order surging power deduced model can calculate the propellers' required power input. Meanwhile, the thrust value is used by the ship dynamic model to predict the ship's speed as feedback and comparison. The propeller power demand is then carried on in the propulsion system model to compute the engines and/or motors' power demand, which can be translated into energy consumption. The consumed energy can be finally transferred into the equivalent amount of fuel for the final comparisons.

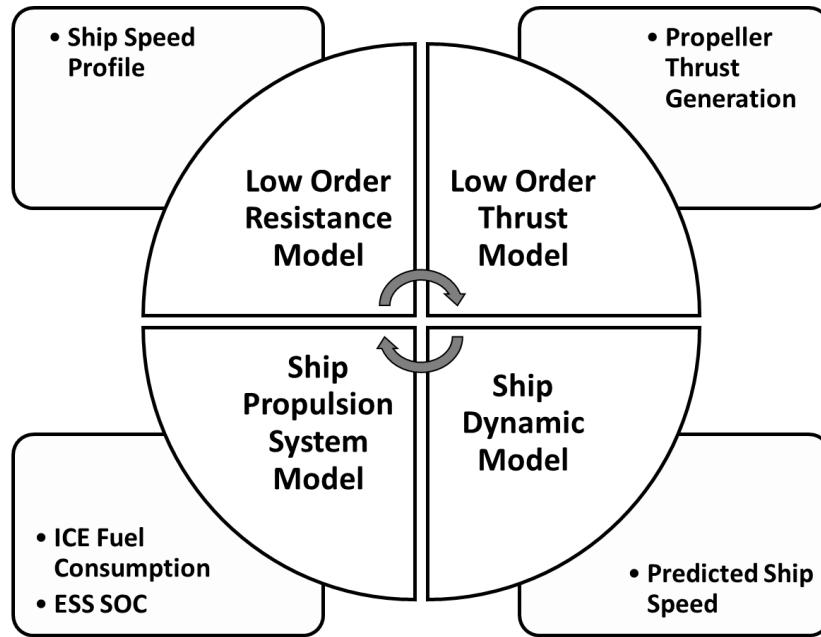


Figure 32: Integrated propulsion system design processes using low-order model

A few assumptions are made to simplify the model:

- a) It is considered that the required thrust is evenly distributed among all four propellers. The advantage of the SKQ system is that four propellers can be individually controlled to achieve maximum efficiency. Ideally, to ensure torque balance, bow and stern propellers can be controlled respectively to achieve front, rear, or all four-propeller drive based on the driving condition. However, if the number of propellers in operation changes, the working propellers' speed and torque need to be changed. Additional gearbox shifts are required to maintain system efficiency, which brings another layer of complexity during the optimization phase. Hence, at the current stage, the four-propeller drive is considered during the entire crossing.
- b) Since the electric related information such as voltage, current, power, and efficiency curve are not available for all components, no electric conversion can be simulated. Ideally, the electric converter needs to be modelled to regulate the voltage and current input/outputs for the motor and generator.
- c) As mentioned before, the simulation is built up for only surge direction. This assumption will lead to less accurate results for the SKQ ferry since the azimuth

propellers utilize a part of the thrust for maneuvering.

- d) For the entire study and comparison, the SKQ ferry is considered to sail at a fully loaded departing condition. The condition suggests the ferry is fully loaded with passengers and vehicle, and the fuel tank and fresh water tank is full. The full loading condition is for testing the extreme sailing condition.
- e) For the entire simulation, only propulsion power is considered. The hotel loads are not included due to the lack of data. For example, for some configurations, the series hybrid electric drive, additional hotel loads can result in different NG generator operation points, which could yield different fuel consumption results.
- f) The electric energy is converted equivalently to fuel consumption for direct comparison. A direct conversion based on fuel energy content and the amount of electric energy usage are considered in this simulation. By dividing the electric power by the fuel heat value, the fuel rate can be estimated. The estimated total equivalent fuel consumption can be generated after cumulative integration over the time steps. Comparing to the Equivalent Fuel Consumption Method established by Paganelli *et al.* [108], the used conversion is a direct simplification. Different optimization methods rather than EFCM are used and detailedly discussed in Chapter 5.
- g) In the benchmark models, battery degradation is not considered. The degradation is more related to system power control and energy management, which will be included in a full case study shown in Chapter 5.
- h) DC buses and DC components are used in all modelling processes. Due to the lack of internal component parameters, conversion losses and phase requirements are hard to determine. The DC bus allows direction efficiency assumption so that the overall model is more consistent.

4.2. Natural Gas (NG) Engine Mechanical Drive

The conventional propulsion system with NG fueled engine(s) and mechanical drive is modelled based on M.A. Sc. Zhu's engine data collected during his thesis research [30]. The overall mechanical model is constructed and shown in Figure 33. According to the assumptions, the propeller evenly delivers the required thrust; hence, only one propeller is modelled. The thrust result is multiplied by four and returned to the vessel dynamics model for velocity simulation. The individual propeller power requirement is transferred to the NG engine through a gearbox. The final fuel consumption can be measured and multiplied by four to yield total fuel consumption.

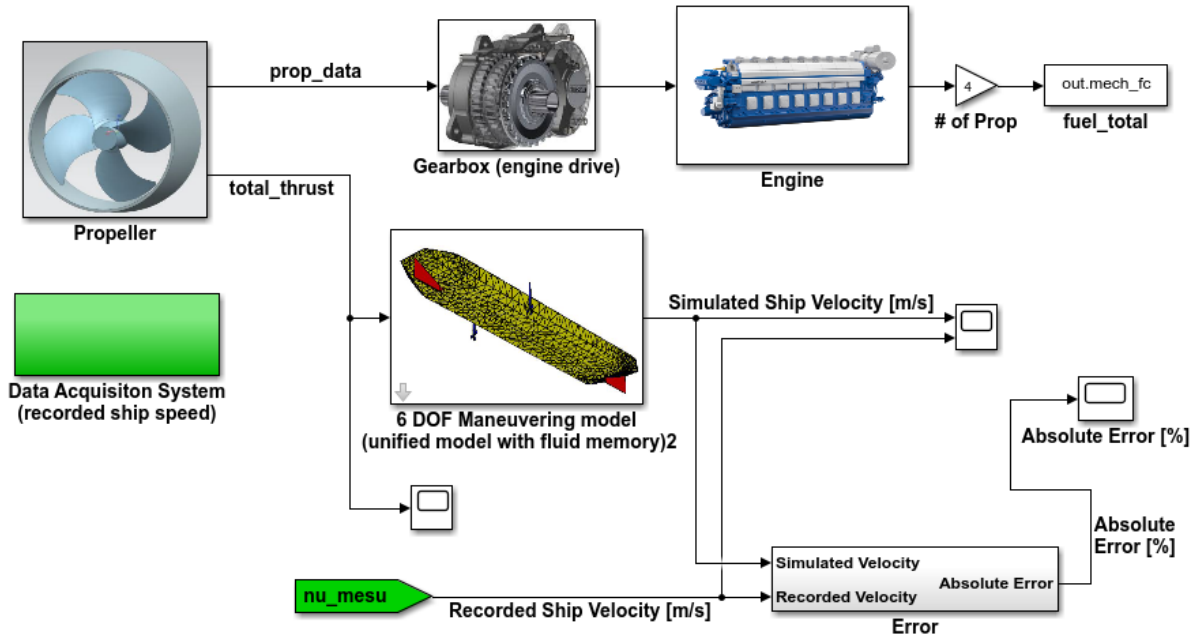


Figure 33: Benchmark model for the NG-mechanical drive propulsion system

The propeller block contains the M-LOM shown in Figure 34. As mentioned in Chapter 3, the resistance model computes the overall hull resistance based on stability characteristics and regression model. The required amount of thrust is the sum of the resistance force and mass acceleration. The surging power deduced model computes the propeller's rotational speed, torque, and efficiency based on the thrust demand and advance ratio. It is worth noting that the propeller block is identical for all configurations and will not be introduced again when illustrating other configuration models.

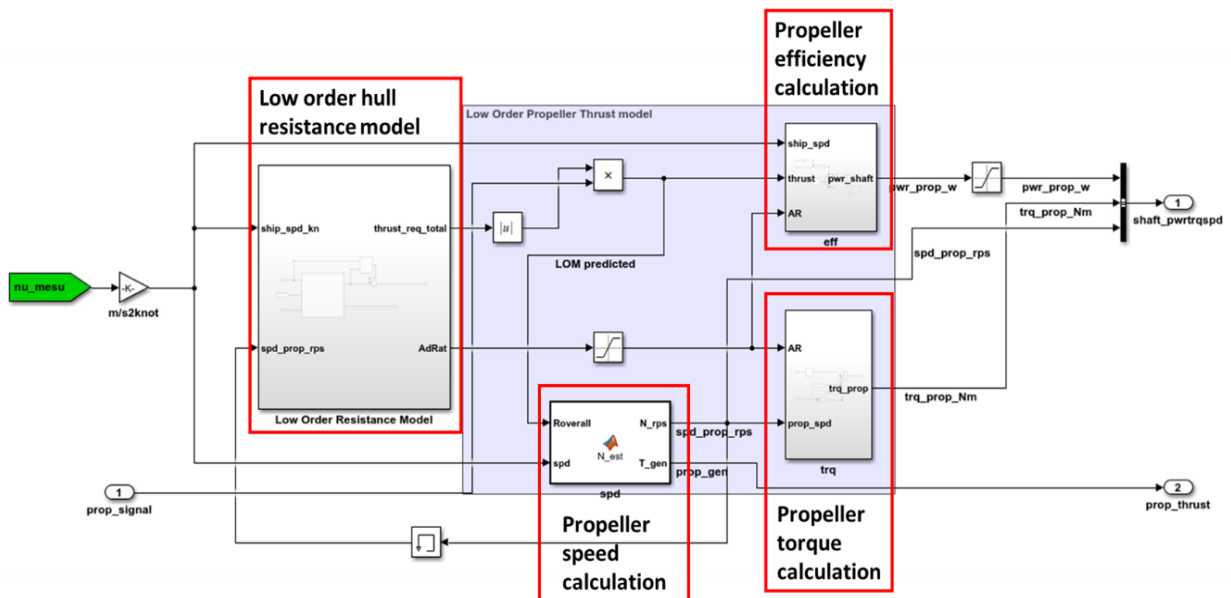


Figure 34: The low-order model block representation

The data accusation block reads the input data from the workspace. The only used external input is the ship's velocity, which is compared to the predicted speed at the end by computing

the absolute error. The engine sizing is governed by the maximum power requirement of the propeller, which is 650 kW. The gearbox block only contains one stage of gear reduction with 95 percent constant efficiency. The gear ratio is calculated based on the propeller's speed under the cruising stage. During the cruising stage, the ship is sailing at 17 knots, under which condition, the propeller is rotating at 22 rad/s (210 RPM). Based on the scaled engine efficiency curve, the adequate engine speed is around 115 rads/s (1098 RPM, corresponding to the high-efficiency zone). Therefore, the gearbox ratio is selected to be 5.2 steps up. The engine model is constructed based on the lookup tables. Since the model uses a backward approach, the engine dynamic can be neglected. The fuel consumption can be looked up in tables and integrated over the simulation time.

4.3. Natural Gas Engine Electric Drive

The NG-electric drive benchmark (shown in Figure 35) is similar to the mechanical drive version, except an additional motor needs to be modelled. The motor model is based on the commonly used TM4 electric machine with a scale specific to the propeller demand. The NG-electric drive requires additional energy converters such as DCDC or ACAC to regulate the voltage and current between the NG generator and electric motor. However, the available motor data does not contain current, voltage, and efficiency curve; thus, control based on the electric current and voltage is not feasible. Therefore, all the simulation is based on torque, speed, and power efficiency instead. Without having information about the voltage and current, the converter performance cannot be modelled, and the efficiency can only be assumed to be constant 95 percent.

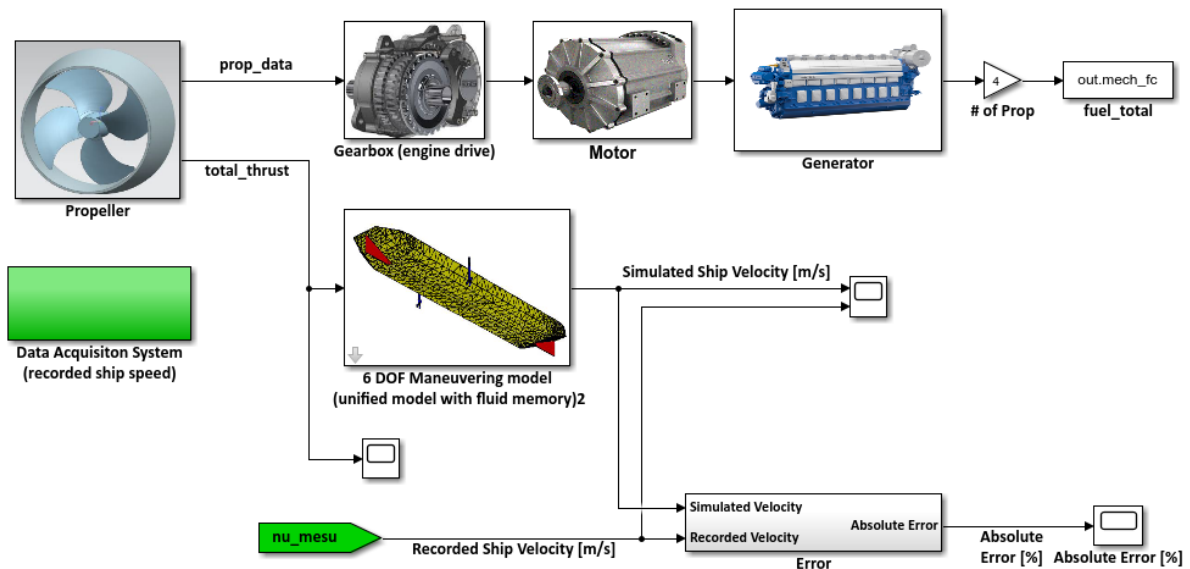


Figure 35: Benchmark model for the NG-electric drive propulsion system

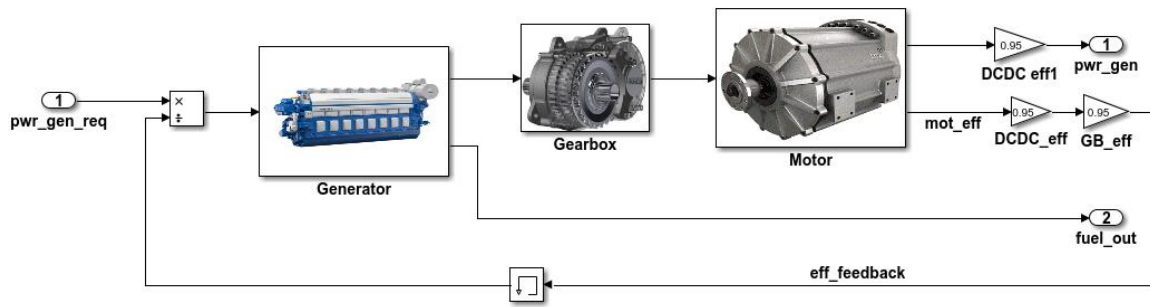


Figure 36: NG generator block representation. The NG generator sub-block contains NG ICE, gearbox, and electric generator.

The NG engine generator is modelled as the engine and motor combination, as shown in Figure 36. In the NG engine generator subblock, a forward approach is considered. The required power is substituted into the engine block, and the resulting torque and speed data are then passed to the gearbox and motor to yield the final power output. Based on the motor operation curve and efficiency, motor efficiency is looked up along with the power output. The efficiency serves as feedback to the power demand input to adjust the input in order to cover the power losses during the processes.

4.4. Pure Electric Drive

The pure-electric drive configuration, shown in Figure 37, is almost identical to the NG-electric drive, except the electric power is provided by a grid-charged battery ESS rather than from the NG engine generator. The subblock ESS model used in the study was developed previously by Li Chen [52]. The battery model is constructed based on the A123 battery. The allowed battery SOC range is selected between 40 percent and 90 percent to maintain a healthy battery condition.

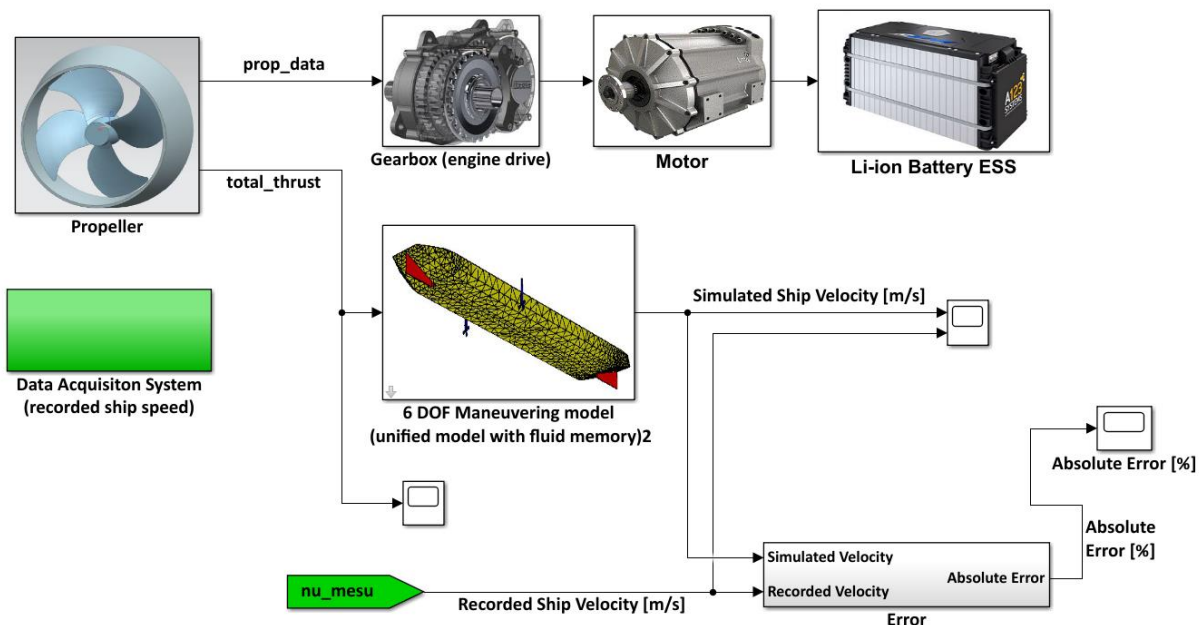


Figure 37: Benchmark model for the pure battery-electric drive propulsion system

4.5. NG Engine Hybrid Electric Drive

In terms of modelling, the hybrid electric configurations are the combinations of the previous three benchmark configurations. However, with additional power sources, usually battery or supercapacitor, the control strategy is necessary to distribute and allocate the energy output between the ESS and the ICE. For the two benchmark models, a simple power follower control is used to emphasize each hybrid architecture's characteristics. For the series hybrid architecture, the NG generator(s) operate in a few best-efficient electric generation points. The battery pack is responsible for providing additional energy for propulsion or consuming excess energy for charging. On the other hand, the parallel architecture allows the engine and motor to provide torque at corresponding synchronized speed jointly.

4.5.1 Series Hybrid Electric Drive

The series hybrid electric drive is modelled and shown in Figure 38. The controller allows the NG generator to operate at 300kW, which can fulfill half of the propeller's continuous power demand. The battery pack releases or collects charges based on the difference between the power demand and the constant generator power rated at 300kW.

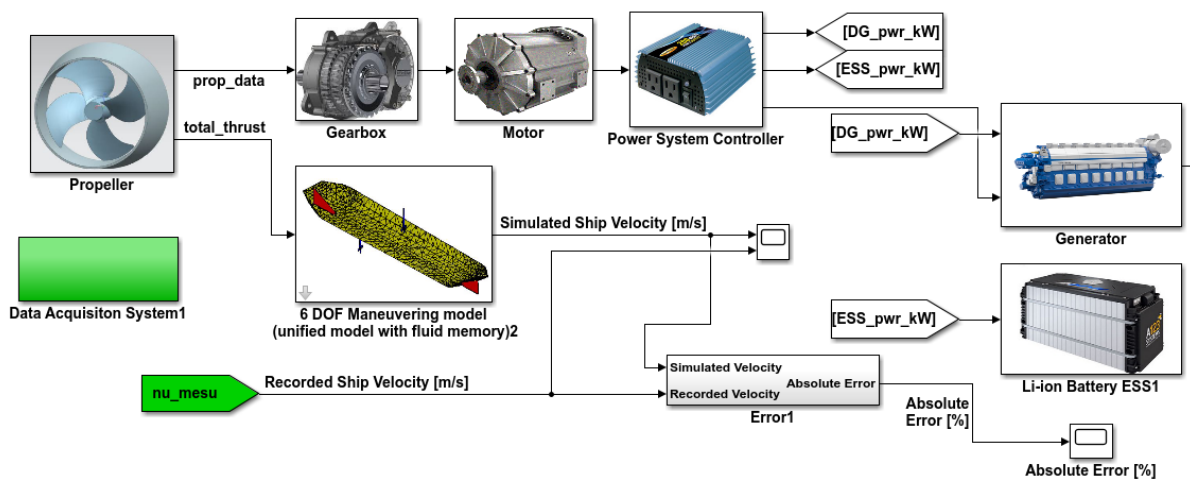


Figure 38: Benchmark model for the series hybrid electric drive propulsion system

4.5.2 Parallel Hybrid Electric Drive

The parallel hybrid architecture (shown in Figure 39) keeps the original mechanical linkage between the ICE and propeller shaft. The additional motor is attached to the shaft through the gearbox. It allocates the power distributions between the ESS and ICE, but the controller also ensures the output rotational speed from ICE and motor after gearbox reduction are identical.

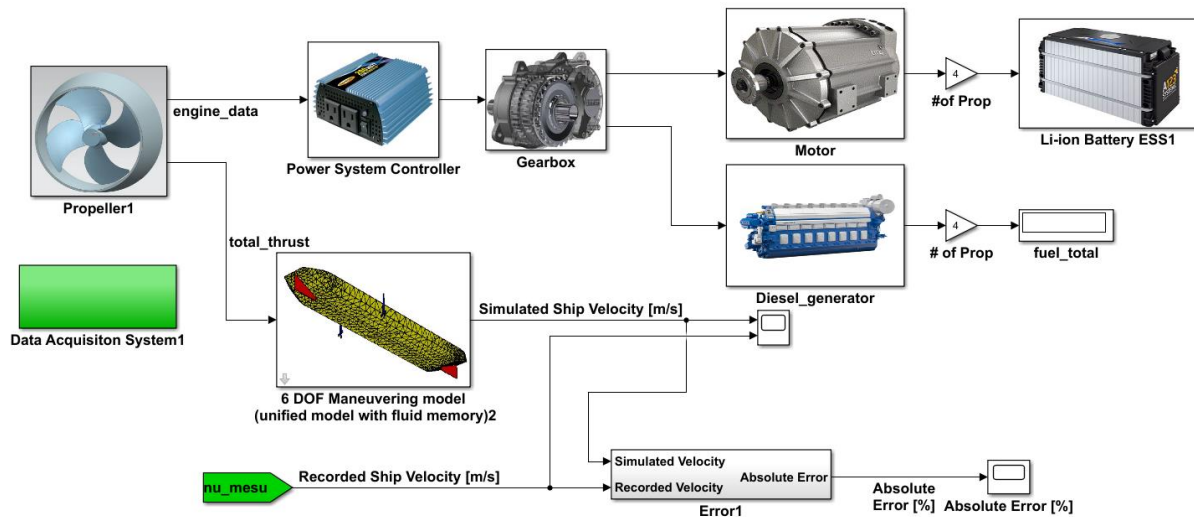


Figure 39: Benchmark model for the parallel electric drive propulsion system

4.6. Benchmark Performance Comparison

To quantitatively compare the performance of all benchmark configurations, the same speed profile is used in calculating fuel consumption. Optimization is carried out on each design to compare the results with the best system components. A global optimization method, discussed in detail in Chapter 5, is used to find the optimal engine size, motor size, and gearbox ratio that minimize the equivalent fuel consumption. Table 4 illustrates the optimization goal and simulation results.

Since the simulation only considers the equivalent fuel consumption, the electric drive can achieve high efficiency with the correct motor size and gearbox ratio; hence, the battery-electric drive has the lowest fuel consumption. As mentioned in the assumption, if battery degradation or SOC penalty is given, the EV's final results can be higher. The NG-electric drive performs the worst due to a few reasons. To regulate the electric voltage, current, and power input/output, multiple stages of electric converters are necessary for the system. The conversion leads to energy losses, which reduces the system's overall efficiency significantly. Meanwhile, since only propulsion power is considered for the active simulation, the NG generator must frequently switch operation points to meet the power demand. Typically, when the hotel loads are considered, the NG generators operate at a fixed narrow region to maintain the output power and phase.

Table 4: Optimized benchmark model result comparison.

Benchmark Configuration	Design Objective of Optimization	Total (Equivalent) Fuel Consumption [kg]
NG engine mechanical drive	<ul style="list-style-type: none"> • Engine size • Engine to propeller gearbox ratio 	170.05
NG-electric drive	<ul style="list-style-type: none"> • Electric motor size • Motor to propeller gearbox ratio • NG generator size • NG engine size • ICE to generator gearbox ration • Generator size 	226.62
Series hybrid electric drive	<ul style="list-style-type: none"> • Electric motor size • Motor to propeller gearbox ratio • NG generator size • NG engine size • Internal engine to generator gearbox ration • Generator size • Battery size • NG generator operation point 	152.30
Parallel hybrid electric drive	<ul style="list-style-type: none"> • Engine size • Motor size • Multi-input gearbox ratio • Battery size • Engine operation point 	123.50
Battery pure electric drive	<ul style="list-style-type: none"> • Electric motor size • Motor to propeller gearbox ratio • Battery size 	73.54

The series hybrid configuration largely resolves the sub-optimal operating points issue that the NG electric configuration encounters by adding a battery pack to the system. The control strategy allows the NG generator to operate at a single high-efficiency point for power generation, whereas the battery covers the power shortage at high efficiency. On the other hand, excess power is consumed by the battery for charging. Overall, the system efficiency can be maintained at a high level during the entire crossing; hence the fuel consumption is lower

compared to the NG-electric drive.

The parallel hybrid drive can be compared to the direct mechanical drive since both systems have ICE operating at variant operation points. The mechanical drive is better for the active simulation than the NG-electric drive since less energy formation conversion occurs. The best-fit gearbox ratio and engine size are obtained through the global optimization method to improve the mechanical drive performance. The parallel hybrid system has an additional motor coupled with the engine to power the shaft jointly. With the additional assistant, the engine operating points can be allocated on the best efficient curve. Unlike the series hybrid drive, where the engine runs at the highest possible efficiency zone, parallel drive locates the operation points to corresponding power with the highest efficiency. For example, regardless of the power demand, the series drive aims at a high-efficiency zone, and the power output may fall far below or above the demand. When the situation occurs, the shortage or excess is covered by the battery. The parallel drive selects a power near the demand. The desired operating points are chosen to be the most efficient speed and torque combination based on the power and speed demand. The coupled motor covers the additional torque.

Chapter 5. Application to Integrated Hybrid Electric Ship Design

In the previous chapters, the fundamental theory of hybrid electric ship propulsion has been thoroughly introduced. With assistance from the developed M-LOM, integrated hybrid ship propulsion can be designed with limited external data. By utilizing the benchmarks modelled in Chapter 4, this chapter illustrates an integrated design of a hybrid electric vessel propulsion system using BC Ferries' ship Skeena Queen (SKQ) as the test platform. The work demonstrates the model-based design processes, including data processing, low-order model construction, model-based system design, system control, and system optimization.

5.1. Propulsion Power Prediction

As stated in Chapter 3, the vessel's propulsion power profile is critical for the model-based design. The power profile reflects the peak and continuous power demand of the sailing, which is the driving factor of component sizing. Meanwhile, this power demand serves as a constraint during model optimization and directly affects power distribution and energy management. Power profile prediction is regarded as the first milestone of the propulsion system design. For the previous studies done on the SKQ by the research group, the speed profile is obtained through real-world measurement. This section of the work utilizes the aforementioned low-order model on the SKQ to predict the required shaft propulsion power.

Detailed in Chapter 3, the low-order model first computes the ship water/wind-induced resistance based on the hull geometry, loading conditions, and stability data. Then, combined with the ship's velocity data and acceleration, the rigid body propulsion power can be estimated. Lastly, merging with the propeller efficiency, the final shaft power demand can be determined.

The M-LOM is developed under the MATLAB environment. However, to combine the model with the simulation processes, a Simulink block needs to be constructed first. When developing the M-LOM, it is assumed that the vessel's stability data is not available. However, for the SKQ ferry, the full stability data under different loading conditions are documented in the stability booklet. Since a fully integrated model is to be constructed at this moment, more accurate data from the stability booklet is used.

In terms of obtaining the propeller's efficiency, the conventional lookup table method is not feasible since the SKQ propeller is specially designed with duct around the blades. A series of CFD simulation needs to be conducted for acquiring the propeller efficiency, torque coefficient, and thrust coefficient curves with respect to the advance ratio. The propeller's designed rotational speed is not recorded on the drawing. The designed ship velocity is estimated first when performing the CFD simulation. Based on the recorded data, the ferry is sailing at 14 knots during the cruising phase, under which condition, the propeller shaft operates at 800 RPM. Based on the shaft to engine speed reduction and the documented engine to propeller speed ratio, the propeller is calculated to run at 285 RPM during the cruising. Naturally, the propeller has the highest efficiency under the designed rotational speed. Meanwhile, to maintain efficiency, the ship is often intended to sail with designed propeller speed. Based on

the analogy, the propeller's design speed is estimated to be 285 RPM for the CFD simulation.

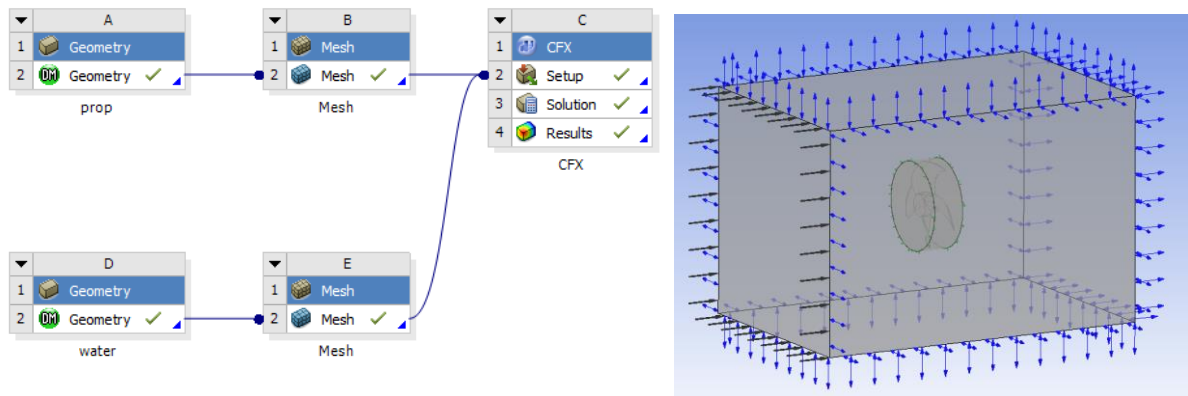


Figure 40: SKQ propeller parameter computation setup using Ansys CFX

Similarly, the propeller CAD model is obtained from BCFS, and the water surrounding is modelled using the Simens NX. The propeller and water region are assembled in the Ansys CFX environment. To mimic the propeller and ship motion under the water, an inlet speed is set up as a control variable for representing the ship's speed, and water-subregion rotational speed is input to serve as the propeller's speed. As mentioned, the controlled inputs for the simulation is forward speed and rotational speed. As stated, the fixed rotational speed (285RPM) is used for all simulations. The ship's speed is ranging from 0 to 23 knots. Such a speed range is investigated due to the disagreement between the CFD simulation result and the ferry sailing speed. The SKQ sails at 14 knots regularly during the cruising phase as recorded; however, the CFD suggests that the propeller has the highest efficiency at 17 knots. Such disagreement affects the designed propeller speed input; but, the issue is resolved by performing the propeller speed backpropagation. The propeller's efficiency, torque coefficient, and thrust coefficient curves are shown in Figure 42.

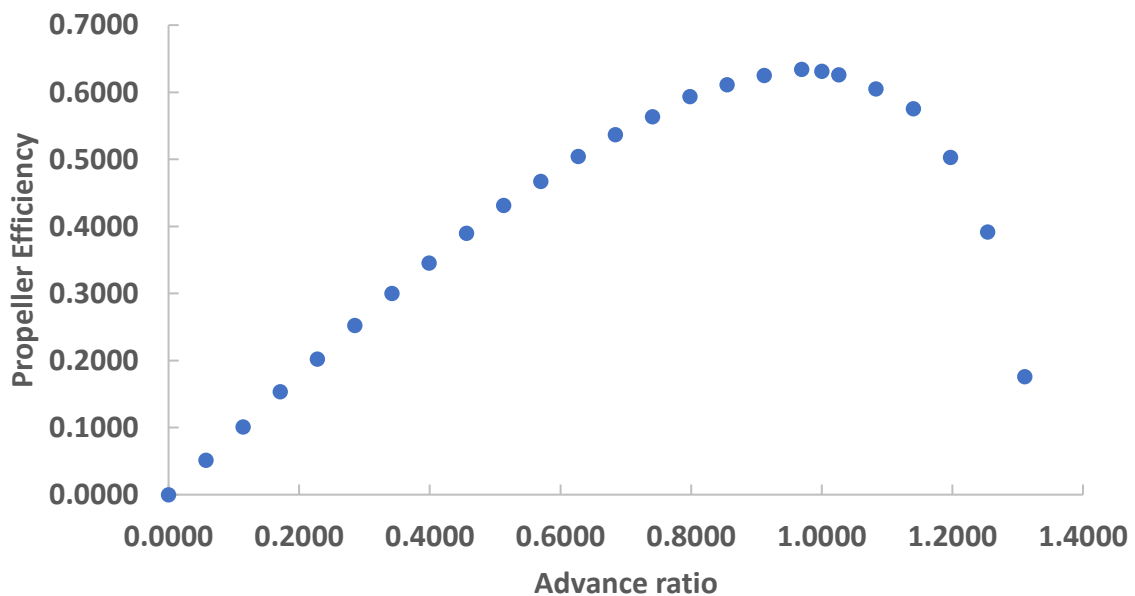
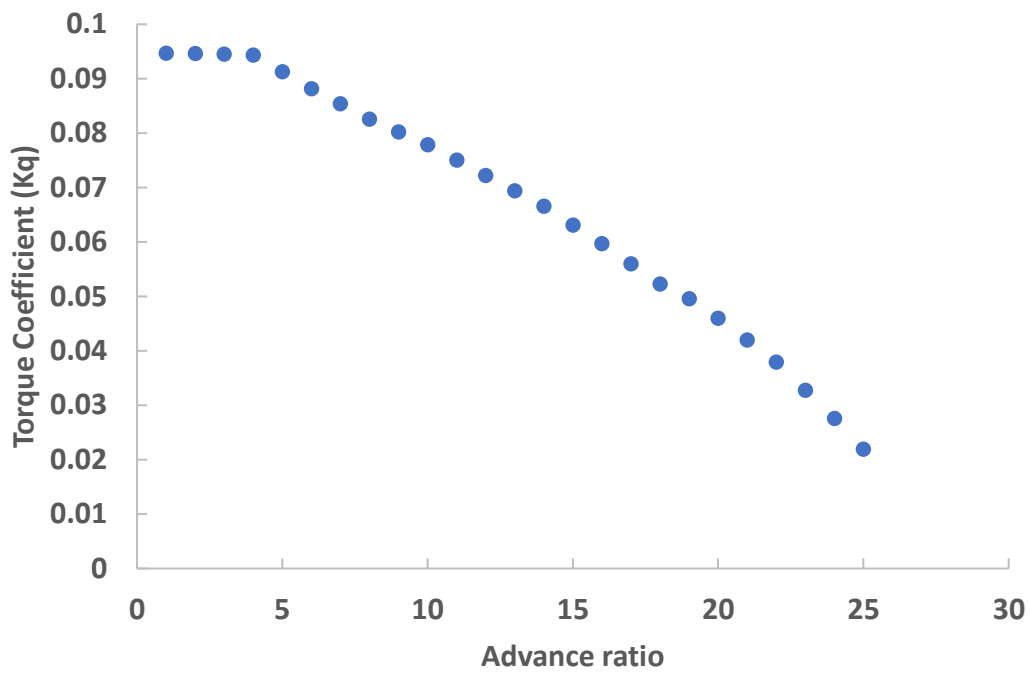
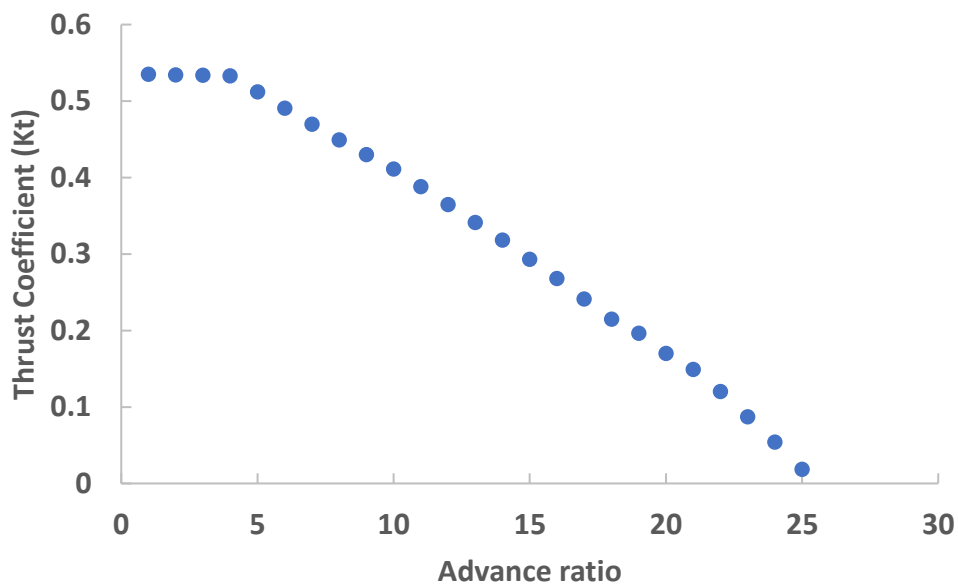


Figure 41: SKQ propeller efficiency results from Aqwa CFD simulation. The horizontal axis represents the propeller's advance ratio, and the vertical axis shows the corresponding efficiency.



(a)



(b)

Figure 42: SKQ propeller parameter results from Aqwa CFD simulation. The horizontal axis represents the propeller's advance ratio. The vertical axis shows the corresponding coefficient value- the upper diagram indicates the torque coefficient Kq and graph (b) shows the thrust coefficient Kt .

After obtaining the propeller efficiency curve, the M-LOM is to be modulized into a Simulink subblock. For the active simulation, the hull resistance model is combined with the propeller thrust model to form the propeller block. The acceleration data of SKQ is not recorded in the

voyage data; instead, it is calculated by taking derivatives of the velocity data. The main problem of taking derivatives is that the data is in the discrete-time domain, where the resulted acceleration is discontinued. Under the simulation environment, a fluctuating acceleration often results in peak power demand. Unlike a direct velocity gauge, the ship's speed is measured using GPS location, where velocity is calculated based on distance change in time. When the ship sailing speed and acceleration are low, the vessel's speed may be marked as constant due to the coarse measurement resolution. Under the situation where the jerk cannot be eliminated, the acceleration data needs to be processed before substituting it into the model.

A moving average method can be used to smooth out the acceleration data damaged by a coarse-resolution GPS tracker. Figure 43 shows the pre and post-processed acceleration data. The main idea is to smooth the data by taking an average of a continuous set of data. Like a filter, the moving average method eliminates the peak data that appeared in the data set; however, rather than simply filtering out the peak data, the moving average method distributes the peak amount among its neighbours. For the active simulation, a five-second (50 data points with 0.1s step size) average is taken. The advantage of the moving average method is that after filtering, the integration of the processed data set remains the same, suggesting that the total amount of velocity increment is the same. This filtering process ensures that the total propulsion energy from prediction remains the same.

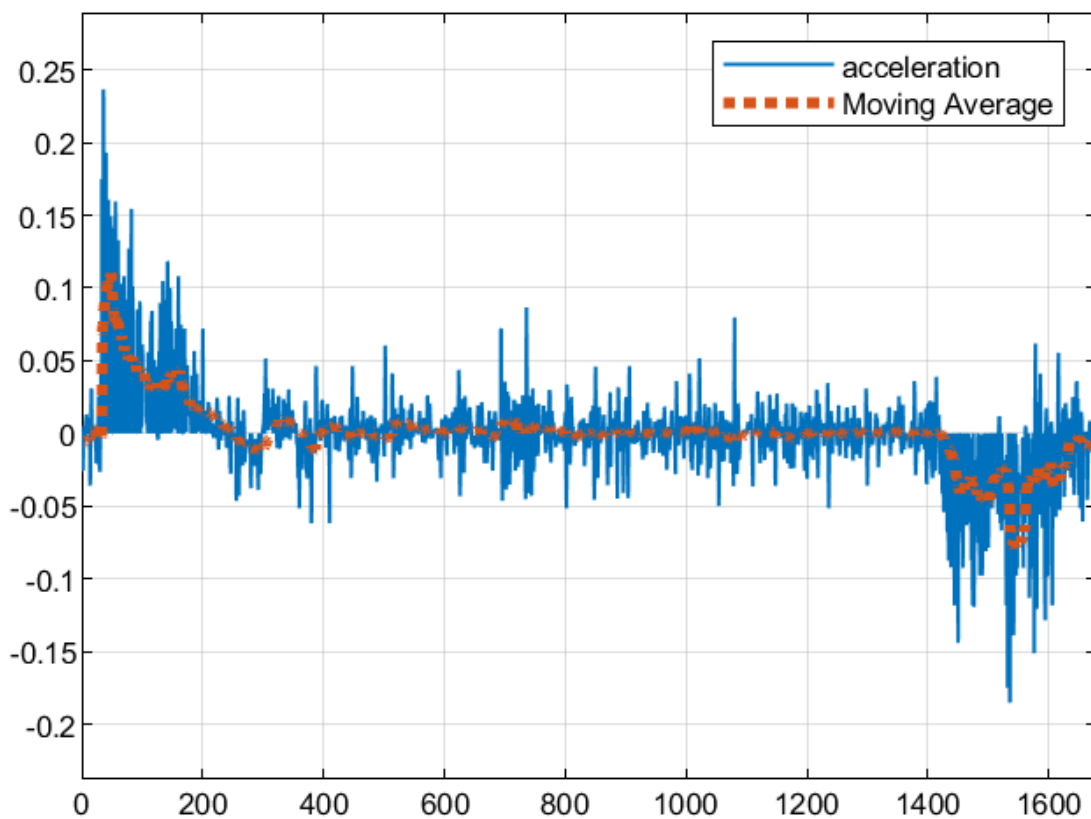


Figure 43: SKQ acceleration results in comparison. The blue line shows the acceleration data obtained by taking a derivative of the vessel's speed data. The red line depicts the acceleration data using a moving average filter.

The improved thrust model remains unchanged, where three subblocks are used to compute the torque, speed, and propulsion power. The efficiency and torque calculation is based on the lookup table extracted from the CFDs. A backpropagation method is used to predict the propellers' rotational speed based on the total thrust and propeller hydrodynamic coefficients obtained from CFDs. The designed propeller speed, 285 RPM, is first plugged into the algorithm to find a reference thrust value. The reference value is then subtracted from the thrust demand for an error response to pass back to the algorithm to adjust the speed of input. The iteration carries until the error is less than 10^{-3} , which suggests that the thrust corresponding to the speed obtained is sufficient for the thrust demand, the speed will be output as the predicted propeller speed. The constant cruising propeller speed is 210 RPM, which is different from the 285 RPM obtained from the output's speed data calculation. According to the ship specifications, the SKQ ferry's best sailing speed is higher than the actual recorded cruising speed, which suggests that the obtained 210 RPM propeller speed is actually representing the recorded velocity.

5.2. Hybrid Electric Propulsion System Design

Typically, a ferry has two fixed-angle propellers located at the stern of the ship. Two propellers rotate at synchronized speed when sailing in a straight line or at different speeds when turning. In comparison, the SKQ has four propellers, which allows more freedom for configuration and control. Utilizing the four propellers on SKQ, a series-parallel configuration is selected for the ferry as shown in Figure 44. The aft propeller set is configured as a parallel drive where TM4 motors and NG engines power the propeller shaft through a gearbox. The fore propeller set is driven by TM4 motors with electric energy from both ESSs and/or the NG generators.

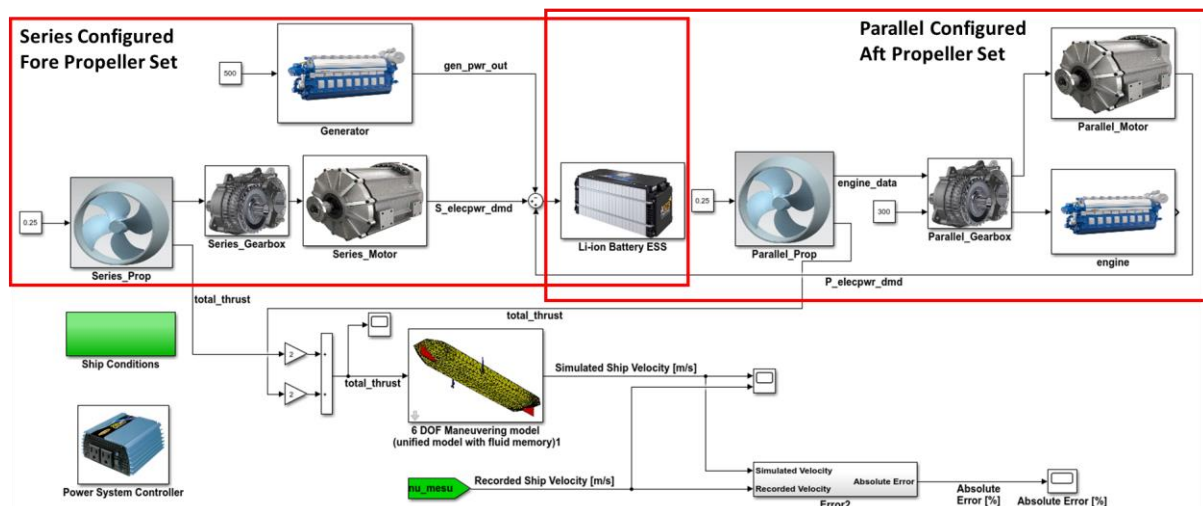


Figure 44: Fully integrated series-parallel hybrid-electric propulsion system design layout for SKQ

In Chapter 4, the disadvantages of the benchmarks are detailedly discussed. The series-parallel configuration vastly reduces the problem. The configuration is inspired by the series-parallel hybrid drive train commonly seen on the ground vehicle. As introduced, a series-parallel architecture combines different configurations and can achieve different driving modes when encountering various conditions. This characteristic is attractive for marine propulsion systems since the marine sailing environment varies due to many conditions such as weather. However,

the central issue of series-parallel hybrid configuration is the complex control strategy. When correctly controlled, the system can remedy each configuration's issues; however, if improperly controlled, the system's inaccuracy will be enlarged.

In the active model, only one side of the system is modelled. The assumption illustrates that the port and starboard propellers operate at the same speed to eliminate the torque generation that may cause turning. The results are multiplied by two to represent the total ferry demand and consumption. For the preliminary sizing, the primary consideration is to have sufficient power ratings for the propulsion components so that the propeller can be driven by one single component upon the failure of the other. For example, in the parallel system, both engine and motor need to have sufficient power rating to drive the propeller alone. From the propulsion power prediction, the maximum propeller power demand is 650 kW. Thus, the size selection criterion is to meet the maximum demand.

5.3. Operation Control of the Hybrid Electric Vessel

As stated, the control is the soul of the hybrid-electric propulsion system, and the system can only benefit from high fuel efficiency if the control is applied correctly. In order to control the system, two control methods are used for the preliminary stage of the system design. A state-flow-driven rule-based power follower control is first programmed to test the system's performance and identify potential design errors embedded. Meanwhile, a simple rule-based control helps choose the component size heuristically for the first stage design. Then, to improve the control strategy for minimizing the system fuel consumption, a dynamic programming method must be constructed to find the global best control scheme. At the first stage of the model-based design, a rule-based control method is applied to validate the system model as well as collect first-hand information about the system performance, such as fuel consumption and emissions level. Such information reflects the improvements that can be made to the system during the optimization phase.

5.3.1 Rule-based Stateflow Control

The rule-based Stateflow control implemented is a basic heuristic power control scheme. Without optimization, the rule is constructed based on the components' initial sizes and intuition. The rules that are driven by the initial sizes serve as constraints. For example, the initial TM4 motor has a maximum power rating of 705 kW. The constructed rule needs to limit the motor's power input under the rated value to ensure it is not damaged. The intuition helps with creating the overall frame of control action and limiting battery performance. The common practice for battery depth of charge is between 40 percent and 90 percent; thus, such practice is intuitively applied to the control scheme.

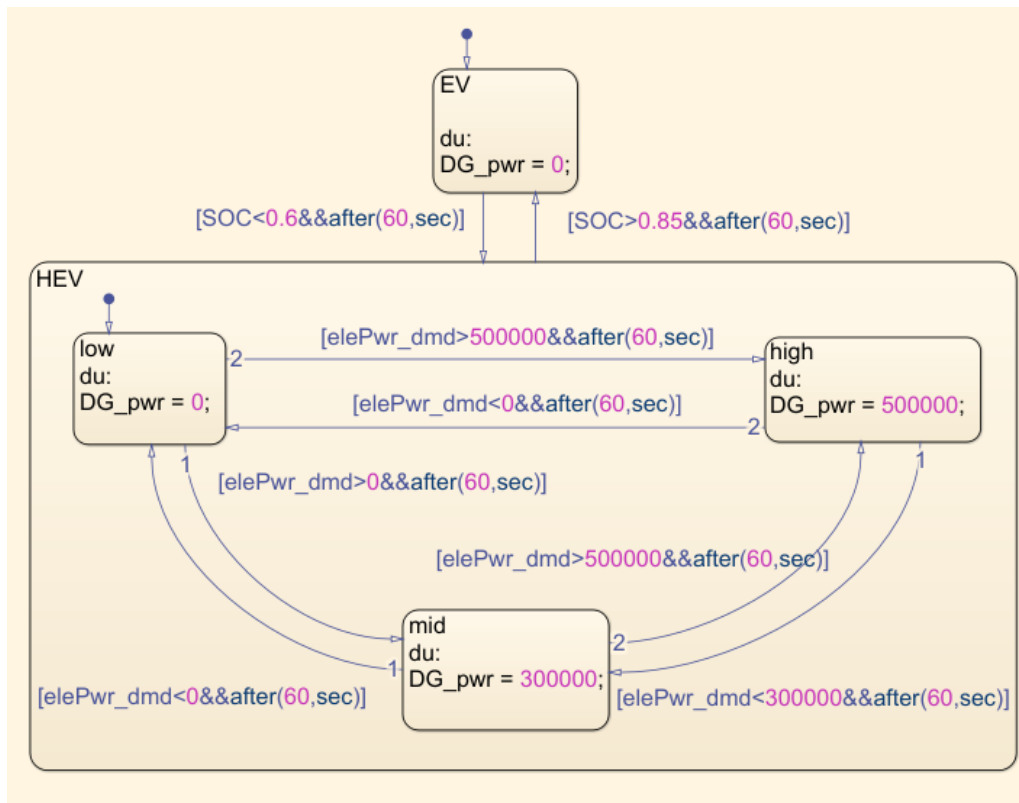


Figure 45: Rule-based control scheme for SKQ series-parallel system. The rule-based controller is a fundamental power follower design with power demand, SOC, and time as a switching condition.

Figure 45 shows the control strategy used in the rule-based controller. Overall, the system switches between pure electric drive and hybrid drive according to the battery SOC. When the SOC is high (above 85 percent), except for the power produced by NG engines in the parallel portion, all the electric energy is provided by the battery. When SOC is below 60 percent, the system enters the hybrid electric drive state. During the hybrid drive condition, the NG generator operates at three different levels depending on the electric power demand. The low level allows NG generators to continually operate at 100 kW, whereas the mid-level and high levels allow 300 kW and 500 kW power output. The ESS will cover the excess or insufficient power in the mean of charging or discharging.

The controller mainly controls the series portion of the system, including the NG generator and ESS. The parallel subsystem has an internal operation strategy to synchronize the output speed and regulate the power. The propeller requires a specific rotational speed, which is stepped up to the rotational speed demand of the NG engine. The embedded control algorithm finds the best operation point for each speed data by finding the highest efficiency along the straight vertical speed line in the efficiency map (as shown in Figure 46). The engine size is selected by matching the shaft rotational speed during constant cruising to the best efficiency zone.

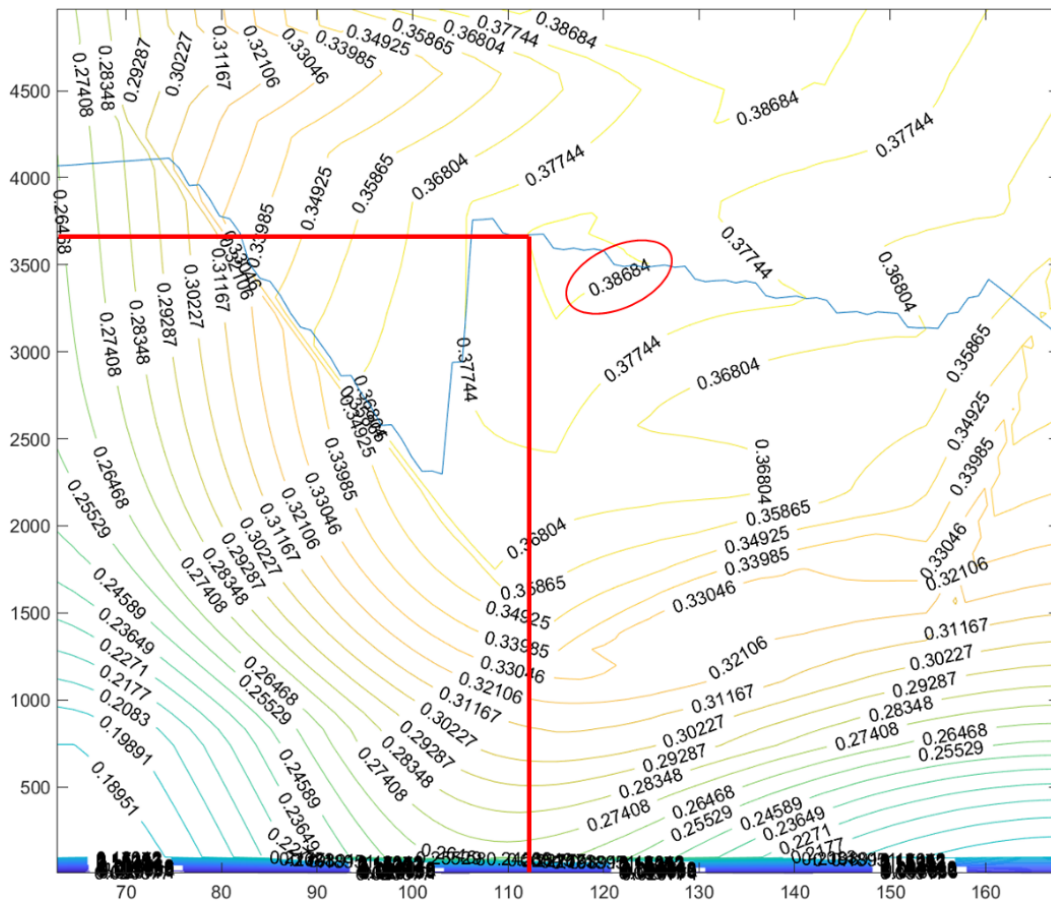


Figure 46: Engine operation curve. For each feasible rotational speed, the thrust value is the best-efficient point along the vertical line.

Figure 47 and Figure 48 shows the results of the rule-based control. It can be observed that the NG generator switches “smoothly” without peak power overshoot. From the SOC result, the system is in charge depleting mode during the entire crossing. Near the end of the mission cycle, the battery is slightly charged back. Such a control strategy requires the plugin (cold ironing) ability to repeat the same performance. If the starting SOC is below 80 percent, more fuel consumption can be expected from the NG generator.

The results show a 152.8 kg of fuel consumption, which is comparable to the series configured benchmark model. Figure 48 contrasts the total power demand and actual power delivery from the motors and engines. It can be observed that power generation matches the trend of power demand. The total delivered power shown in red colour is larger than the power demand depicts in blue. The primary reason is that the output power needs to encounter the system efficiency. With the assumed 95 percent efficiency of converters and the gearboxes, more massive power output is expected.

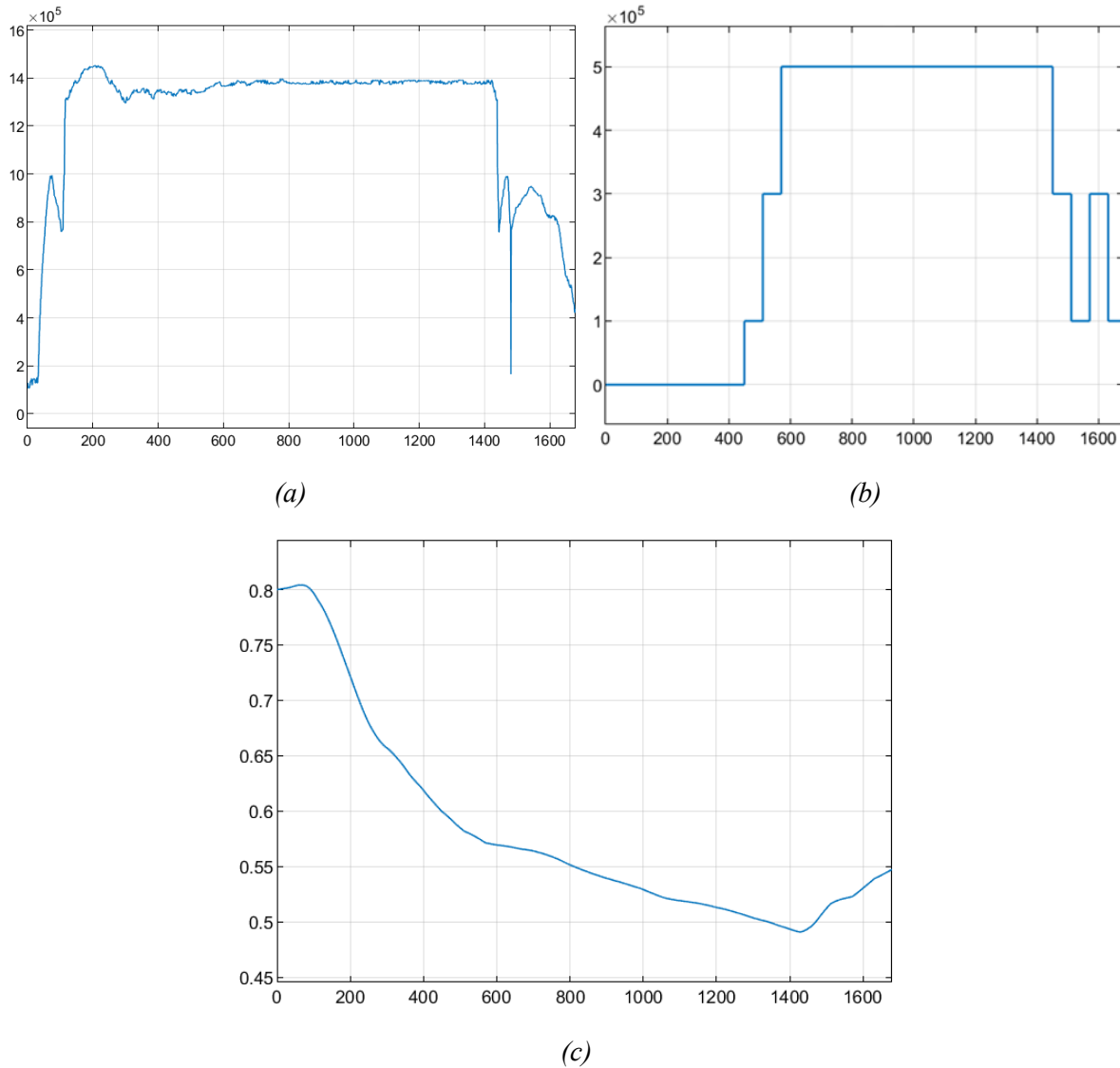


Figure 47: Simulation result for series-parallel configured SKQ using rule-based control. (a) shows the ICE power output in W, (b) shows the NG-electric generator output in W, and (c) shows the battery SOC state. For all figures, the horizontal axis shows the time step in [second].

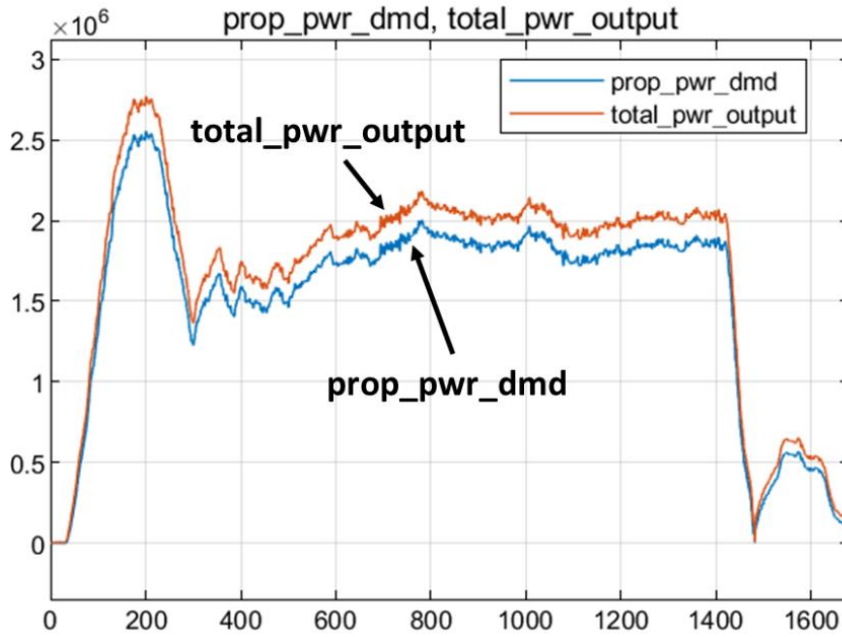


Figure 48: Comparison between simulation results and recorded results. The red line shows the simulated power generation, whereas the blue line indicates the recorded total SKQ power demand. It can be observed that the simulated power generation is greater than the recorded demand since the power generation needs to overcome power losses and efficiency.

5.3.2 Dynamic Programming (DP)

When comparing to the rule-based control, the dynamic programming searches all control combinations in the entire possible design space for the best operation path that optimizes the objective. At the first stage, it is assumed that all four propellers rotate at the same speed. Additional control can be applied for allocating the thrust distributions between the aft and fore propeller sets. However, currently for dynamic programming, with three control variables, namely NG generator power, NG engine power, and battery power, the program time complexity is n^3 , an additional control parameter will increase the complexity to n^4 . After the dynamic programming, nested optimization that optimizes the component sizes of each dynamic programming loop will be performed, which will add one more complexity to reach n^5 . Such algorithms can be time-consuming to perform, which is not desired.

Developed by R. Bellman [109], dynamic programming is an optimization method that breaks a large complex problem into a series of small sub-problems. The idea is that the optimal solution to the overall complex problem is the sum of the optimal solutions to the breakdown problems. DP is generally evaluated from the back, known as backpropagating DP. The forward DP is also achievable but not commonly practiced. A backpropagating example based on SOC and time steps shown in Figure 49 is used to illustrate the DP processes.

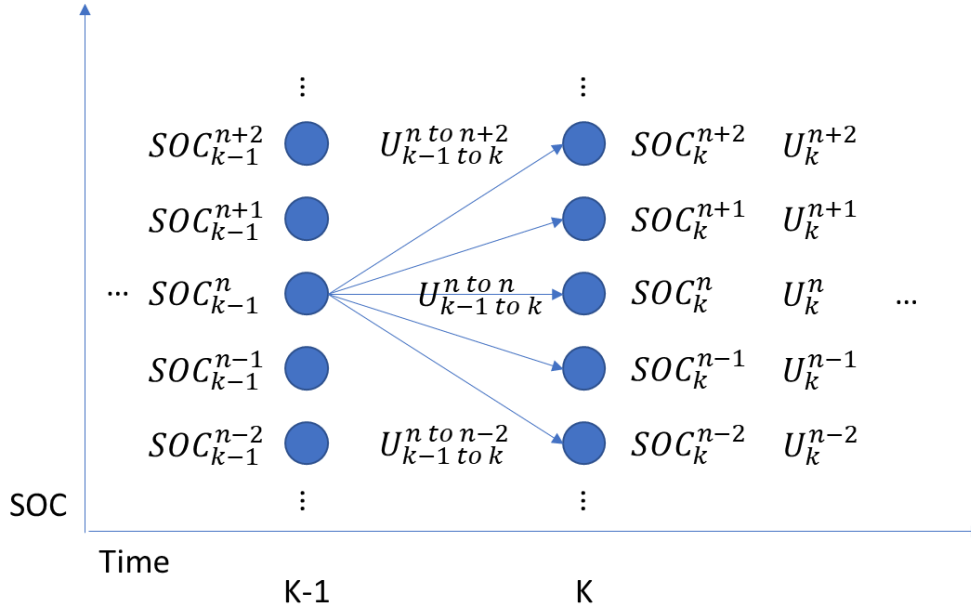


Figure 49: Dynamic programming processes demonstration

The diagram shows two adjacent time steps, each with several available SOC. Assuming the n^{th} SOC in the $k - 1$ stage is under evaluation: the n th SOC can be charged into $n + 2$ or $n + 1$ states, remain unactivated to reach n , or discharged into $n - 1$ or $n - 2$ states when reaching time k . A cost U is associated with each path taken from time $k - 1$ to time k . For each state under time k , a cumulative cost U_k is corresponding to it. Therefore, considering backpropagation, for every single node from the $k - 1$ step, the total cost of moving to every node from k step is $U_{k-1}^i + U_k^i$. A minimum can be found among all possible moves, which will be recognized as the total cost to the specific nodes in the $k - 1$ step. Then, the $k - 1$ becomes the k for the next iteration, and the new $k - 1$ is calculated. When a single start and a single end is given, a unique sequence of the path can be obtained. The sequence represents the sum of all the minimum path costs.

To test different control strategies and compare the potential outputs, two variations of DP are conducted. The control parameters are the NG generator power output, NG engine power output, and the battery power output. The first strategy is to let the NG engines in the parallel subsystem operate at a fixed constant and allow the NG generator and battery to adjust the power output accordingly. Under such a situation, the first layer of the stationary condition is the NG engine output. The engine power output range is selected from 0 to 700 kW, where 0 represents the case when the propellers are electrically propelled, and 700 kW suggests the propellers are powered mechanically. A “for loop” is used to search the whole space. Inside of the first loop, a time and SOC based conventional two-variable DP is performed. For each time constant traced from the back, the algorithm evaluates the possible change of SOC that represents the battery energy input/output. Then, NG generator demand is calculated based on the DG and ESS power. The SOC resolution is chosen to be 0.0002, and the SOC bound for each time is determined by maximum charging and discharging power to eliminate unnecessary invalid calculation. For example, if the algorithm searches the entire SOC space, it will calculate when SOC changes from 0.4 to 0.9. Such a change in SOC in a single time step is not

feasible for a 900 kW generator to a 600Ah battery. Thus, such calculation is omitted for time-saving. The pseudo-code that represents the situation with the fixed NG engine output reads as:

```

1  Initialize the simulation environment, set up the searching boundary
2      for engine power = 100, 200, 300, ..., 900 kW
3      Run simulation to calculate the required discrete-time electric power based on
        the engine power
4      Calculate the maximum and minimum achievable SOC boundary
5      for j = 1:number of discrete-time data point n
6          Set current SOC group SOC(n-j+1) and previous group SOC(n-j)
7          for k = 1:number of SOC(n-j)
8              Calculate ess power based on the change of SOC
9              Calculate NG generator power based on ess power and NG
                engine power
10             Calulcate fuel_consumption(k)
11         end
12         Find the minimum fuel_consumption among k data and its
                corresponding location
13         Add the selection SOC and NG generator power to the (n-j) location
14         Set current SOC(n-j+1) = SOC(n-j)
15     end
16     Calculate overall fuel consumption by simulation
17 end

```

The second method allows the NG engine to continually switch the operation condition along its best operation curve shown in Figure 46. Generally, the embedded NG engine control method is the same as the strategy used in rule-based control, where based on the rotational power demand, the highest efficiency point is selected for power output. The dynamic programming is responsible for searching the optimal NG generator operation profile and the battery input/output. The pseudo-code for the variant NG engine power method is similar to the code listed above, except that the “for loop” in the second line is no longer needed since the engine power is predetermined by the shaft rotational speed demand. Table 5 compares the outcomes of the two illustrated methods. The results compare the quantitative value of the control objective and matching performance.

Table 5: Detailed results comparison of two different dynamic programming strategies

	DP Optimized Control for Fixing Power Output of Parallel-connected Engine	DP Optimized Control for Varying Power Output of Parallel-connected Engine
Fuel Consumption [kg]	148.6	152.6
PHEV Drive Engine Output [W]	500000, Figure 50, (a)	Variant, Figure 50, (b)
NG Generator Output [W]	Figure 51, (a)	Figure 51, (b)
Battery SOC [percent]	Figure 52, (a)	Figure 52, (b)
Power Delivery Performance	Figure 53, (a)	Figure 53, (b)

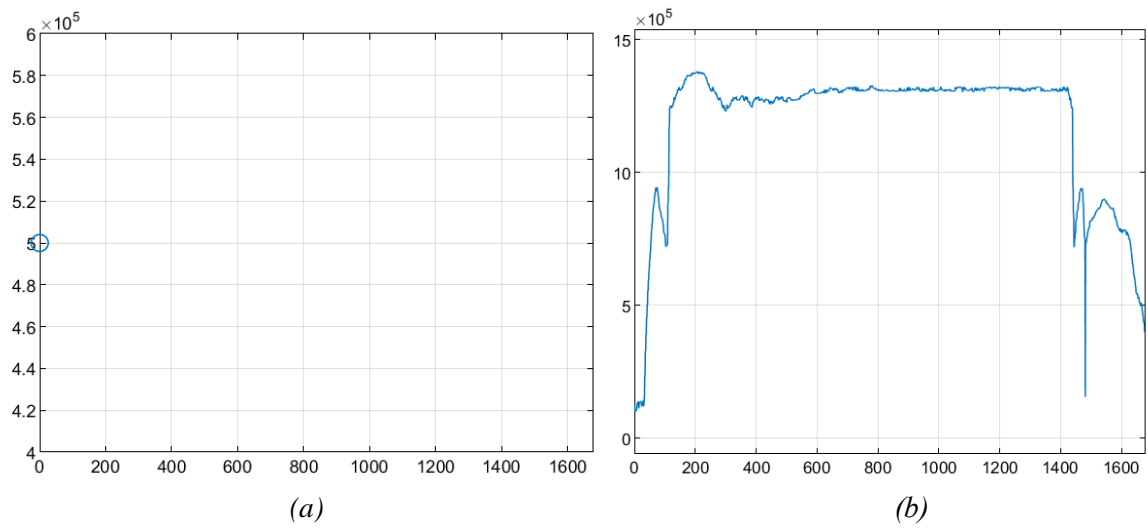


Figure 50: ICE power production comparison between two DP strategies

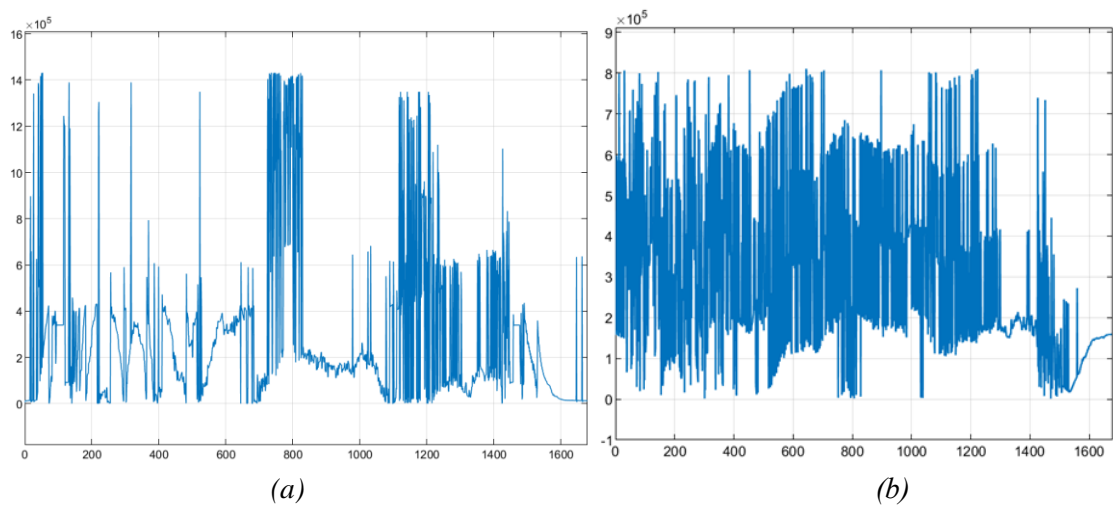


Figure 51: NG generator power generation comparison between two DP strategies

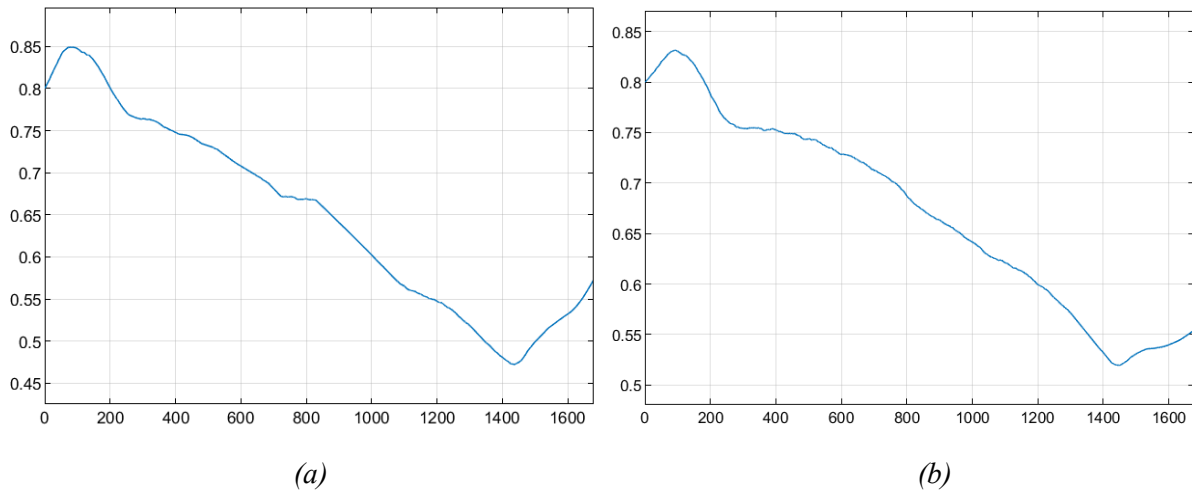


Figure 52: Battery SOC comparison between two DP strategies

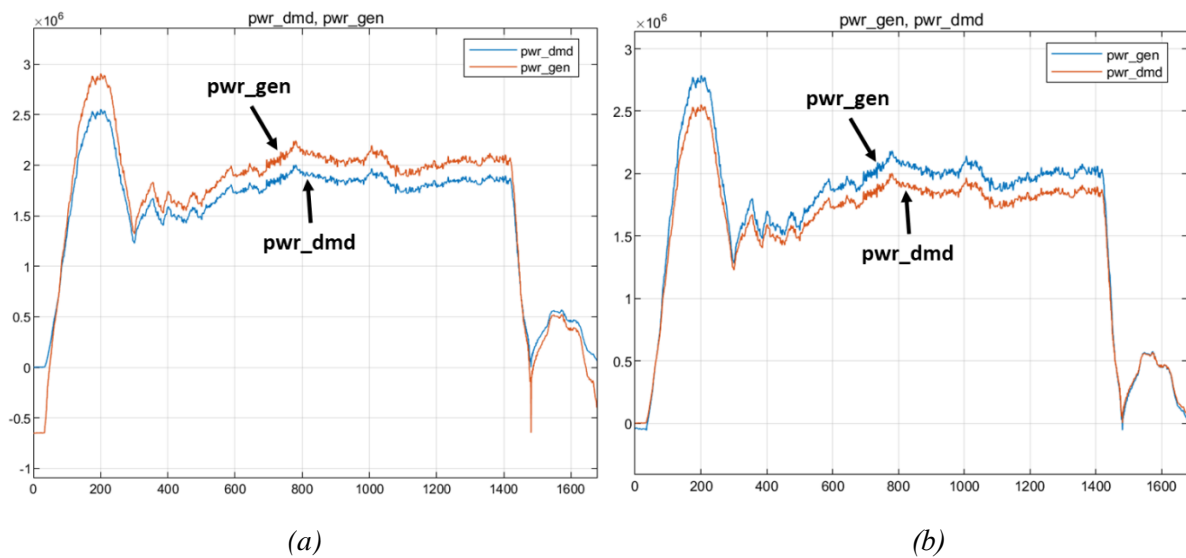


Figure 53: Comparison between simulated power output and recorded power demand for both control strategies. For (a), the red line depicts the simulated power generation, whereas for (b), the red line shows the recorded power demand instead.

5.4. Integrated Propulsion System Design and Control Optimization

A hybrid electric vehicle or ship is a mechatronics system with behaviours determined by the system design and built-in controls. The best energy efficiency and emission reduction potential can only be achieved through the joint optimization of the system design and the control algorithms used to operate the system, as identified in our team's recent research [114]-[117].

The joint optimization aims to achieve the optimal component sizing and the system control strategy simultaneously. Traditionally the component size optimization is conducted first based on a simple power follower control strategy, and optimal control is carried out for the predetermined system design. Such an approach can not guarantee a globally optimal solution [116, 117]. In this work, the same nested global optimization method simultaneously optimizes

component sizes and controls of the fully integrated system.

The nested optimization involves multiple loops of optimization, where the solution of the inner loop algorithm is the parameter for the outer optimization. For the series-parallel system optimization, two layers of optimization are considered. The internal loop search for the best control processes using dynamic programming based on the size parameters. The outer loop uses a global optimization method to optimize the component sizes based on the returned optimal control strategy and results. The selection of the algorithms for both loops is essential to the results. Since the DP produces the absolute optimal control strategy, which outperforms other the reviewed control strategies, it becomes the exclusive selection for the inner loop. The outer loop global optimization has several options. Besides the mathematical (gradient/hessian-based) model and the heuristic (GA, particle swarm method) model, the metamodel is an excellent solution to use.

Metamodelling, also known as surrogate models, is a type of advanced searching based global optimization method. The metamodelling method constructs a computationally inexpensive model to represent the original objective function. Metamodelling algorithms often solve an optimization by sampling in the feasible design space first. After sampling, the sample points are used to construct a mathematical model for the conventional gradient-based optimization method to find the “optimal” candidates and their location easily. After finding the promising candidate(s), further samplings are done in the promising region(s) to update the metamodel for a better representation. The iteration goes on until reaching the stopping criteria. Since the nested optimization's inner loop is the computationally intensive DP, stochastic searching methods like GA will be time-consuming, especially when the number of variables increases. The metamodelling method, on the other hand, only samples the entire workspace once to initialize the surrogate model, for the further iteration, only promising regions are searched. For the outer-loop optimization, the conventional gradient and hessian based mathematical model are not considered as feasible. The main reason is that the objective function for this optimization is the solution of dynamic programming. The model is not strictly convex and linear, which makes the conventional method such as LP and SQP not feasible to run or get caught at the local minimum.

The specific metamodel method selected is the Multi-Start Space Reduction (MSSR) method. Developed by Huachao Dong during his Ph.D. research, MSSR is a surrogate-based search method for global optimization of computational intensive or black box problems [110]. For MSSR, the optimized Latin Hypercube Sampling method is used to select sample points to be evaluated. After obtaining the desired number of sample points, a kriging based surrogate model is constructed. Multi-start SQP is then used to optimize the surrogate model in global space, medium-sized space, and local space. The selected optima are considered new sample points for expensive fitness function evaluation to update the model. The iteration carries to reduce the feasible space size. When the stopping criteria are met (number of allowable objective function computations), the algorithm terminates.

Figure 54 shows the general process flow of the nested optimization used to obtain the optimal component sizes under the best control strategy. It is worth mentioning that the best control strategy corresponds to the control objective mentioned in the previous section which is to

minimize the total equivalent fuel consumption. With different control objectives, the inner loop solution varies, influencing the component size results from the outer loop. In the integrated design, additional conditions are considered on top of the control strategy for the original preliminary design and optimization.

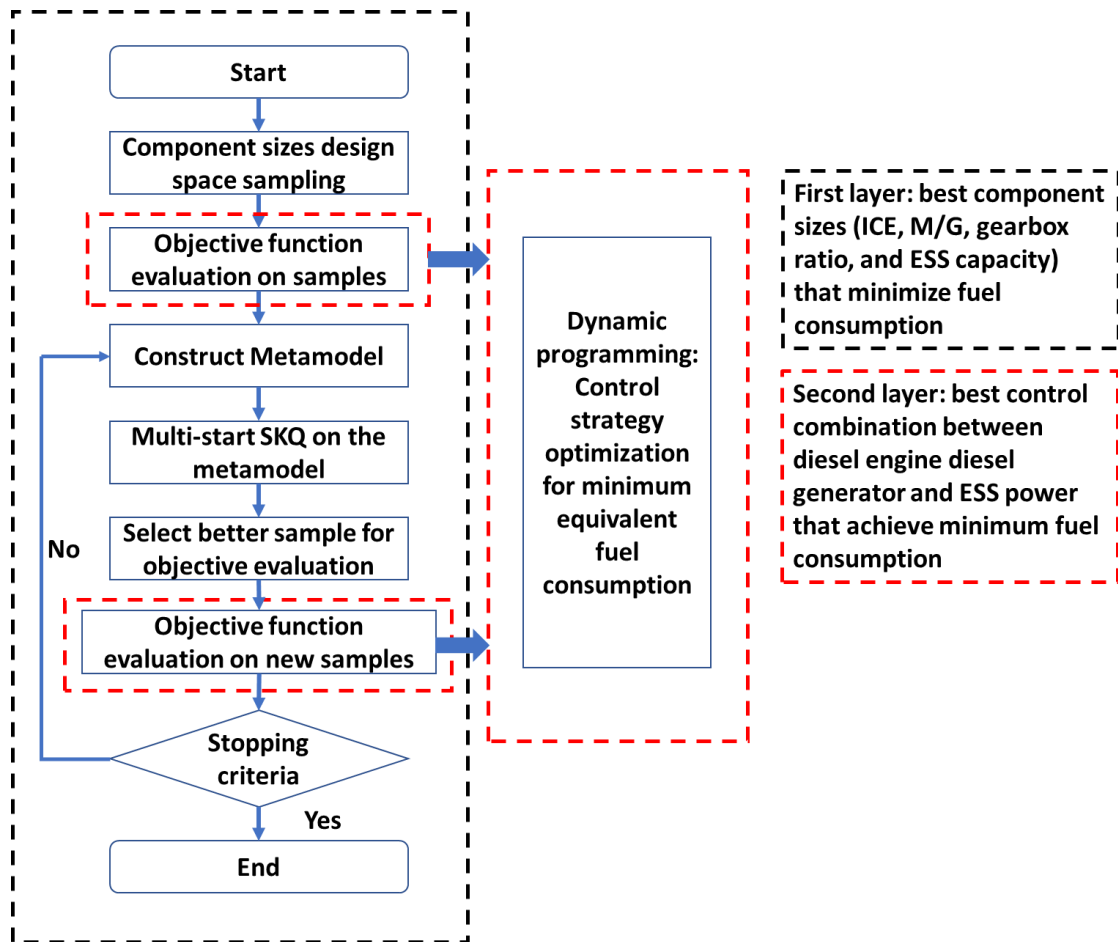


Figure 54: Flowchart demonstration of nested two-layer optimization. The outer layer utilizes the multi-start space reduction surrogate method, whereas the inner loop uses dynamic programming.

First of all, equivalent fuel consumption is considered. The equivalent fuel consumption method is a well-established optimization method for hybrid electric system optimization. Introduced by Paganelli *et al.* [108], the technique has been tested thoroughly. The newly constructed objective function assumes that consuming electric energy is equivalent to consuming fossil fuel since the ESS is charged through NG-electric generation. Of course, such consideration is built up on top of the assumption that the ship is not plugged in through cold ironing during docking. Otherwise, if the ESS is charged after each sailing cycle, the optimization method can favour electric propulsion. If considering external charges, another layer of complexity for total equivalent energy can be considered. However, such consideration is beyond the scope of the current stage of the study. The plugin or battery swap will be considered in future work. The idea of the equivalent consumption in this study is that spending electric energy from the ESS is translated into the same amount of fuel when considering the energy content. On the other hand, burning additional fuel for electric generation at the current time step will reduce the fuel expense for the future time step since electric energy is stored in

ESS. After considering the equivalent consumption methods, the algorithm can determine the balance among burning fuel for ICE propulsion, consuming fuel for ESS charging, and using ESS charges for propelling.

Furthermore, to ensure that the system does not favour electric propulsion since fuel consumption is the main objective to minimize, the battery degradation and corresponding penalty are considered objective. The battery degradation model used in this study is initially developed by Wang *et al.* [61] based on the equations established by Bloom *et al.* [52]. Calibrated by Song *et al.* [111], the battery power is substituted into the degradation model to yield the final capacity loss throughout the crossing. A penalty is then applied to the amount of degradation and added to the final equivalent fuel consumption. At the current stage, a heuristic penalty function is used. Since the degradation amount for each crossing is small, a multiplier is used to bring the capacity loss to the same order of magnitude as the fuel consumption. Ideally, such a penalty function needs to be selected with caution since a large penalty will lean towards the ICE mechanical drive. Typically, the penalty multiplier is optimized through a global optimization algorithm. However, because the current optimization method is a nested optimization, an additional objective is not considered. Alternative methods for obtaining adequate penalty value will be tried in future studies.

Since two control strategies are tested during the DP processes illustrated in the previous section, both methods are continuously tested and optimized for the final design. As introduced, the first strategy considers a fixed power delivery for the NG engines in the parallel configured aft propeller set. In comparison, the second method allows variant engine power output, which is similar to the internal control strategy during the rule-based control. The former puts the engine in a fixed operating point so that the NG generator and ESS work jointly to cover the power demand fluctuation. The latter allows all three devices to respond to the varying power demands. The former's advantage is that the engine efficiency remains at a single high point during the entire crossing. This strategy is beneficial since the NG engine suffers from low efficiency during the departing and approaching phase. However, such management shifts the burden to the NG generator since it has to shift operation conditions. The latter is the complete opposite situation where NG generator can remain in a high-efficiency zone for electric generation, and the engine operation points vary with the power demand.

Table 6 compares the final results after the nested optimization. For the system, the gearbox ratio in between the parallel-configured ICE and output shaft is not optimized. That is because only the torque is scaled during engine scaling. The engine output speed will remain unchanged for all considered combinations in DP. Thus, a fixed gearbox ratio of 5 is used to step down the engine speed to ensure the engine operates at the highest efficiency zone.

Table 6: Simulation results of two nested optimizations using fixed ICE power output strategy and variant ICE power generation

Parameters	Explanation	Upper Bound	Lower Bound	Fixed Parallel-connected Engine's Power Output	Variant Parallel-connected Engine's Power Output
DieGenScale	The ICE scale factor of the NG generator set based on a 2000kW model	2	4	3.120686	3.66
DieGengb	Gearbox ratio between the NG engine and generator	1	3	1.982316	1.8074
DieGenMotScale	generator scale factor of the NG generator set based on a 2000kW model	1	2	1.823520	1.5629
PHEVengScale	The engine scale factor for ICE used in the parallel drive	2	3	2.340012	2.4323
PHEVmotScale	The motor scale factor for the electric machine used in the parallel drive	1	2	1.776608	1.2902
PHEVgbMRatio	Gearbox ratio for the motor in parallel drive	4	7	4.188485	4
SHEVmotScale	The motor scale factor for the electric machine used in the series drive	1	2	1.387967	1
SHEVgbRatio	Gearbox ratio for the motor in series drive	4	7	5.363653	6.1043
V_ess	Battery pack voltage [V]	600	900	753.6112	710.9279
E_ess	Battery pack capacity [Ah]	500	800	616.2959	555.9510
Total equivalent fuel consumption [kg]				139.6	147.5

Figures 54, 55 and 56 show the simulation results after the joint optimization. The figures on the left show the results from the fixed parallel engine generation designs and the figures on the right present results from the flexing parallel engine output. Figure 55 shows the NG generator operation curve that reflects the optimal control strategy. The horizontal axis shows the time in second, and the vertical axis indicates the NG generator power in Watt. The simulation's time step is one second; thus, the resultant output power of the NG generator changes every second. However, an NG engine with a slower dynamic response is not ideal for operations under constantly changing power demand alone. Hence, a time constraint is added to limit the minimum engine operation time. Figure 56 shows the limited operation time considering 60 second time window by applying a 60-second long zero-order-hold during the simulation. During the held time frame, the engine output value is maintained at the same level.

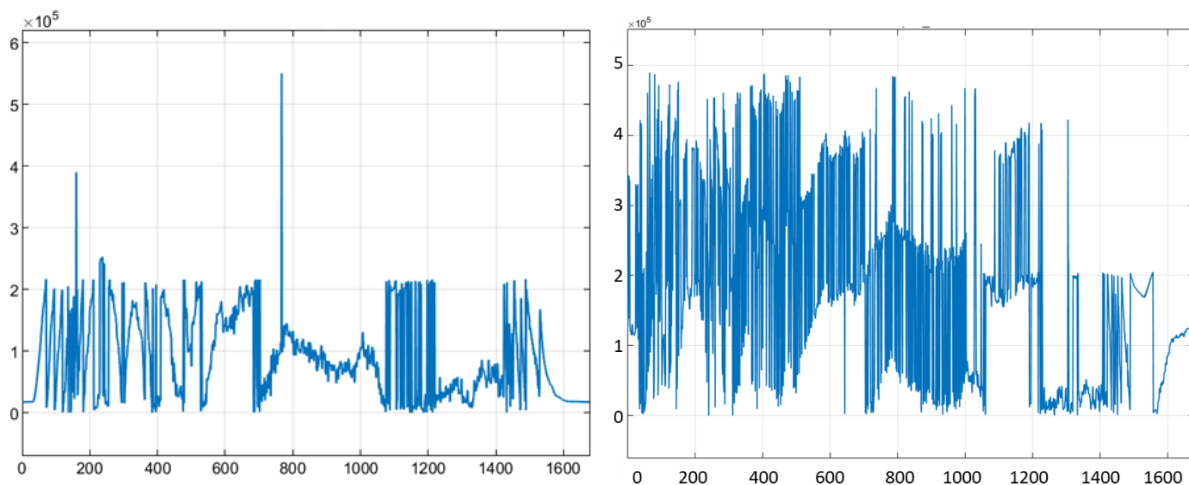


Figure 55: NG generator power production for two different control strategies. The left figure shows the fixed ICE power generation variation, and the right figure indicates the flexible ICE outputs variation. The horizontal axis shows the time steps in second. The vertical axis shows the power output in 10^5 W.

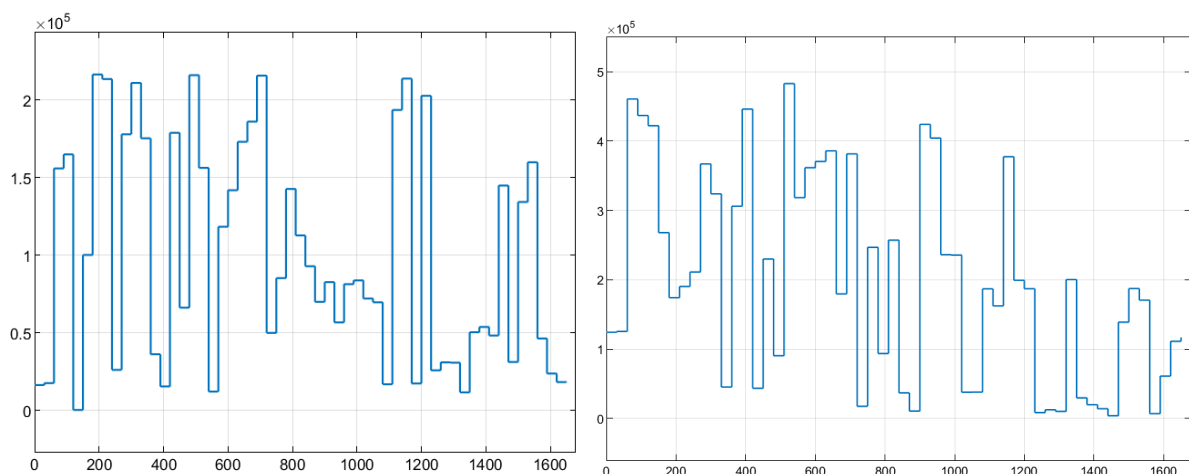


Figure 56: NG generator power profile filtrated using a 60-second moving average filter.

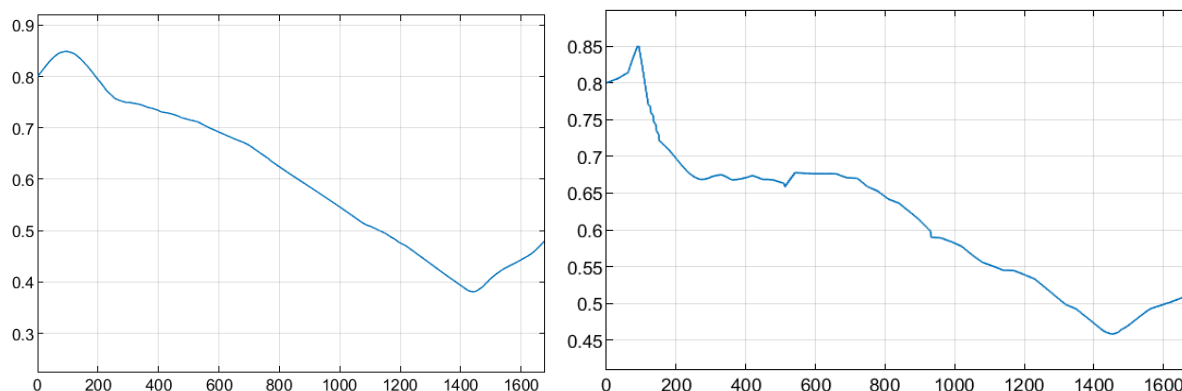


Figure 57: Battery SOC profile comparison between control strategies.

Figure 57 shows the battery SOC during the entire simulation. It is worth noting that although the DP limits the final SOC to be 60 percent, the final SOC demonstrated in the results is lower than the limit. This is due to the applied hold during the simulation. After applying the hold, the generator's high power output stage may be replaced by a low-level hold value, which results in insufficient generator output. Such shortage is covered by the battery, which in consequence, the final battery SOC is lower than the applied limits.

The yielded fuel consumption results are similar. Compared to all the benchmark models, the designed series-parallel configurations' fuel consumptions fall between the series and parallel hybrid drive. However, since the battery degradation is not considered during the benchmark modelling, the active designed configuration could have better performance than all the other benchmark configurations. The signature properties of the series-parallel hybrid configuration are not reflected in this first stage benchmark modelling. Ideally, more complex control that regulates the fore, aft, and all propeller drives can boost fuel consumption performance.

Currently, the only control and optimization objective is the equivalent fuel consumption, which is adequate for the first stage proof of concept but can be too narrow for advanced system design. Analogy argues that the less fuel is consumed, the less overall emissions will be generated. Such consideration is valid when considering minimizing the total amount of emissions; however, the situation can be different in terms of specific pollutant content in the emissions. When two configurations A and B are compared, the total amount of emissions, measured in kg for example, of configuration A can be less than the amount of emission from B, but the total amount of harmful emissions from B, NO_x and SO_x , for instance, may outnumber the same pollutant from A. It is inevitable that based on the different situations, the definition of harmful emissions varies. For some conditions, low GHG and hydrocarbon emissions are the top priority, whereas NO_x , SO_x , and PM need to be strictly regulated. Thus, the equivalent fuel consumption for this functional design considers the general case. When specific requirements are raised, the optimization objective needs to be changed accordingly for the best system size and control strategy.

The simulation estimates the ship velocity based on the thrust generation and ship hydrodynamic model. Figure 58 compares the simulation obtained ship velocity and actual ship velocity from VDR. In the diagram, the vertical axis indicates the velocity in m/s, and the horizontal axis represents the time in second. The blue line in the graph shows the simulated

results, contrasting the recorded velocity shown in red. Two significant regions of difference can be observed. For the large area of difference, which occurs during the “constant speed” cruising phase, the primary reason for such a difference is the lack of wind resistance representation in the hydrodynamic model. The used ship hydrodynamic toolbox is developed and masked by Fossen [112]. The block cannot be modified with additional wind resistance. In order to make the comparison, the wind resistance effect is temporarily removed from the LOM, and the velocity difference after removing the wind resistance is depicted in Figure 59. It can be observed that, after removing the wind resistance, the velocity difference reduced from 60 percent to 20 percent on average during the cruising phase.

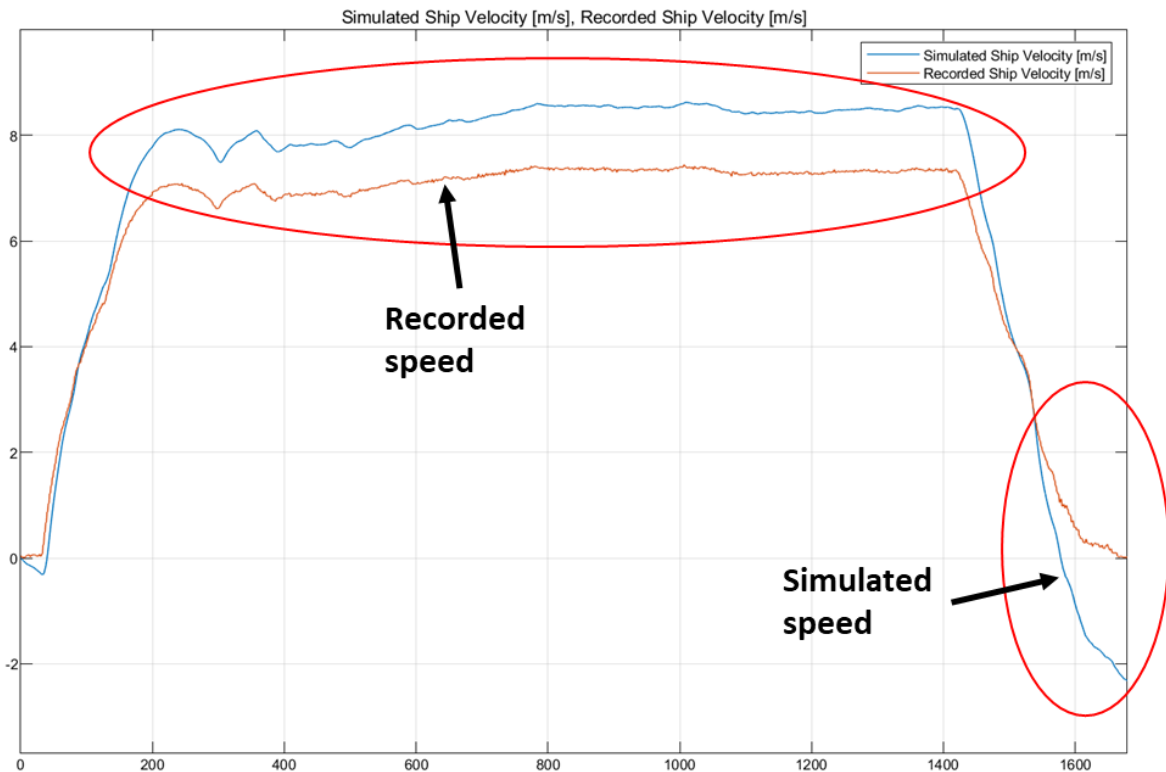


Figure 58: Comparison between simulated ship velocity and the VDR recorded velocity data. The red line shows the recorded sailing data, and the blue line indicates the simulated ship velocity. The horizontal axis shows the time in [second] and the vertical axis shows the speed in [m/s].

Another major region of velocity difference is near the approaching and docking phase. From the diagram, the predicted velocity changes direction after reaching a complete stop. This behaviour suggests that the counter thrust is so large that the vessel is pushed back after stopping. The main reason for such strange behaviour is the large deceleration demand. As aforementioned, the ship experiences a total resistance force and a total thrust force and results in mass acceleration. Since the velocity is the only input to the system, as the ship’s velocity reduces, the ship encounters a diminishing resistance. The resultant mass acceleration dominates the low-order thrust model. Thus a large negative (reverse of surge direction) propulsion force is generated. Once input into the hydrodynamic model, the velocity reverses in direction due to the large counter force.

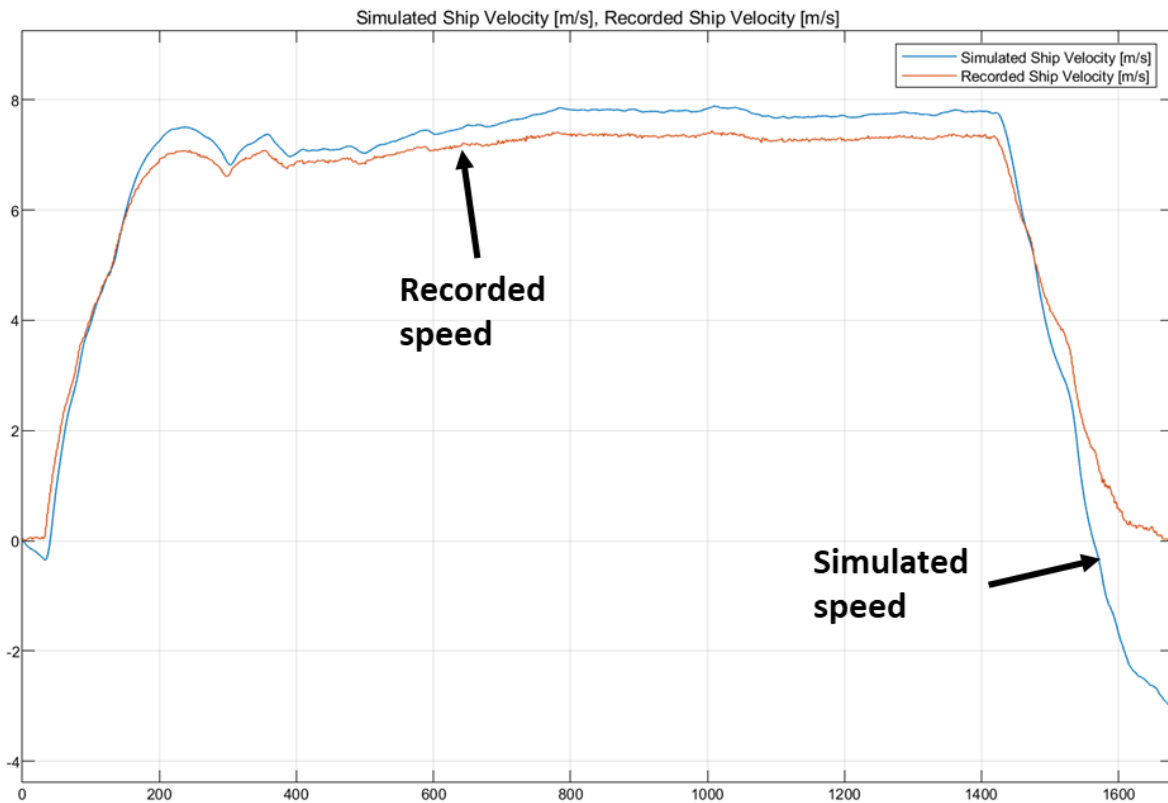


Figure 59: Improved simulated ship speed comparing to the recorded ship speed.

The potential reason for such mismatch is the resistance prediction error during approaching or hydrodynamic model error. As mentioned in Chapter 3 of the thesis, the M-LOM resistance model mainly relies on the ship's speed. During the approaching phase, the ship's velocity reduces, and consequently, the predicted resistance reduces. When the resistance reduces, a counter-thrust is needed to fulfill the large deceleration demand, which can lead to the reversed velocity as the counter thrust is over predicted. On the other hand, the hydrodynamic model block may not fully represent environmental conditions. One noticeable lack is the wind resistance shortage in the dynamic model. Lastly, the overall simulation generalizes the wind, current, and wave resistance in an open water condition. Such generalization can represent the constant cruising phase well, which can be proven from the matching predicted vessel speed; however, the water condition is more complicated during departing and docking. At nearshore, the water becomes shallow, where propeller thrust can cause current and vortexes. Such water conditions may introduce additional resistance forces on the ship's body. Such additional resistance is not detailedly modelled in either the M-LOM or ship CFD data used in the hydrodynamic tool block. All of these mentioned shortages contribute to the mismatches, especially during the nearshore sailing period. To resolve the error, a PID controller is added to the model to interrupt and regulate the thrust generation, directly affecting the system output.

The implemented ship speed control is a PID controller (shown in Figure 60) that takes the predicted (achieved) ship speed as feedback and compares it to the reference recorded speed. Although the controller is implemented in the Simulink environment, where a PID control toolbox is available, the modulized block and tuning method is not used. Instead, a manually

constructed PID is used in the model and tuned using an optimization method. The optimization method searches for the best K_p , K_i , and K_d combination that minimizes the sum of the absolute error between the reference ship speed and predicted speed.

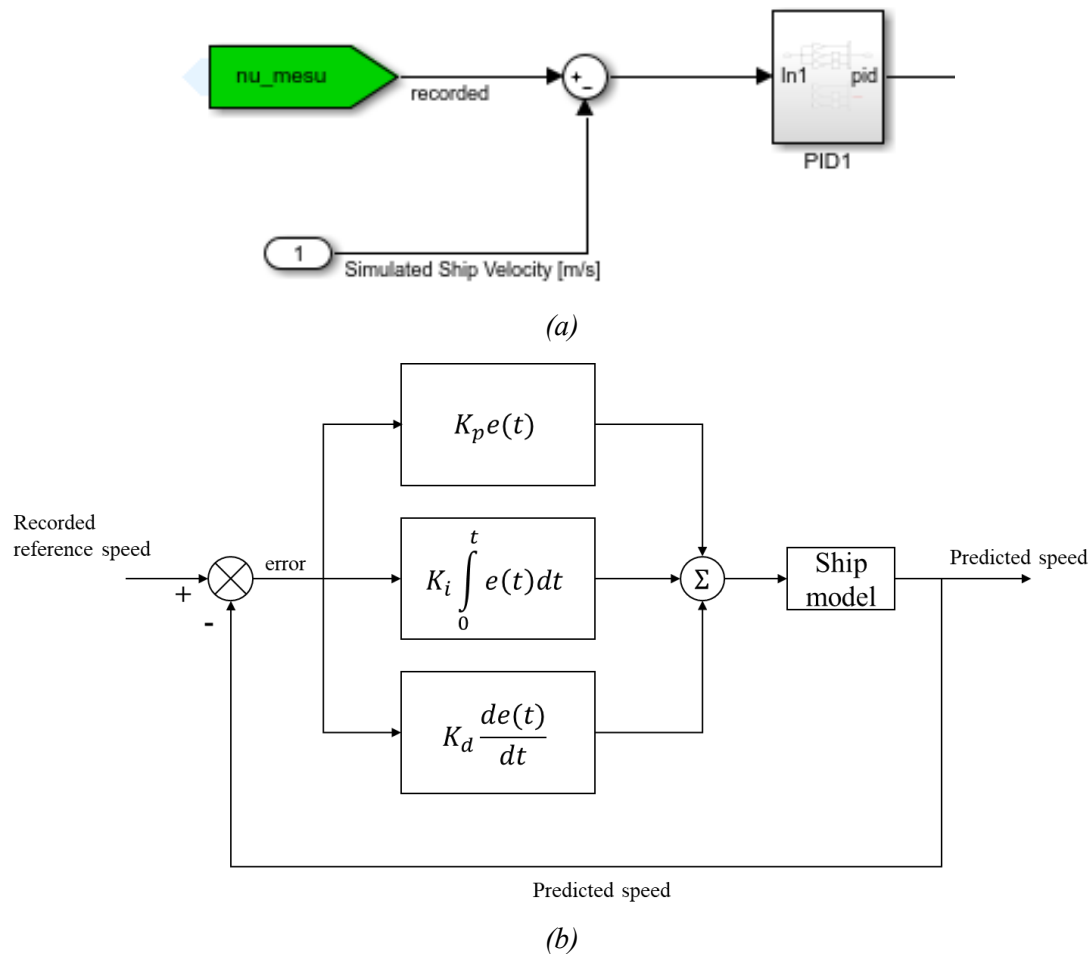


Figure 60: Ship “helmsman” speed PID controller implementation

Figure 61 shows the speed simulation results after implementing the PID controller. The blue line shows the simulated ship speed, whereas the dashed red line indicates the recorded ship velocity. It can be observed that, after the implementation, the speed prediction accuracy increased drastically. On average, the absolute error is 3 percent. The PID controller serves as a ship’s master to a large degree, “who” controls the power output in order to achieve ship speed that is close to the desired reference speed.

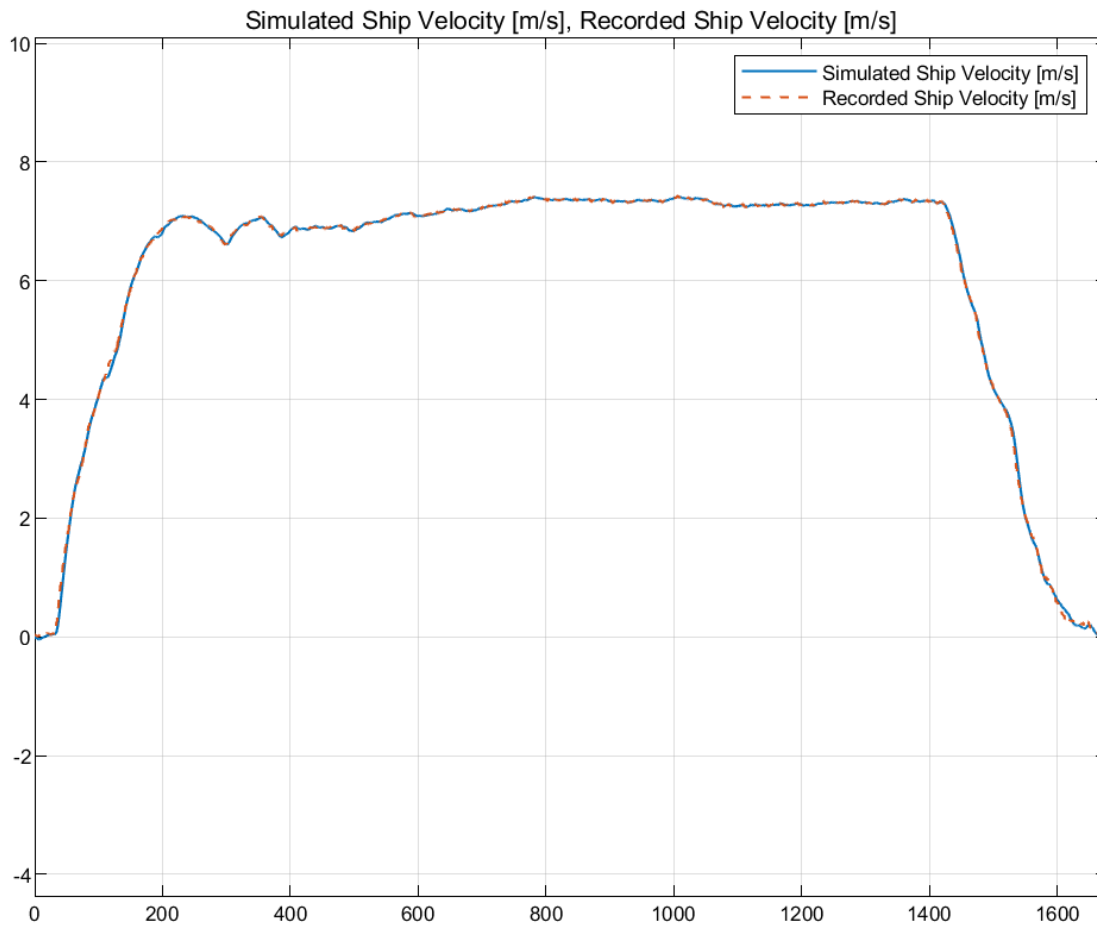


Figure 61: Speed controller module regulated ship speed in comparison to recorded ship speed.

The “captain” control model is not originally intended to be modelled in the system but only tested here to check the system's closed-loop response and prediction performance. The initially simulated model focuses on open-loop performance since the central area of interest is to use M-LOM in integrated model-based system design and its ability to predict the propulsion power accurately. Meanwhile, with the additional ship hydrodynamic model in place, the simulation aims at testing the feasibility of system design using only speed data. Suppose the controller is modelled at the beginning, the potential errors caused by the LOM and benchmark model may be veiled since a properly designed closed-loop control can always regulate the system input to yield the current speed output. Meanwhile, unlike the ground vehicle driver model, the ship’s captain or helmsman model is hard to model. The active PID control model represents a “delicate” captain model “who” controls the system strictly close to the desired ship speed. However, a real captain may pilot a ship based on personal preference or experience. For example, the captain may ramp up the power output and let the system reach its desired speed slowly or cut off the power completely to allow ship cruising during docking. Such a control method achieves the final control goal, but the response time and overshoot may vary significantly from the reference. The implemented PID controller is currently tuned optimally so that no noticeable overshoot and delay can be found in the final speed output. However, such a controller requires constant manipulation of the power output, causing undesired power fluctuation. Figure 62 shows the shaft power, torque, and speed demand. It is evident that the

demand is not smooth, and such constant changes can damage the power output devices such as motors and NG engines. A filter can be applied to the system to eliminate the peaks, but the absolute error is increased to 6 percent.

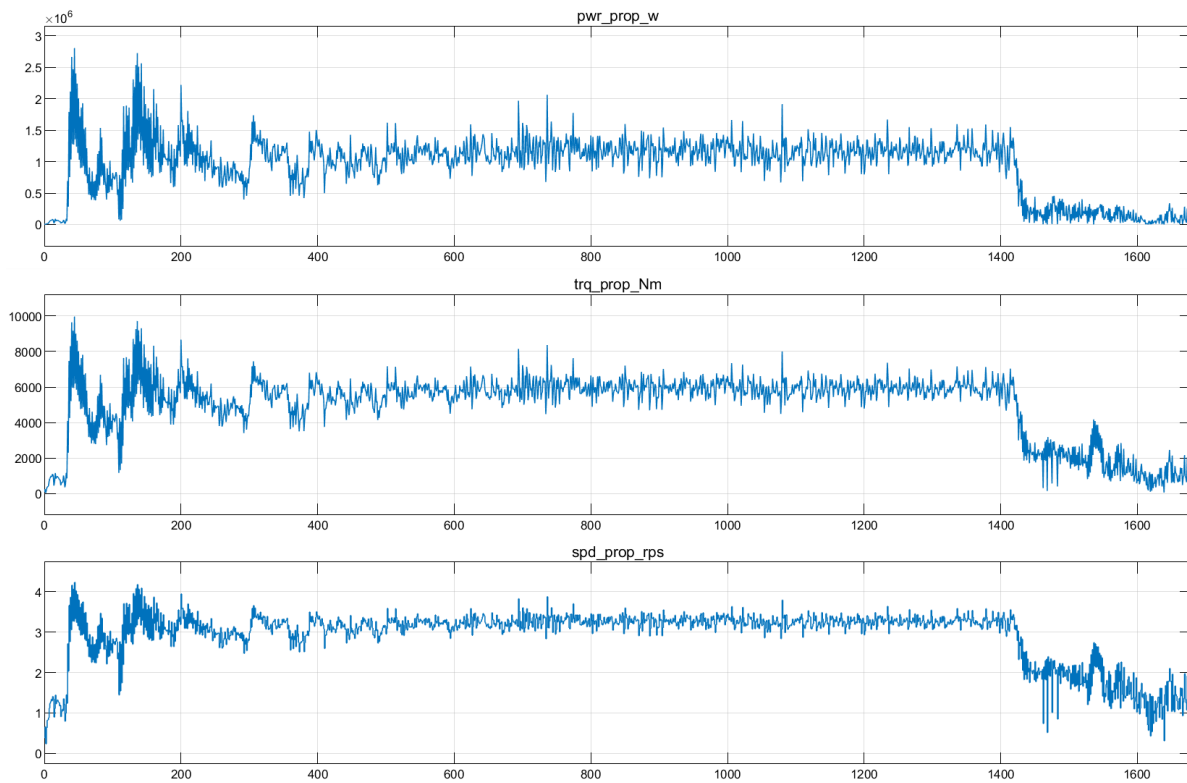


Figure 62: Predicted shaft power, torque, and speed demand after PID controller implementation. It can be observed that the demands experience constant fluctuation. A filter is required to eliminate the peaks so that the components, such as motors and ICEs, can run smoothly without damaging them.

Chapter 6. Conclusion and Future Works

6.1. Summary

This thesis first reviewed the hybrid-electric propulsion system and its potentials on ships and vessels. Since the propulsion system of vessels is similar to ground vehicles, the application of HEPS to ships is feasible and has enormous potential for fuel efficiency improvements and emissions reduction. However, with all advantages illustrated for hybrid-electric ship applications, the main challenge is to predict the ship's shaft power demand during the mission. Thus, the thesis looks into the ship's power profile prediction methods and develops an improved vessel's speed and stability-data-driven, modified low-order model (M-LOM) for hull resistance and propeller thrust. Compared to the conventional power prediction methods, M-LOM combines the one-pass CFD and stability-data-driven regression model to ensure the power prediction accuracy and short computation time. To test model performance, the M-LOM is then used for the benchmark comparison of vessel propulsion systems. Conventional NG engine-mechanical, NG engine-electric, pure electric, series hybrid electric, and parallel hybrid electric propulsion systems are modelled for the BC Ferries' vessel Skeena Queen (SKQ). The study proved the M-LOM's functionalities in predicting vessel power demand and demonstrated the feasibility and benefit of applying hybrid electric technology on a ferry ship. With the benchmark propulsion system models and the M-LOM, an integrated series-parallel hybrid-electric propulsion system was designed for the SKQ for fuel consumption and associated CO_2 emission reduction. Using a nested two-layer optimization method that combined DP and the MSSR global optimization algorithm, the system's optimal component sizes and control strategy were identified.

The optimization also considered the equivalent fuel consumption when using the battery ESS and the additional cost penalty from battery performance degradation. With the optimal component sizes and control strategy, the hybrid electric propulsion system design consumed 139 kg of fuel during the entire simulated sailing trip, an 18.2 percent and a 38.4 percent improvements compared to the optimized NG engine-mechanical and NG engine-electric systems, respectively. The M-LOM was validated by substituting the predicted power profile into a 6-DOF ship hydrodynamic model representing the SKQ for ship speed prediction. The yielded ship speed was compared to the recorded ship speed. Without a speed controller model, the open-loop result had a 20 percent average absolute error. The closed-loop simulation that used a PID controller to function as the "captain" of the vessel reduced the error to 6 percent (for filtered results) and 3 percent (for unfiltered results), compared to measured vessel speed data.

The results suggested that M-LOM could accurately predict the ship's shaft power demand. Meanwhile, the hybrid electric propulsion system could achieve improved fuel consumption with optimal component sizes and control strategy compared to the conventional ship propulsion technologies.

6.2. Conclusions

The environmental issue is getting severe, which requires immediate action. As a larger contributor to GHG emissions and air pollution, the transportation sector has become the main focus for implementing clean transportation propulsion technology. Maritime activities also contribute to significant air pollutions, and the cost benefits of clean marine transportation are higher than the automotive industry, making research on reducing maritime pollution necessary and urgent. Meanwhile, successful clean propulsion technologies can be transferred to the marine sector to accelerate progress.

Hybrid electric propulsion technology, primarily implemented in automotive applications, has proven its benefits towards fuel and emissions reduction. Configured with series, parallel, and series-parallel, different powertrains architectures better suit various applications. The maturing model based design (MBD) technique, which accurately predicts the performance, fuel economy, and emissions of a hybrid electric vehicle, made the development and optimization of hybrid electric powertrain systems and corresponding controls possible. Since the ship's mission cycles vary greatly, a specific design is needed for each application.

Traditional marine propulsion systems are based on diesel-mechanical or diesel-electric drives, and the diesel hybrid electric drive with a battery ESS is becoming a popular design choice for new vessels. Other clean engine and propulsion system technologies are also quickly maturing for commercial applications, including NG compression ignition (CI) engine, LNG, hydrogen fuel cells, large electric propulsion motors, marine propulsion battery ESS, DC power bus and efficient power converters, and hybrid electric propulsion system (HEPS).

Due to the diversified hull/propulsor design and operation cycle, the development of a hybrid electric marine propulsion system demands the model-based design and control optimization for each unique and small batch production vessel. The integrated design and control optimization further require accurate and computation efficient hull resistance and propulsor thrust calculation methods that can be used to predict needed propulsion power and gauge vessel performance, energy efficiency, and emissions. This research focused on improving the low-order Holtrop and Mennen's hull resistance regression method and propulsor thrust models in the longitudinal direction by extracting model parameters from one-pass computational fluid dynamics (CFD) simulation and testing the acquired models in integrated design optimization of the marine propulsion system. The model is implemented in MATLAB/Simulink and ANSYS Aqwa and validated using operation data from BC Ferries' ship Tachek. The modified low-order model and calculation method as well as the surging power deduced model (M-LOM) was then used in the integrated optimizations of propulsion system component sizes and operation control strategies for another BC Ferries' ship, Skeena Queen. The performance, energy efficiency, and emissions of various propulsion options, including NG-mechanical and NG-electric benchmarks, and hybrid electric alternatives of series hybrid, parallel hybrid, and battery/pure electric systems were compared to demonstrate the benefits of the new method in completing these complex tasks and hybrid electric marine propulsion. The test results showed that the M-LOM could accurately predict the propulsion power demands to define the design target of various hybrid electric marine propulsion systems without the computation-intensive full-scale CFD simulations, as in the past work of the

research team in using the numerical simulations, and reduced-order hydrodynamics model [29].

Application of the new M-LOM and the model generation method to the integrated modelling, design, and control optimization showed the feasibility for carrying out the global optimization of the hybrid electric marine propulsion system with minimum design inputs of vessel hull/propeller geometry and expected operation speed. The combination of the vessel propulsion demand prediction, propulsion system design, and control optimizations makes MBD and model based optimization (MBO) feasible and beneficial design tools. The new approach allowed different marine propulsion technologies to be fairly compared for a given marine application and specific vessel hull and propeller design to identify the optimal propulsion system design and controls.

The quantitative vessel performance and energy efficiency evaluations using the newly developed modelling method and simulation tools allowed different vessel propulsion systems to be compared at the early design stage, supporting the critical design and investment decisions. The simulation results from the Skeena Queen showed significant energy efficiency improvement and emission reduction, effectively illustrating the benefit of hybrid electric marine propulsion technology.

The research formed a foundation for further studies to achieve more accurate propulsion demand prediction and a more comprehensive lifecycle cost assessment of clean marine propulsion solutions. The newly developed modelling method and tools will also support more comprehensive hybrid electric propulsion design optimization and intelligent real-time optimal control research in the future.

6.3. Research Contributions

In this work, an improved low-order hull resistance/propeller thrust model and model building method for ship propulsion power prediction is introduced and validated. The new model and calculation method is then applied to the benchmark study on a representative BC Ferries' ship, Skeena Queen (SKQ) ferry, to perform the integrated series-parallel hybrid electric propulsion system design and control optimization. The detailed research contributions include:

- The research developed the improved stability and speed data based M-LOM for calculating ship hull resistance, propeller thrust, and the ship's propulsion power demand. Aiming at generating the power profile based on the minimum amount of vessel operation data, the M-LOM can generate ships' power profile using only the design speed and the CAD model of the vessel. The newly introduced M-LOM avoids extensive numerical computation and ensures good accuracy by combining the conventional regression method and the one-pass CFD on hull and propellers.
- The work validated the M-LOM and model generation method using acquired vessel operation data from BC Ferries' ship, Tachek, and the verified hydrodynamic model of BC Ferries' ship, Skeena Queen, to prove the feasibility and accuracy of the modified LOM and model generation method. The operation data and verified hydrodynamic model were obtained and created by the UVic Green Transportation team in recent years.

- The study introduced propulsion system models for the ferry ship, Skeena Queen, including the conventional NG-engine mechanical/electric drive, hybrid electric drive, and pure electric drive. By examining their equivalent fuel consumption, these models provide a quantitative comparison of fuel efficiency and emissions among different vessel propulsion options. The models and comparison prove the feasibility and benefit of a hybrid-electric propulsion system for midsized passenger and vehicle ferries and provide an excellent start point for future research and developments.
- Modelling and designing a series-parallel hybrid propulsion system for SKQ utilizing the vessel's propulsion power profile obtained from the M-LOM under given vessel speed were carried out. A comparison is made between the predicted vessel speed of the modelled hybrid electric vessel and the recorded speed of the vessel to examining the accuracy of the integrated propulsion system model.
- The research has carried out integrated design optimization of key powertrain component sizes and vessel's operation control to achieve the minimum equivalent fuel consumption (EFC), using a nested two-layer optimization method. The EFC accounts for fuel consumption cost, battery electricity equivalent fuel consumption cost, and battery performance degradation associated cost. The nested optimization combines the traditionally separated design optimization on the sizes of the key hybrid electric propulsion system and control optimization on the operation of the propulsion system. The joint optimization searches for the best control for each variant powertrain component size combination to achieve the optimal system design and control solution.

6.4. Future work

To further develop the M-LOM as well as the fully integrated design, several improvements can be introduced in the future.

- Ideally, the low-order model should capture 3 DOF, including transverse, longitudinal, and yaw (or surge, sway, and yaw). At present, the M-LOM only calculates drag in sailing direction (transverse direction). Additional DOFs can be added to improve the model accuracy and, more importantly, the model's robustness. Since the model contains only 1 DOF, it works the best for the ship with fix-angle propellers. The propellers' angle needs to be considered to improve the model's prediction performance for vessels with azimuth drive.
- A better CFD or regression model is needed for low-speed hull resistance and shaft power prediction. The open-loop results reveal that the error of the yielded results is relatively large when the vessel is departing and approaching the dock. Since the model assumes open water conditional for the entire sailing trip, a better modelling approach is needed to capture the dynamic behaviours of the vessel at low-speed or during maneuvering to accurately account for the associated propulsion power/energy.
- In the integrated propulsion system, the models on total equivalent fuel consumption need to be improved. At present, the simulation is only based on one simple mission cycle in which the battery degradation is relatively small. Meanwhile, the penalty parameter is intuitively selected. These penalty functions need to be improved

especially during a lifecycle assessment.

- Lifecycle assessment needs to be conducted for both the benchmark vessel propulsion system and the new series-parallel electric propulsion system. Currently, the choice of the equivalent conversion factor balances the usage of NG fuel and electricity. In addition, the initial investment costs, and long-term maintenance cost, and a better battery performance-degradation/life-shortening associated penalty cost should be included.
- At present, emission reduction is limited to the GHG that is proportional to the fuel consumption. A more comprehensive objective function of the design optimization that covers all emissions can be introduced. Hydrocarbon (HC) and carbon monoxide (CO) emissions are a significant issue for NG fuelled compression ignition engines; an additional measure for reducing the separated HC and CO emissions is thus needed on top of the existing total fuel consumption minimization.
- In the nested two-layer optimization, the optimal control strategy is obtained through dynamic programming (DP). The approach produces the best control strategies through intensive optimization search. However, the off-line method cannot be applied in real-time control operation when the vessel departs from the “standard sailing mission cycle” in real operation. An intelligent, real-time optimal control method that is based on vessel operation pattern recognition and operation-pattern and DP based optimal control strategies is needed.

Reference

- [1] O. US EPA, “Global Greenhouse Gas Emissions Data,” *US EPA*, Jan. 12, 2016. <https://www.epa.gov/ghgemissions/global-greenhouse-gas-emissions-data> (accessed Mar. 04, 2020).
- [2] “Everything You Need to Know About the Fastest-Growing Source of Global Emissions: Transport,” *World Resources Institute*, Oct. 16, 2019. <https://www.wri.org/blog/2019/10/everything-you-need-know-about-fastest-growing-source-global-emissions-transport> (accessed Mar. 04, 2020).
- [3] “Shipping Pollution,” *Oceana EU*. <https://eu.oceana.org/en/shipping-pollution-1> (accessed Jan. 13, 2020).
- [4] J. Nedwidek, “Ferry Industry Facts,” *Interferry*. <https://interferry.com/ferry-industry-facts/> (accessed Sep. 03, 2020).
- [5] “Traffic Statistics System - Total Vehicle and Passenger Counts by Route for July 2020,” BC Ferries, STTR 190, Aug. 2020. Accessed: Sep. 03, 2020. [Online]. Available: https://www.bcferries.com/files/AboutBCF/traffic_stats/July_2020_Traffic_Stats.pdf.
- [6] “GHG Emissions.” <http://www.imo.org/en/OurWork/Environment/PollutionPrevention/AirPollution/Pages/GHG-Emissions.aspx> (accessed Jan. 13, 2020).
- [7] L. van Biert, M. Godjevac, K. Visser, and P. V. Aravind, “A review of fuel cell systems for maritime applications,” *J. Power Sources*, vol. 327, pp. 345–364, Sep. 2016, doi: 10.1016/j.jpowsour.2016.07.007.
- [8] L. K. C. Tse, S. Wilkins, N. McGlashan, B. Urban, and R. Martinez-Botas, “Solid oxide fuel cell/gas turbine trigeneration system for marine applications,” *J. Power Sources*, vol. 196, no. 6, pp. 3149–3162, Mar. 2011, doi: 10.1016/j.jpowsour.2010.11.099.
- [9] “Air Pollution.” <http://www.imo.org/en/OurWork/Environment/PollutionPrevention/AirPollution/Pages/Air-Pollution.aspx> (accessed Jan. 13, 2020).
- [10] F. Vogler and G. Würsig, “Fuel Cell in Maritime Applications Challenges, Chances and Experiences,” Sep. 2011, Accessed: Dec. 23, 2020. [Online]. Available: <https://www.h2knowledgecentre.com/content/conference546>.
- [11] Ed. C. Ågren, “Air pollution from ships.” Miljöinformation Åström & Nilsson AB. Printed by TRydells, Laholm, Sweden, Nov. 2011, [Online]. Available: https://www.airclim.org/sites/default/files/documents/Air%20pollution%20from%20ships_Nov_2011.pdf.
- [12] K. H. Strand and K. J. Aarskog, “Life cycle assessment of Fuel Cells onboard ships,” *Livssyklusanalyse av bruk av brenselceller om bord i skip*, 2010, Accessed: Oct. 21, 2019. [Online]. Available: <https://ntnuopen.ntnu.no/ntnu-xmlui/handle/11250/237857>.
- [13] T. Tronstad, H. H. Åstrand, G. P. Haugom, and L. Langfeldt, “STUDY ON THE USE OF FUEL CELLS IN SHIPPING,” *EMSA Eur. Marit. Saf. Agency*, p. 108, Jan. 2017.
- [14] “The Future of Hydrogen,” IEA, Paris, Report prepared by the IEA for the G20, Japan, 2019. [Online]. Available: <https://www.iea.org/reports/the-future-of-hydrogen>.
- [15] C. Bourne, T. Nietsch, D. Griffiths, and J. Morley, “Application of fuel cells in surface

- ships,” ETSU F/03/00207/REP. Accessed: Oct. 09, 2019. [Online]. Available: <https://www.osti.gov/etdeweb/servlets/purl/20249928>.
- [16] M. Mench, *Fuel Cell Engines*, 1st ed. John Wiley & Sons, Ltd, 2008.
- [17] “Fuel Cell Handbook (Seventh Edition),” *EGG Tech. Serv. Inc*, p. 427.
- [18] R. D. Geertsma, R. R. Negenborn, K. Visser, and J. J. Hopman, “Design and control of hybrid power and propulsion systems for smart ships: A review of developments,” *Appl. Energy*, vol. 194, pp. 30–54, May 2017, doi: 10.1016/j.apenergy.2017.02.060.
- [19] J. Brouwer, “Hybrid Gas Turbine Fuel Cell System.” National Fuel Cell Research Center University of California Irvine, CA.
- [20] J. Ahn *et al.*, “Performance and availability of a marine generator-solid oxide fuel cell-gas turbine hybrid system in a very large ethane carrier,” *J. Power Sources*, vol. 399, pp. 199–206, Sep. 2018, doi: 10.1016/j.jpowsour.2018.07.103.
- [21] J. Markowski and I. Pielecha, “The potential of fuel cells as a drive source of maritime transport,” *IOP Conf. Ser. Earth Environ. Sci.*, vol. 214, p. 012019, Jan. 2019, doi: 10.1088/1755-1315/214/1/012019.
- [22] S. Molloy *et al.*, “HybridTechnology Review_NSBA.pdf,” Nova Scotia Boatbuilders Association, Halifax, Nova Scotia, Mar. 2015. Accessed: Mar. 02, 2020. [Online]. Available: https://nsboats.com/wp-content/uploads/2018/03/HybridTechnologyReview_NSBA.pdf.
- [23] H. Menana, J.-Y. Billard, N. Bennabi, J.-F. Charpentier, and P. Genet, “Hybrid Propulsion Systems for Small Ships: Context and Challenges,” Sep. 2016, doi: 10.1109/ICELMACH.2016.7732943.
- [24] E. K. Dedes, D. A. Hudson, and S. R. Turnock, “Assessing the potential of hybrid energy technology to reduce exhaust emissions from global shipping,” *Energy Policy*, vol. 40, pp. 204–218, Jan. 2012, doi: 10.1016/j.enpol.2011.09.046.
- [25] H. Lan, S. Wen, Y.-Y. Hong, D. C. Yu, and L. Zhang, “Optimal sizing of hybrid PV/diesel/battery in ship power system,” *Appl. Energy*, vol. 158, pp. 26–34, Nov. 2015, doi: 10.1016/j.apenergy.2015.08.031.
- [26] N. Xiao, R. Zhou, and X. Lin, “Type selection and design of hybrid propulsion system of ship,” *IOP Conf. Ser. Mater. Sci. Eng.*, vol. 157, no. 1, p. 012034, Nov. 2016, doi: 10.1088/1757-899X/157/1/012034.
- [27] K. Niklas and H. Pruszko, “Full-scale CFD simulations for the determination of ship resistance as a rational, alternative method to towing tank experiments,” *Ocean Eng.*, vol. 190, p. 106435, Oct. 2019, doi: 10.1016/j.oceaneng.2019.106435.
- [28] K. Andersen, “Development of a Time-Domain Modeling Platform for Hybrid Marine Propulsion Systems,” p. 313.
- [29] Z. Dong, P. Oshkai, and S. Molloy, “Characterization of Canadian Marine Vessel Operational Profiles and Hybrid Electric Propulsion System Modelling Tool Improvement for GHG and Ship Noise Reduction,” Transport Canada, UVic Clean Transportation and Glas Ocean Research Teams, T8156-160029, Dec. 2019.
- [30] H. Zhu, “Modelling, design and energy management of a hybrid electric ship – a case study,” Master Thesis, University of Victoria, Victoria, BC, Canada, 2020.
- [31] K. Çağatay Bayindir, M. A. Gözüküçük, and A. Teke, “A comprehensive overview of hybrid electric vehicle: Powertrain configurations, powertrain control techniques and

- electronic control units,” *Energy Convers. Manag.*, vol. 52, no. 2, pp. 1305–1313, Feb. 2011, doi: 10.1016/j.enconman.2010.09.028.
- [32] V. Krithika and C. Subramani, “A comprehensive review on choice of hybrid vehicles and power converters, control strategies for hybrid electric vehicles,” *Int. J. Energy Res.*, vol. 42, no. 5, pp. 1789–1812, 2018, doi: 10.1002/er.3952.
- [33] T. M. Henriques, “Life Cycle Assessment of the Hybrid Vehicle – Toyota Prius,” Master Thesis, Technische Universität Braunschweig, Braunschweig, 2013.
- [34] C. Lin, T. Wu, X. Ou, Q. Zhang, X. Zhang, and X. Zhang, “Life-cycle private costs of hybrid electric vehicles in the current Chinese market,” *Energy Policy*, vol. 55, pp. 501–510, Apr. 2013, doi: 10.1016/j.enpol.2012.12.037.
- [35] M. Kebriaei, A. H. Niasar, and B. Asaei, “Hybrid electric vehicles: An overview,” in *2015 International Conference on Connected Vehicles and Expo (ICCVE)*, Oct. 2015, pp. 299–305, doi: 10.1109/ICCVE.2015.84.
- [36] J. W. Pratt and A. P. Harris, “Vessel Cold-Ironing Using a Barge Mounted PEM Fuel Cell: Project Scoping and Feasibility,” Sandia National Lab. (SNL-CA), Livermore, CA (United States), SAND2013-0501, Jan. 2013. doi: 10.2172/1117104.
- [37] R. Tang, X. Li, and J. Lai, “A novel optimal energy-management strategy for a maritime hybrid energy system based on large-scale global optimization,” *Appl. Energy*, vol. 228, pp. 254–264, Oct. 2018, doi: 10.1016/j.apenergy.2018.06.092.
- [38] H. H. Zhu and Z. Dong, “Modeling and Simulation of Hybrid Electric Ships with AC Power Bus - A Case Study,” in *2018 14th IEEE/ASME International Conference on Mechatronic and Embedded Systems and Applications (MESA)*, Jul. 2018, pp. 1–8, doi: 10.1109/MESA.2018.8449163.
- [39] C. C. Chan, “The State of the Art of Electric, Hybrid, and Fuel Cell Vehicles,” *Proc. IEEE*, vol. 95, no. 4, pp. 704–718, Apr. 2007, doi: 10.1109/JPROC.2007.892489.
- [40] Y. M. A. Welaya, M. M. El Gohary, and N. R. Ammar, “A comparison between fuel cells and other alternatives for marine electric power generation,” *Int. J. Nav. Archit. Ocean Eng.*, vol. 3, no. 2, pp. 141–149, Jun. 2011, doi: 10.2478/IJNAOE-2013-0057.
- [41] J. W. Pratt and S. H. Chan, “Maritime Fuel Cell Generator Project,” Sandia National Laboratories, Albuquerque, New Mexico, SAND2017-5751, May 2017.
- [42] “Maritime Electrical Installations And Diesel Electric Propulsion.” Accessed: Oct. 15, 2019. [Online]. Available: http://www.trpa.org/wp-content/uploads/ABB-AS_2003.pdf.
- [43] J. J. de-Troya, C. Álvarez, C. Fernández-Garrido, and L. Carral, “Analysing the possibilities of using fuel cells in ships,” *Int. J. Hydrog. Energy*, vol. 41, no. 4, pp. 2853–2866, Jan. 2016, doi: 10.1016/j.ijhydene.2015.11.145.
- [44] L. E. Klebanoff, “Feasibility of the Zero-V: A Zero-emission Hydrogen Fuel Cell Coastal Research Vessel,” SAND2018-4664, 1527303, May 2018. doi: 10.2172/1527303.
- [45] “A review on production, storage of hydrogen and its utilization as an energy resource - ScienceDirect.” <https://www.sciencedirect.com/science/article/pii/S1226086X13003481> (accessed Jan. 14, 2020).
- [46] Y. Bicer and I. Dincer, “Clean fuel options with hydrogen for sea transportation: A life cycle approach,” *Int. J. Hydrog. Energy*, vol. 43, no. 2, pp. 1179–1193, Jan. 2018, doi: 10.1016/j.ijhydene.2017.10.157.
- [47] J. Wang, H. Wang, and Y. Fan, “Techno-Economic Challenges of Fuel Cell

- Commercialization,” *Engineering*, vol. 4, pp. 352–360, May 2018, doi: 10.1016/j.eng.2018.05.007.
- [48] “Alternative Fuels Data Center: Hydrogen Production and Distribution.” https://afdc.energy.gov/fuels/hydrogen_production.html (accessed Oct. 08, 2019).
- [49] I. Staffell *et al.*, “The role of hydrogen and fuel cells in the global energy system,” *Energy Environ. Sci.*, vol. 12, no. 2, pp. 463–491, Feb. 2019, doi: 10.1039/C8EE01157E.
- [50] H. Prastowo, F. T. Pinto, and Semin, “Advanced Ship Propulsion Technology: A Review,” *Asian J. Appl. Sci.*, vol. 04, no. 03, Jun. 2016.
- [51] L. Chen, Y. Tong, and Z. Dong, “Li-Ion Battery Performance Degradation Modeling for the Optimal Design and Energy Management of Electrified Propulsion Systems,” p. 19, 2020.
- [52] I. Bloom *et al.*, “An accelerated calendar and cycle life study of Li-ion cells,” *J. Power Sources*, vol. 101, no. 2, pp. 238–247, Oct. 2001, doi: 10.1016/S0378-7753(01)00783-2.
- [53] K. A. Severson *et al.*, “Data-driven prediction of battery cycle life before capacity degradation,” *Nat. Energy*, vol. 4, no. 5, Art. no. 5, May 2019, doi: 10.1038/s41560-019-0356-8.
- [54] R. Deshpande, M. Verbrugge, Y.-T. Cheng, J. Wang, and P. Liu, “Battery Cycle Life Prediction with Coupled Chemical Degradation and Fatigue Mechanics,” *J. Electrochem. Soc.*, vol. 159, no. 10, p. A1730, Aug. 2012, doi: 10.1149/2.049210jes.
- [55] J. Wang *et al.*, “Degradation of lithium ion batteries employing graphite negatives and nickel–cobalt–manganese oxide + spinel manganese oxide positives: Part 1, aging mechanisms and life estimation,” *J. Power Sources*, vol. 269, pp. 937–948, Dec. 2014, doi: 10.1016/j.jpowsour.2014.07.030.
- [56] M. Doyle, T. F. Fuller, and J. Newman, “Modeling of Galvanostatic Charge and Discharge of the Lithium/Polymer/Insertion Cell,” *J. Electrochem. Soc.*, vol. 140, no. 6, p. 1526, Jun. 1993, doi: 10.1149/1.2221597.
- [57] P. Ramadass, B. Haran, P. M. Gomadam, R. White, and B. N. Popov, “Development of First Principles Capacity Fade Model for Li-Ion Cells,” *J. Electrochem. Soc.*, vol. 151, no. 2, p. A196, Jan. 2004, doi: 10.1149/1.1634273.
- [58] L. Ren, L. Zhao, S. Hong, S. Zhao, H. Wang, and L. Zhang, “Remaining Useful Life Prediction for Lithium-Ion Battery: A Deep Learning Approach,” *IEEE Access*, vol. 6, pp. 50587–50598, 2018, doi: 10.1109/ACCESS.2018.2858856.
- [59] G. Ning and B. N. Popov, “Cycle Life Modeling of Lithium-Ion Batteries,” *J. Electrochem. Soc.*, vol. 151, no. 10, p. A1584, Sep. 2004, doi: 10.1149/1.1787631.
- [60] M. Ecker *et al.*, “Development of a lifetime prediction model for lithium-ion batteries based on extended accelerated aging test data,” *J. Power Sources*, vol. 215, pp. 248–257, Oct. 2012, doi: 10.1016/j.jpowsour.2012.05.012.
- [61] J. Wang *et al.*, “Cycle-life model for graphite-LiFePO₄ cells,” *J. Power Sources*, vol. 196, no. 8, pp. 3942–3948, Apr. 2011, doi: 10.1016/j.jpowsour.2010.11.134.
- [62] W. Raza *et al.*, “Recent Advancements in Supercapacitor Technology,” *Nano Energy*, vol. 52, Aug. 2018, doi: 10.1016/j.nanoen.2018.08.013.
- [63] A. Khaligh and Z. Li, “Battery, Ultracapacitor, Fuel Cell, and Hybrid Energy Storage Systems for Electric, Hybrid Electric, Fuel Cell, and Plug-In Hybrid Electric Vehicles: State of the Art,” *IEEE Trans. Veh. Technol.*, vol. 59, no. 6, pp. 2806–2814, Jul. 2010, doi:

- 10.1109/TVT.2010.2047877.
- [64] C. Kagiri and X. Xia, “Optimal Control of a Hybrid Battery/Supercapacitor Storage for Neighborhood Electric Vehicles,” *Energy Procedia*, vol. 105, pp. 2145–2150, May 2017, doi: 10.1016/j.egypro.2017.03.605.
- [65] R. Dhaouadi, Y. Hori, and H. Xiaoliang, “Robust control of an ultracapacitor-based hybrid energy storage system for electric vehicles,” in *2014 IEEE 13th International Workshop on Advanced Motion Control (AMC)*, Mar. 2014, pp. 161–166, doi: 10.1109/AMC.2014.6823275.
- [66] K. V. Singh, H. O. Bansal, and D. Singh, “A comprehensive review on hybrid electric vehicles: architectures and components,” *J. Mod. Transp.*, vol. 27, no. 2, pp. 77–107, Jun. 2019, doi: 10.1007/s40534-019-0184-3.
- [67] A. M. Bassam, A. B. Phillips, S. R. Turnock, and P. A. Wilson, “An improved energy management strategy for a hybrid fuel cell/battery passenger vessel,” *Int. J. Hydrog. Energy*, vol. 41, no. 47, pp. 22453–22464, Dec. 2016, doi: 10.1016/j.ijhydene.2016.08.049.
- [68] K. Kim, K. Park, G. Roh, and K. Chun, “DC-grid system for ships: a study of benefits and technical considerations,” *J. Int. Marit. Saf. Environ. Aff. Shipp.*, vol. 2, no. 1, pp. 1–12, Nov. 2018, doi: 10.1080/25725084.2018.1490239.
- [69] S. Upadhyay and M. P. Sharma, “A review on configurations, control and sizing methodologies of hybrid energy systems,” *Renew. Sustain. Energy Rev.*, vol. 38, pp. 47–63, Oct. 2014, doi: 10.1016/j.rser.2014.05.057.
- [70] V. V. Budashko, “Design of the three-level multicriterial strategy of hybrid marine power plant control for a combined propulsion complex,” *Электротехника И Электромеханика*, no. 2 (eng), Art. no. 2 (eng), 2017, Accessed: Mar. 02, 2020. [Online]. Available: <https://cyberleninka.ru/article/n/design-of-the-three-level-multicriterial-strategy-of-hybrid-marine-power-plant-control-for-a-combined-propulsion-complex>.
- [71] R. D. Geertsma, R. R. Negenborn, K. Visser, and J. J. Hopman, “Parallel Control for Hybrid Propulsion of Multifunction Ships,” *IFAC-Pap.*, vol. 50, no. 1, pp. 2296–2303, Jul. 2017, doi: 10.1016/j.ifacol.2017.08.229.
- [72] M. Kalikatzarakis, R. D. Geertsma, E. J. Boonen, K. Visser, and R. R. Negenborn, “Ship energy management for hybrid propulsion and power supply with shore charging,” *Control Eng. Pract.*, vol. 76, pp. 133–154, Jul. 2018, doi: 10.1016/j.conengprac.2018.04.009.
- [73] M. Amiri, M. Esfahanian, M. R. Hairi-Yazdi, and V. Esfahanian, “Minimization of power losses in hybrid electric vehicles in view of the prolonging of battery life,” *J. Power Sources*, vol. 190, no. 2, pp. 372–379, May 2009, doi: 10.1016/j.jpowsour.2009.01.072.
- [74] T. E. Lipman and M. A. Delucchi, “A retail and lifecycle cost analysis of hybrid electric vehicles,” *Transp. Res. Part Transp. Environ.*, vol. 11, no. 2, pp. 115–132, Mar. 2006, doi: 10.1016/j.trd.2005.10.002.
- [75] A. Nordelöf, M. Messagie, A.-M. Tillman, M. Ljunggren Söderman, and J. Van Mierlo, “Environmental impacts of hybrid, plug-in hybrid, and battery electric vehicles—what can we learn from life cycle assessment?,” *Int. J. Life Cycle Assess.*, vol. 19, no. 11, pp. 1866–1890, Nov. 2014, doi: 10.1007/s11367-014-0788-0.
- [76] F. D. Pero, M. Delogu, and M. Pierini, “Life Cycle Assessment in the automotive sector:

- a comparative case study of Internal Combustion Engine (ICE) and electric car,” *Procedia Struct. Integr.*, vol. 12, pp. 521–537, 2018, doi: 10.1016/j.prostr.2018.11.066.
- [77] L. L. P. de Souza, E. E. S. Lora, J. C. E. Palacio, M. H. Rocha, M. L. G. Renó, and O. J. Venturini, “Comparative environmental life cycle assessment of conventional vehicles with different fuel options, plug-in hybrid and electric vehicles for a sustainable transportation system in Brazil,” *J. Clean. Prod.*, vol. 203, pp. 444–468, Dec. 2018, doi: 10.1016/j.jclepro.2018.08.236.
- [78] C. Tagliaferri *et al.*, “Life cycle assessment of future electric and hybrid vehicles: A cradle-to-grave systems engineering approach,” *Chem. Eng. Res. Des.*, vol. 112, pp. 298–309, Aug. 2016, doi: 10.1016/j.cherd.2016.07.003.
- [79] M. Rupp, S. Schulze, and I. Kuperjans, “Comparative Life Cycle Analysis of Conventional and Hybrid Heavy-Duty Trucks,” *World Electr. Veh. J.*, vol. 9, no. 2, p. 33, Aug. 2018, doi: 10.3390/wevj9020033.
- [80] F. Boureima *et al.*, “Comparative LCA of electric, hybrid, LPG and gasoline cars in Belgian context,” 2009, doi: 10.3390/wevj3030469.
- [81] G. Jungmeier *et al.*, “Key issues in life cycle assessment of electric vehicles — Findings in the International Energy Agency (IEA) on Hybrid and Electric Vehicles (HEV),” in *2013 World Electric Vehicle Symposium and Exhibition (EVS27)*, Barcelona, Spain, Nov. 2013, pp. 1–7, doi: 10.1109/EVS.2013.6914862.
- [82] A. Lajunen, “Energy consumption and cost-benefit analysis of hybrid and electric city buses,” *Transp. Res. Part C Emerg. Technol.*, vol. 38, pp. 1–15, Jan. 2014, doi: 10.1016/j.trc.2013.10.008.
- [83] A. Lajunen and T. Lipman, “Lifecycle cost assessment and carbon dioxide emissions of diesel, natural gas, hybrid electric, fuel cell hybrid and electric transit buses,” *Energy*, vol. 106, pp. 329–342, Jul. 2016, doi: 10.1016/j.energy.2016.03.075.
- [84] J. Dumortier *et al.*, “Effects of providing total cost of ownership information on consumers’ intent to purchase a hybrid or plug-in electric vehicle,” *Transp. Res. Part Policy Pract.*, vol. 72, pp. 71–86, Feb. 2015, doi: 10.1016/j.tra.2014.12.005.
- [85] G. J. Offer, D. Howey, M. Contestabile, R. Clague, and N. P. Brandon, “Comparative analysis of battery electric, hydrogen fuel cell and hybrid vehicles in a future sustainable road transport system,” *Energy Policy*, vol. 38, no. 1, pp. 24–29, Jan. 2010, doi: 10.1016/j.enpol.2009.08.040.
- [86] H. Mousazadeh, A. Keyhani, A. Javadi, H. Mobli, K. Abrinia, and A. Sharifi, “Life-cycle assessment of a Solar Assist Plug-in Hybrid electric Tractor (SAPHT) in comparison with a conventional tractor,” *Energy Convers. Manag.*, vol. 52, no. 3, pp. 1700–1710, Mar. 2011, doi: 10.1016/j.enconman.2010.10.033.
- [87] M. Messagie, “Life Cycle Analysis of the Climate Impact of Electric Vehicles,” Transport and Environment, Vrije Universiteit Brussel, Brussels, Belgium, 2017. Accessed: Sep. 09, 2019. [Online]. Available: <https://www.transportenvironment.org/sites/te/files/publications/TE%20-%20draft%20report%20v04.pdf>.
- [88] B. Manouchehrinia, S. Molloy, Z. Dong, T. A. Gulliver, and C. Gough, “Emission and life-cycle cost analysis of hybrid and pure electric propulsion systems for fishing boats,” *J. Ocean Technol.*, vol. 13, pp. 64–87, Jul. 2018.

- [89] H. Wang, E. Oguz, B. Jeong, and P. Zhou, “Life cycle cost and environmental impact analysis of ship hull maintenance strategies for a short route hybrid ferry,” *Ocean Eng.*, vol. 161, pp. 20–28, Aug. 2018, doi: 10.1016/j.oceaneng.2018.04.084.
- [90] E. Oguz, B. Jeong, H. Wang, and P. Zhou, “Life Cycle and Cost Assessment on Engine Selection for an Offshore Tug Vessel,” p. 8.
- [91] B. Jeong, H. Wang, E. Oguz, and P. Zhou, “An effective framework for life cycle and cost assessment for marine vessels aiming to select optimal propulsion systems,” *J. Clean. Prod.*, vol. 187, pp. 111–130, Jun. 2018, doi: 10.1016/j.jclepro.2018.03.184.
- [92] J. Ling-Chin and A. P. Roskilly, “A comparative life cycle assessment of marine power systems,” *Energy Convers. Manag.*, vol. 127, pp. 477–493, Nov. 2016, doi: 10.1016/j.enconman.2016.09.012.
- [93] J. Ling-Chin and A. P. Roskilly, “Investigating the implications of a new-build hybrid power system for Roll-on/Roll-off cargo ships from a sustainability perspective – A life cycle assessment case study,” *Appl. Energy*, vol. 181, pp. 416–434, Nov. 2016, doi: 10.1016/j.apenergy.2016.08.065.
- [94] E. Blanco-Davis and P. Zhou, “LCA as a tool to aid in the selection of retrofiting alternatives,” *Ocean Eng.*, vol. 77, pp. 33–41, Feb. 2014, doi: 10.1016/j.oceaneng.2013.12.010.
- [95] J. Holtrop and G. G. J. Mennen, “An approximate power prediction method,” *Int. Shipbuild. Prog.*, vol. 29, no. 335, pp. 166–170, Jul. 1982, doi: 10.3233/ISP-1982-2933501.
- [96] L. Birk, *Fundamentals of Ship Hydrodynamics: Fluid Mechanics, Ship Resistance and Propulsion*, 1st ed. Wiley, 2019.
- [97] J. M. J. Journée and W. W. Massie, “Offshore Hydromechanics.” Delft University of Technology, Jan. 2001, Accessed: May 18, 2020. [Online]. Available: https://ocw.tudelft.nl/wp-content/uploads/OffshoreHydromechanics_Journee_Massie.pdf.
- [98] “The Resistance Committee: Final Report and Recommendations to the 28th ITTC.” International Towing Tank Conference, 2017.
- [99] “ITTC – Recommended Procedures and Guidelines: Description and Rules of the ITTC.” International Towing Tank Conference, 2014, Accessed: Jun. 11, 2020. [Online]. Available: <https://itc.info/media/4008/10-01.pdf>.
- [100] T. Jaster, “Modeling and Simulation of a Hybrid Electric Vessel,” Master Thesis, University of Victoria, Victoria, BC, Canada, 2013.
- [101] M. Rahimpour, “A Preliminary Study on Low-Order Hull Resistance and Propeller Thrust Model on BCFS Clisser.” University of Victoria, Jan. 15, 2020.
- [102] W. A. L. Truelove, “A general methodology for generating representative load cycles for monohull surface vessels,” Thesis, 2018.
- [103] M. M. Bernitsas, D. Ray, and P. Kinley, “KT, KQ, and Efficiency Curves for the Wageningen B-Series Propellers.” Department of Naval Architecture and Marine Engineering, University of Michigan, Accessed: May 13, 2020. [Online]. Available: https://deepblue.lib.umich.edu/bitstream/handle/2027.42/91702/Publication_No_237.pdf?sequence=1&isAllowed=y.
- [104] L. Pivano, “Thrust Estimation and Control of Marine Propellers in FourQuadrant

- Operations,” Norwegian University of Science and Technology, Trondheim, 2008.
- [105] K. Zelazny, “A Simplified Method for Calculating Propeller Thrust Decrease for a Ship Sailing on a Given Shipping Lane,” *Pol. Marit. Res.*, vol. 21, no. 2, pp. 27–33, Apr. 2014, doi: 10.2478/pomr-2014-0015.
- [106] A. H. Techet, “Hydrodynamics for Ocean Engineers.” Massachusetts Institute of Technology, 2004, [Online]. Available: <http://hdl.handle.net/1721.1/35850>.
- [107] “Skeena Queen | BC Ferries.” <https://www.bcferries.com/on-the-ferry/our-fleet/skeena-queen/SKEN?redir=301> (accessed Sep. 29, 2020).
- [108] G. Paganelli, S. Delprat, T. M. Guerra, J. Rimoux, and J. J. Santin, “Equivalent consumption minimization strategy for parallel hybrid powertrains,” in *Vehicular Technology Conference. IEEE 55th Vehicular Technology Conference. VTC Spring 2002 (Cat. No.02CH37367)*, May 2002, vol. 4, pp. 2076–2081 vol.4, doi: 10.1109/VTC.2002.1002989.
- [109] R. Bellman, “Dynamic programming and stochastic control processes,” *Inf. Control*, vol. 1, no. 3, pp. 228–239, Sep. 1958, doi: 10.1016/S0019-9958(58)80003-0.
- [110] H. Dong, B. Song, Z. Dong, and P. Wang, “Multi-start Space Reduction (MSSR) surrogate-based global optimization method,” *Struct. Multidiscip. Optim.*, vol. 54, no. 4, pp. 907–926, Oct. 2016, doi: 10.1007/s00158-016-1450-1.
- [111] Z. Song *et al.*, “Multi-objective optimization of a semi-active battery/supercapacitor energy storage system for electric vehicles,” *Appl. Energy*, vol. 135, pp. 212–224, Dec. 2014, doi: 10.1016/j.apenergy.2014.06.087.
- [112] T. I. Fossen, *Handbook of Marine Craft Hydrodynamics and Motion Control: Fossen/Handbook of Marine Craft Hydrodynamics and Motion Control*. Chichester, UK: John Wiley & Sons, Ltd, 2011.

Appendix A Coefficients for Holtrop's method of resistance calculation

$$C_1 = 2223105C_7^{3.78613} \left(\frac{T}{B}\right)^{1.07961} (90 - i_E)^{-1.37565} \quad (\text{A1})$$

$$C_2 = \exp(-0.89\sqrt{C_3}) \quad (\text{A2})$$

$$C_3 = \frac{0.56A_{BT}^{1.5}}{B * T(0.31\sqrt{A_{BT}} + T_F - h_B)} \quad (\text{A3})$$

$$C_4 = \begin{cases} \frac{T_F}{L} & \text{when } \frac{T_F}{L} \leq 0.04 \\ 0.04 & \text{when } \frac{T_F}{L} \geq 0.04 \end{cases} \quad (\text{A4})$$

$$C_5 = 1 - \frac{0.8A_T}{B * T * C_M} \quad (\text{A5})$$

$$C_6 = \begin{cases} 0.2(1 - 0.2F_{nT}) & \text{when } F_{nT} < 5 \\ 0 & F_{nT} \geq 5 \end{cases} \quad (\text{A6})$$

$$C_7 = \begin{cases} 0.229577 \left(\frac{B}{L}\right)^{0.3333} & \text{when } B/L < 0.11 \\ \frac{B}{L} & \text{when } 0.11 < B/L < 0.25 \\ 0.5 - 0.0625 \frac{L}{B} & \text{when } B/L > 0.25 \end{cases} \quad (\text{A7})$$

$$C_{12} = \begin{cases} (T/L)^{0.2228446} & \text{when } T/L > 0.05 \\ 48.2(T/L - 0.02)^{2.078} + 0.479948 & \text{when } 0.02 < T/L < 0.05 \\ 0.479948 & \text{when } T/L < 0.02 \end{cases} \quad (\text{A8})$$

$$C_{13} = 1 + 0.003C_{stern} \quad (\text{A9})$$

$$C_{15} = \begin{cases} 0 & \frac{L^3}{\nabla} < 512 \\ -0.169385 + \frac{\frac{L}{1} - 8}{2.36} & 512 < \frac{L^3}{\nabla} < 1727 \\ -1.69385 & \frac{L^3}{\nabla} > 1727 \end{cases} \quad (\text{A10})$$

$$C_{16} = \begin{cases} 8.07981C_P - 13.8673C_P^2 + 6.984388C_P^3 & \text{when } C_P < 0.8 \\ 1.73014 - 0.7067C_P & \text{when } C_P > 0.8 \end{cases} \quad (\text{A11})$$

$$m_1 = 0.0140407 \frac{L}{T} - 1.75254 \frac{\nabla^{\frac{1}{3}}}{L} - 4.79323 \frac{B}{L} - C_{16} \quad (\text{A12})$$

$$m_2 = C_{15} C_P^2 \exp(-0.1 F_n^{-2}) \quad (\text{A13})$$

$$\lambda = \begin{cases} 1.446 C_P - \frac{0.03L}{B} & \text{when } \frac{L}{B} < 12 \\ 1.446 C_P - 0.36 & \text{when } \frac{L}{B} > 12 \end{cases} \quad (\text{A14})$$

$$C_{stern} = \begin{cases} -10 & \text{for } V - \text{shaped section} \\ 0 & \text{for Normal section shape} \\ 10 & \text{for } U - \text{shaped sections with Hogner stern} \end{cases} \quad (\text{A15})$$

where, i_E is the angle of the waterline at the bow

$$i_E = 1 + 89 \exp \left[- \left(\frac{L}{B} \right)^{0.80856} (1 - C_{WP})^{0.30484} (1 - C_P - 0.0225 lcb)^{0.6367} \left(\frac{L_R}{B} \right)^{0.34574} \left(\frac{100 \nabla}{L^3} \right)^{0.16302} \right] \quad (\text{A16})$$

h_B is the height of the center of the transverse area A_{BT} above the keel line; A_{BT} is the transverse area above the keel line; and T_F is the forward draft.

Approximate k_2 Values	
Rudder behind skeg	1.5-2.0
Rudder behind stern	1.3-1.5
Twin-screw balance rudders	2.8
Shaft brackets	3.0
Skeg	1.5-2.0
Structure bossings	3.0
Hull bossings	2.0
Shafts	2.0-4.0
Stabilizer fins	2.8
Dome	2.7
Bilge keels	1.4

Appendix B Coefficients for wind resistance calculation

α_{rw} [°]	A ₀	A ₁	A ₂	A ₃	A ₄	A ₅	A ₆
0	2.152	-5.000	0.243	-0.164	0.000	0.000	0.000
10	1.714	-3.330	0.145	-0.121	0.000	0.000	0.000
20	1.818	-3.970	0.211	-0.143	0.000	0.000	0.033
30	1.965	-4.810	0.243	-0.154	0.000	0.000	0.041
40	2.333	-5.990	0.247	-0.190	0.000	0.000	0.042
50	1.726	-6.540	0.189	-0.173	0.348	0.000	0.048
60	0.913	-4.680	0.000	-0.104	0.482	0.000	0.052
70	0.457	-2.880	0.000	-0.068	0.346	0.000	0.043
80	0.341	-0.910	0.000	-0.031	0.000	0.000	0.052
90	0.355	0.000	0.000	0.000	-0.247	0.000	0.018
100	0.601	0.000	0.000	0.000	-0.347	0.000	-0.020
110	0.651	1.290	0.000	0.000	-0.582	0.000	-0.031
120	0.564	2.540	0.000	0.000	-0.748	0.000	-0.024
130	-0.142	3.580	0.000	0.047	-0.700	0.000	-0.028
140	-0.677	3.640	0.000	0.069	-0.529	0.000	-0.032
150	-0.723	3.140	0.000	0.064	-0.475	0.000	-0.032
160	-2.148	2.560	0.000	0.081	0.000	1.270	-0.027
170	-2.707	3.970	-0.175	0.126	0.000	1.810	0.000
180	-2.529	3.760	-0.174	0.128	0.000	1.550	0.000

Appendix C Coefficients for propeller efficiency calculation

Coefficients and terms of the K_T and K_Q polynomials for the Wageningen B-screw
Series for $R_n=2 \times 10^6$. Reproduced from [1]

$$K_T = \sum_{s,t,u,v} C_{s,t,u,v}^T \cdot (J)^s \cdot (P/D)^t \cdot (A_E/A_O)^u \cdot (z^v)$$

$$K_Q = \sum_{s,t,u,v} C_{s,t,u,v}^Q \cdot (J)^s \cdot (P/D)^t \cdot (A_E/A_O)^u \cdot (z^v)$$

K_T	$C_{s,t,u,v}^T$	s (J)	t (P/D)	u (A_E/A_O)	v (Z)	$C_{s,t,u,v}^Q$	s (J)	t (P/D)	u (A_E/A_O)	v (Z)
	+0.00880496	0	0	0	0	+0.00379368	0	0	0	0
	-0.204554	1	0	0	0	+0.00886523	2	0	0	0
	+0.166351	0	1	0	0	-0.032241	1	1	0	0
	+0.158114	0	2	0	0	+0.00344778	0	2	0	0
	-0.147581	2	0	1	0	-0.0408811	0	1	1	0
	-0.481497	1	1	1	0	-0.108009	1	1	1	0
	+0.415437	0	2	1	0	-0.0885381	2	1	1	0
	+0.0144043	0	0	0	1	+0.188561	0	2	1	0
	-0.0530054	2	0	0	1	-0.00370871	1	0	0	1
	+0.0143481	0	1	0	1	+0.00513696	0	1	0	1
	+0.0606826	1	1	0	1	+0.0209449	1	1	0	1
	-0.0125894	0	0	1	1	+0.00474319	2	1	0	1
	+0.0109689	1	0	1	1	-0.00723408	2	0	1	1
	-0.133698	0	3	0	0	+0.00438388	1	1	1	1
	+0.00638407	0	6	0	0	-0.0269403	0	2	1	1
	-0.00132718	2	6	0	0	+0.0558082	3	0	1	0
	+0.168496	3	0	1	0	+0.0161886	0	3	1	0
	-0.0507214	0	0	2	0	+0.00318086	1	3	1	0
	+0.0854559	2	0	2	0	+0.015896	0	0	2	0
	-0.0504475	3	0	2	0	+0.0471729	1	0	2	0
	+0.010465	1	6	2	0	+0.0196283	3	0	2	0
	-0.00648272	2	6	2	0	-0.0502782	0	1	2	0
	-0.00841728	0	3	0	1	-0.030055	3	1	2	0
	+0.0168424	1	3	0	1	+0.0417122	2	2	2	0
	-0.00102296	3	3	0	1	-0.0397722	0	3	2	0
	-0.0317791	0	3	1	1	-0.00350024	0	6	2	0
	+0.018604	1	0	2	1	-0.0106854	3	0	0	1
	-0.00410798	0	2	2	1	+0.00110903	3	3	0	1
	-0.000606848	0	0	0	2	-0.000313912	0	6	0	1
	-0.0049819	1	0	0	2	+0.0035985	3	0	1	1
	+0.0025983	2	0	0	2	-0.00142121	0	6	1	1
	-0.000560528	3	0	0	2	-0.00383637	1	0	2	1
	-0.00163652	1	2	0	2	+0.0126803	0	2	2	1
	-0.000328787	1	6	0	2	-0.00318278	2	3	2	1
	+0.000116502	2	6	0	2	+0.00334268	0	6	2	1
	+0.000690904	0	0	1	2	-0.00183491	1	1	0	2
	+0.00421749	0	3	1	2	+0.000112451	3	2	0	2
	+0.0000565229	3	6	1	2	-0.0000297228	3	6	0	2
	-0.00146564	0	3	2	2	+0.000269551	1	0	1	2
						+0.00083265	2	0	1	2
						+0.00155334	0	2	1	2
						+0.000302683	0	6	1	2
						-0.0001843	0	0	2	2
						-0.000425399	0	3	2	2
						+0.0000869243	3	3	2	2
						-0.0004659	0	6	2	2
						+0.0000554194	1	6	2	2

$$R_n = 2 \times 10^6$$